Fault facies modelling:
3D representation of faults in petroleum reservoirs.

Master of Science thesis
by
Geir Christian Kjeldaas

Acknowledgments

I would like to extend a further thanks to all my friends and fellow students in Bergen, who have made my days as a student a wonderful and unforgettable experience. Without you I would not have finished what I started. I am sure to miss the time spent with you all as it literally has been the time of my life. Let us hope all our days to come are as fun and rewarding.

Finally, I would like to thank my mother and father for having influenced me to study earth sciences, and for their loving support through my student years.

Geir Christian Kjeldaas

Bergen, June 30, 2008

Abstract

The purpose of a reservoir model is to act as a tool for optimizing development and production strategies for subsurface hydrocarbon reservoirs. Such a model is intended to be predictive, and to act as a map for the ones placing and drilling wells into the reservoir. For a model to be as predictive as possible, it is important that it represents the geology as accurately as possible. In present day models faults are modelled as 2D transmissibility multipliers. Such a representation is not optimal as it excludes the effect the actual 3D architecture of faults have on fluid flow. To rectify this, a technique to model faults as 3D bodies has been developed by the Fault Facies group at CIPR.

The aim of this thesis was to conduct a practical test of the fault facies modelling method. The work is a part of the Fault Facies groups' effort to improve the modelling technique.

My assignments in the project can be summarised as follows:

1.   Recreate reservoir models previously presented by Sæther (2006), and use these as a base for the test. The models were reproduced geometries mapped at Kilve on the South coast of the Bristol Channel (UK). Simulation results for these models, using conventional methods, were available, thus allowing comparison with results obtained from the fault facies modelling.

2.   Beta-testing of the fault facies modelling algorithms included in Havana, a fault modelling tool developed by the Norwegian Computing Center (NR)) and used in conjunction with Irap RMS™ as a base for implementing the fault facies modelling method. The work involved identifying bugs and problems with the work flow and implementation, reporting them to NR and finding workarounds.

3.   Strain- and facies modelling of fault zones. This was done using a Havana as well as scripts in the internal programming language of RMS (IPL).

4.   Assign and model porosity and permeability for the fault facies. The values used were based on published and unpublished data collected by the Fault Facies group and supplemented by data from other published sources.

5.   Flow simulation and testing of the models. Results were analyzed compared with simulation results obtained by Sæther (2006) using conventional fault modelling techniques.

The reservoir modelling tool used to create the model grids in this assignment has been Irap RMS™ from Roxar. This is a common standard modelling tool used in both research and the petroleum industry to generate petroleum reservoir geo- and simulation models. The ECLIPSE 100 fluid flow simulator from Schlumberger was used to perform the flow simulations. A third program, Havana (chapter 2.3), by the Norwegian Computing Centre (NR), was used to implement advanced functions needed in the modelling process.

Chapter overview:

Chapter 1

The first two parts of chapter 1 will give an introduction to the concept of fault facies modelling, an explanation of what part this thesis plays in the Fault Facies Project and what the overall aim of the project is. Further, a brief review is given of some of the previous studies which have been done on fault zone geometries and modelling, and a short description and definition of a fault zone and the fault zone structural elements.

Chapter 2

This chapter covers the work performed with regard to the modelling. It contains an overview of the geometry of the three chosen cases, an explanation of the workflow used when recreating the geo-models and fault models, used by Sæther (2006), in RMS, a description of the creation of the local grid refinements (LGRs) and the fault facies and how the strain and displacement models work.

Chapter 3

Chapter 3 explains what facies are being used in both the sedimentary and the fault zone facies models. It also contains a description of the different facie types and petrophysical values used in the modelling and simulation, outlining and explaining the choices made when assigning petrophysical values for the fault facies.

Chapter 4

Chapter 4 describes the different simulation setups and presents the flow parameters used. It contains a description of the setups used in the different simulation scenarios, and a qualitative and quantitative analysis of the simulation results.

Chapter 5

Chapter 5 contains description of the beta-test problems encountered when running the workflows with the fault facies software.

Chapter 6

Chapter 6 contains the discussion.

Chapter 7

Chapter 7 is the conclusion chapter.

1 Chapter 1 Introduction

1.1 Introduction:

The purpose of a reservoir model is to act as a tool for optimizing development and production strategies for subsurface hydrocarbon reservoirs. A geological reservoir model is a numerical representation of the spatial distribution and organization of geological architecture elements and properties. This static model serves as input to fluid flow simulation models which can be used to forecast reservoir behaviour during production. The simulation model allows us to test and evaluate different development scenarios and optimise recovery. It furthermore facilitates risk assessment and economical evaluation of different scenarios.

Two main groups of features need to be captured when building a geological reservoir model: Sedimentological heterogeneities and structural heterogeneities. The correct representation of these is critical for the credibility and predictive power of the model.

Sedimentological modelling has progressed significantly during the last twenty years, from deterministic, coarse, boxlike representation of sedimentary bodies with constant petrophysical properties to a stochastic modelling of facies and petrophysical properties with complex, realistic geometries and interrelationships where multiple facies and heterogeneities down to a relatively small scale can be used to populate a grid. The level of detail which can be included in reservoir models is presently only constrained by input data resolution and time and computational power available to the modeller.

Structural modelling, on the other hand, appears far less sophisticated. There are two main reasons for this; one related to interpretation, the other to conventions of model implementation:

1) The seismic signature of faults is often weak and and/or heterogeneous and poorly defined, which adds ambiguity and uncertainty to the interpretation of fault positions and geometries. Thus fault interpretation is prone to be subjective. For modelling purposes this tendency is commonly exacerbated by deterministic use of fault data and insufficient or wholly lacking uncertainty analysis ;

2) Traditional reservoir modelling and simulation tools incorporate faults in a very simplified manner as displacements across grid-splits. Faults are represented as planes along which offset takes place and their impact on fluid flow included as 2D

transmissibility multipliers between cells on either side of the plane (Manzocchi et al 1999, 2008).

Unfortunately, previous efforts at implementing faults and fault properties in reservoir models (see Chapter 1.3.1) have largely focused on how to adapt geological reality to these technical constraints, rather than addressing the technical inadequacy of this modelling paradigm to realistically represent faults as seen in nature.

Seismic scale faults in nature commonly exhibits an envelope of complex structures surrounding the main slip plane called a fault zone. This can be subdivided into a core, where most of the displacement is accommodated, and a surrounding damage zone (Caine et al. 1996). Representing fault zones as 2D planes with transmissibility multipliers accounting for the cumulative effect of the fault zone on fluid flow across faults is obviously an oversimplification, as a number of features of fluid flow in reservoirs can not be included in the model (Tveranger et al. 2005). Most important of these is flow inside and parallel to the fault zone. There are at present no standard tools which allow explicit modelling of this. Furthermore, although commonly seen to extend tens to hundreds of meters away from the fault core and displaying petrophysical properties modified by the faulting process, damage zones are rarely included as a feature in reservoir models. This may lead to overestimation of in place volumes and underestimation of reservoir complexity when drilling well close to or through faults. Also, there is the fact that a fault modelling method lacking the means to reproduce all known fluid flow effects occurring in faults, gives a misleading picture of actual uncertainty, thereby potentially severely underestimating risk and range of reservoir behaviour to given production strategies. A new way of including faults, reproducing fault zone structures and properties as seen in nature, is clearly needed.

Recent research has developed a new approach for handling fault zones in reservoir models (Tveranger et al. 2005, Syversveen et al 2006, Fredman 2007, in press, Soleng et al. 2007, Cardozo et al. in press, Braathen et al. submitted, Nøttveit et al. submitted). The method involves describing fault zones as volumetric entities populated by "fault facies" or volumetrically expressed building blocks. A fault facies is informally defined as "any feature or rock body deriving its present properties from tectonic deformation" (Tveranger et al. 2005). For all practical purposes fault facies can be handled using the same modelling tools as are currently employed for modelling sedimentary facies. The main differences lie in the use of a fault zone grid and conditioning factors derived from strain modelling to account for fault facies types, distributions and properties. Thus the method allows fault zone structures and properties to be represented in realistic detail.

The modelling method is still in its early stages with regard to practical application. Although a functional workflow has been developed only a limited number of prototype models using synthetic fault configuration and data have been built. An extensive series of testing is needed to map out strengths, weaknesses and shortcomings before it can be applied routinely in reservoir modelling.

The aim of the present thesis was to conduct a practical test of the fault facies modelling method. The work is a part of the Fault Facies groups' effort to improve the modelling technique.

My assignments in this project can be summarised as follows:

6.   Recreate reservoir models previously presented by Sæther (2006), and use these as a base for the test. The models were reproduced geometries mapped at Kilve on the South coast of the Bristol Channel (UK). Simulation results for these models, using conventional methods, were available, thus allowing comparison with results obtained from the fault facies modelling.

7.   Beta-testing of the fault facies modelling algorithms included in Havana, a fault modelling tool developed by the Norwegian Computing Center (NR)) and used in conjunction with Irap RMS™ as a base for implementing the fault facies modelling method. The work involved identifying bugs and problems with the work flow and implementation, reporting them to NR and finding workarounds.

8.   Strain- and facies modelling of fault zones. This was done using a Havana as well as scripts in the internal programming language of RMS (IPL).

9.   Assign and model porosity and permeability for the fault facies. The values used were based on published and unpublished data collected by the Fault Facies group and supplemented by data from other published sources.

10.   Flow simulation and testing of the models. Results were analyzed compared with simulation results obtained by Sæther (2006) using conventional fault modelling techniques.

The reservoir modelling tool used to create the model grids in this assignment has been Irap RMS from Roxar. This is a common standard modelling tool used in both research and the petroleum industry to generate petroleum reservoir geo- and simulation models. The Eclipse 100 fluid flow simulator from Schlumberger was used to perform the flow simulations. A third program, Havana (chapter 2.3), by the Norwegian Computing Centre (NR), was used to implement advanced functions needed in the modelling process.

Before progressing to the description of the modelling and testing performed as part of this Master thesis, a short review of fault zone structures and how they traditionally have been incorporated in reservoir models is required.

1.2 Fault zones and structural elements of faults

1.2.1 Introduction

A fault can be defined as a planar or curved fracture where compressional or tensional forces cause a relative displacement of the rock on the opposite sides of the fracture. Faults are created due to differential stresses on the rock building up to a level exceeding the strength of the host rock, causing it to break, or fracture (Fossen and Gabrielsen 2005). The process of faulting introduces two main changes to the host rock: 1) A geometrical change caused by displacement along the fault, and 2) a modification of the rock volume surrounding the fault (also termed the fault envelope or fault zone). Faults occur at all scales exhibiting displacements from cm to km scale and displaying lengths from cm to several hundred km. The extent of the fault envelope is dependant on the scale of the fault, the nature of the host rock (mechanical strength, lithology etc.), tectonic setting, at which burial depth faulting occurred and temporal evolution of the fault. Consequently fault envelope thickness may vary from mm to several hundred meters. Faults rarely occur as isolated features, and depending on the stress field complex patterns of faults may develop (Figure 1.2.1, Figure 1.2.4, Figure 2.2.2 and Figure 2.2.3). A fault may be composed of several minor faults which occur so close to one another that the displacement and individual fault envelopes overlap and intertwine, creating thick composite fault zones.

Fault zones show great variability and complexity in terms of geometry and the distribution of petrophysical properties (Figure 1.2.1) (Antonellini and Aydin 1994, Caine et al. 1996, Fossen & Gabrielsen 2005, Tveranger et al. 2008). The fault core commonly includes a central fault plane. In larger faults the core may consist of several interconnected slip planes commonly with associated membranes of gouge and cataclasites or shale encased in breccia and lenses consisting of fault rock of variously deformed lenses of host rock. The damage zone may display deformation bands, minor slip planes with or without membranes and host rock lenses exhibiting internal deformation such as folding, minor slip planes and deformation bands.

The petrophysical heterogeneity introduced by the presence of a fault zone strongly influence the way fluids and gases will move in a faulted reservoir. Faults are known to act as both seals and conduits for fluid flow in reservoirs (Antonellini and Aydin 1994, Caine et al. 1996,). However,

establishing the actual impact of a given fault on reservoir fluid flow constitutes a large source of uncertainty (Hesthammer et al. 2000, Yielding et al. 2002, Manzocchi et al. 2008).
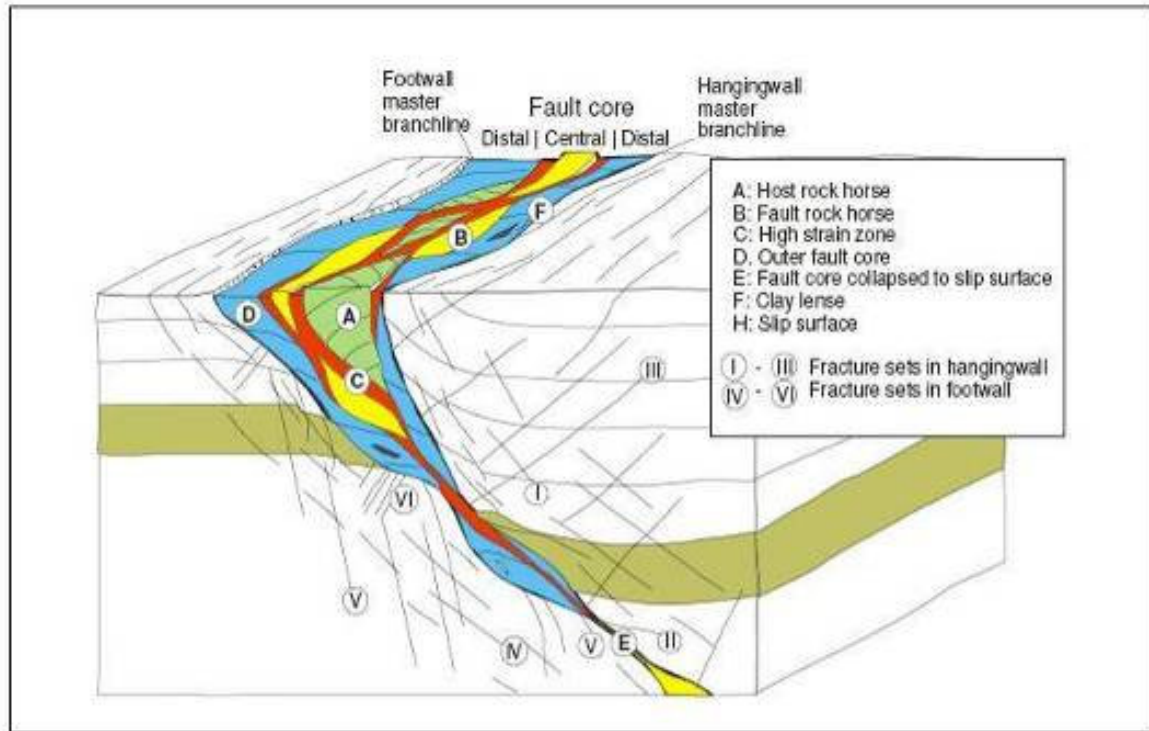
Figure 1.2.1 (Gabrielsen et al. in prep)

1.2.2 Structural elements

The main structural elements to take into account when modelling a reservoir are the overall geometries, the fault core, the outer and the inner damage zone.

Geometry:

There are three main end-member types of fault displacement methods:

- Normal faulting, generated by extensional forces acting on the rock.
- Reverse faulting, generated by compressional forces acting on the rock.
- Strike-slip faulting, by a horizontal sliding of the rock bodies past each other.

Each of these end-members creates a set of distinct geometries. Many fault contain elements of all three types, although one may be dominant, giving rise to some rather complicated geometries. In this thesis only normal faults have been modelled.

Common normal-fault geometries include (Fossen & Gabrielsen 2005):

- Single faults with sub-planar fault planes which die out at shallow depths.
- Single faults with listric fault planes dipping shallower with depth

- Bookshelf-fault (or domino-fault) type geometries, where several faults with fairly similar strike and dip create a bookshelf-like image in side view of the seismic image. An example is shown in Figure 1.2.2 and the straightest three faults in Figure 2.2.3.

- Fault drag folding, sub-seismic faulting or ductile deformation of faults leading to a drag folding of the hanging wall against the footwall.

- Fault interaction can lead to linkage (displacement being relieved from one fault set being taken over by a close by fault). This creates special geometries such as relay and broken relay ramps (Gougel 1952, Larsen 1988) (Figure 1.2.4). This type of overlapping geometry can be seen in three dimensions, but is generally only referred to as a relay ramp if seen in plane-view.

- Horst- Graben structures, where normal faults dipping in opposite directions create a relatively long and narrow trough and/or a horst structure (Peacock et al. 2000 from Reid et al. 1913 and Dennis 1967 (Figure 2.2.4).

- Parallel or sub-parallel faults, grabens and relay ramps etc., may all be listric and link up at depth, creating a y shaped faults (Larsen 1988).

Getting the geometries of a fault right in a reservoir model is of vital importance, as making a mistake here could lead to a completely erroneous understanding of the reservoir architecture and thus render the model with severely compromised forecasting abilities.
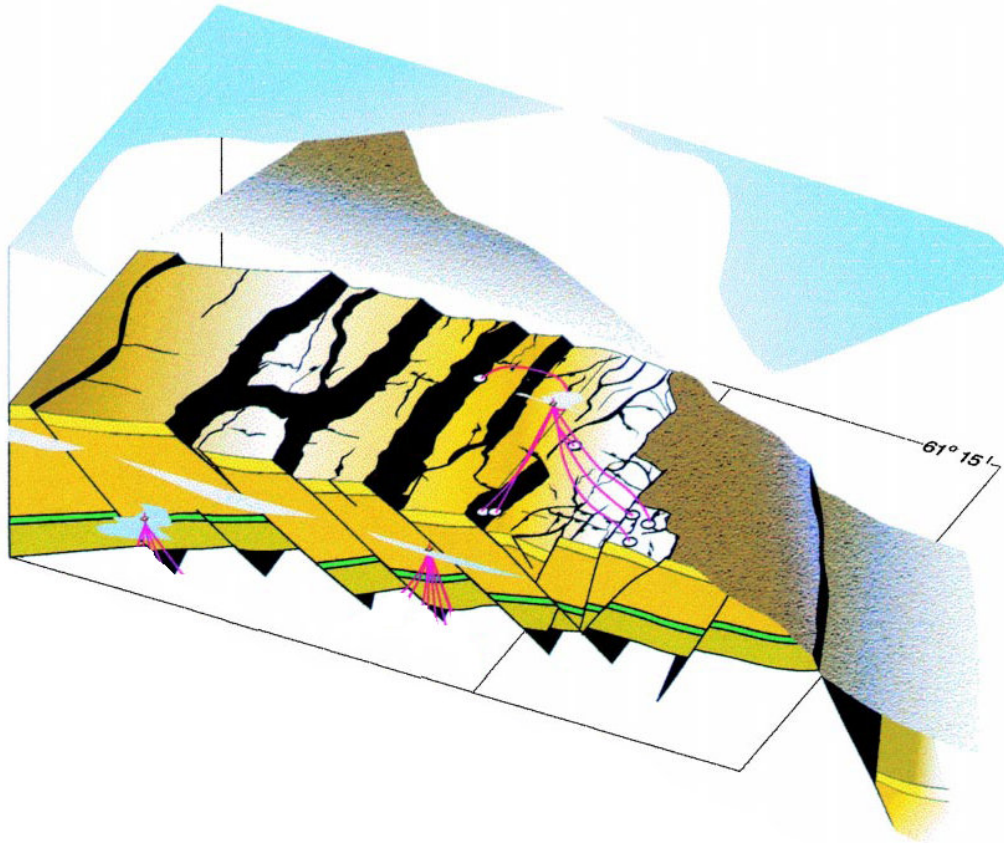
Figure 1.2.2   Modified from Fossen & Hesthammer (2000) From the Gullfaks Field, North Sea.

Damage zone

The damage zone is a transitional volume between the high-strain central part of the fault (inner damage zone and core), and the undeformed host rock. This volume commonly accommodates only a minor part of the total fault displacement. The zone exhibits deformation bands occurring as single band, clusters and networks with generally increasing frequencies towards the core, and occasionally lenses of undeformed or weakly deformed host rock surrounded by low-displacement shearplanes. The deformation-bands criss-cross each other at low angles to the fault plane, creating lozenge shape compartments separated by the low-permeability bands (Figure 1.2.3) (Parnell et al. 2004, Fossen & Bale 2007, Ma & Couples 2007). This leads to a highly anisotropic permeability pattern around the fault, where flow in general is highest parallel to the main fault plane and perpendicular the slip direction, and decreasing in the direction towards the plane. The petrophysical parameters of the damage zone are detailed in chapter 3.2.2.

$$k_{\parallel} > k_{\perp}$$

Wellbore

Hydraulic fracture

$k_{\perp}$

Fault

$k_{\parallel}$

Deformation bands in damage zone
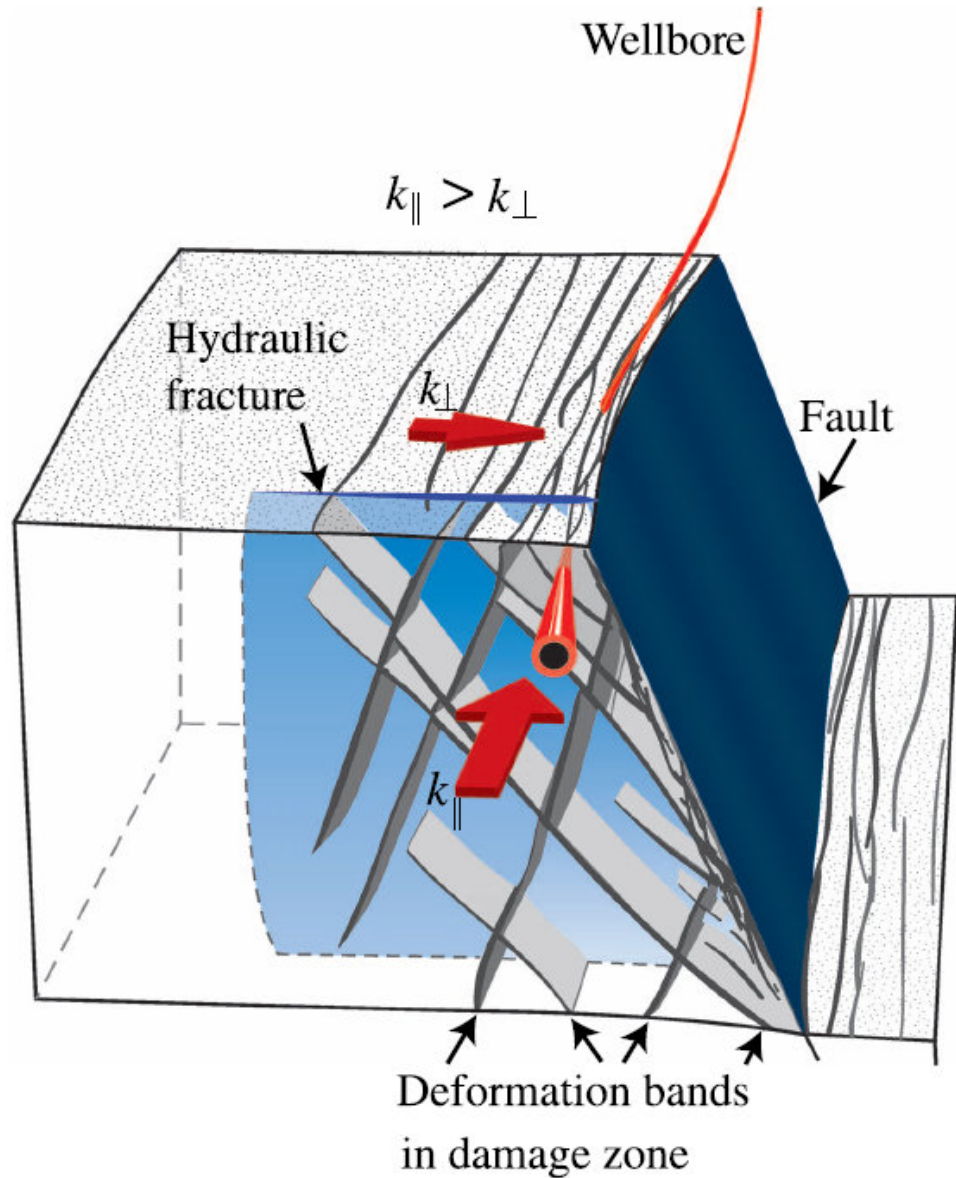
Figure 1.2.3   Fossen & Bale (2007)

Inner damage zone

The inner damage zone is the volume of rock which immediately surrounds the fault core, similar to what Gabrielsen et al. (in prep.) has named "Outer fault core" in Figure 1.2.1 (Gabrielsen et al. in prep). This zone consists of a higher density of deformation bands, small shear fractures and breccias. The breccias and shearplanes of the inner damage zone generally cause a decrease in permeabilities due to cataclasis and compaction. The petrophysical characteristics of this facies are described in chapter 3.2.3.

Fault core:

The fault core normally accommodates most of the strain. It can be a thin, single, sub-planar or slightly curved fault plane or a thicker chaotic zone displaying several anastomosing, curved or sub planar fault planes,. An example of the latter is shown in figure 1.2.4, where two overlapping faults are hard-linked. This creates a lens in the fault zone, which may express itself as a thick and chaotic segment of the fault core. The fault plane or planes are made up of a smooth wall, polished by the slip of the fault, or a volume of intensely deformed rock such as fine fault gouge, breccia or cataclasites.

Relay breached by hard linking of segments, creating lens in between.
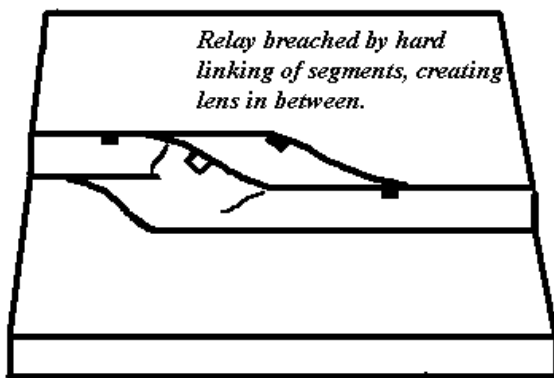
Figure 1.2.4

Fault cores often have a lowered permeability (chapter 3.2.3) compared to the surrounding rock (Antonellini and Aydin, 1994, Shipton et al., 2002, Shipton et al., 2005), due to the fine grain size of crushed material, fault-plane parallel alignment of phyllosilicate grains, and sometimes due to clays having been dragged into the fault-plane and creating clay smears (Yielding et al. 1997). The sealing effect of the fault core mainly depends on its thickness (Shipton et al. 2005) and the amount of clay (Yielding et al. 1997). It appears that a high ratio of clay in the faulted stratigraphy and consequently in the fault core, leads to sealing. The thicker the zone is, the lower is its permeability. Conversely, if the fault-zone is active (Caine et al. 1996) or contains high permeability lenses (Fredman et al. 2007), more or less connecting the hanging wall block to the footwall block, the fault core may increase the overall cross-fault and along fault permeability.

1.3 Fault modelling

1.3.1 Current modelling techniques

It is extremely difficult to create simulation models which include high resolution fault representations. This is partly due to insufficient grid resolution in conventional, field sized reservoir models, partly due to a lack of comprehensive databases on faulted rocks for various lithologies and different tectonic settings and their property distributions in 3D, and partly due to a lack of proper modelling tools allowing realistic representation. Consequently, present day fault modelling uses simplified fault rock descriptions and proxies which can be applied within the current limitations of present day modelling tools (i.e. fault planes and transmissibility multipliers).

Previous studies of modelling flow across faults (generated at shallow depths (i.e. <2000 m) in siliciclastic rocks generally fall into three categories:

- Defining and reviewing various kinds of algorithms for generation of transmissibility multipliers based on clay/shale content or thickness and amount of displacement, and studies on clay smearing in faults (CSP – Bouvier et al. 1989, SSF – Lindsay et al. 1993, SGR – Yielding et al. 1997) (Freeman et al. 1998, Manzocchi et al. 1999, Sperrevik et al. 2000, Flodin et al. 2001, Yielding 2002, Doughty 2005)
- The effect of juxtaposition of permeable and impermeable layers. (Knipe 1997, Clarke et al. 2005, Manzocchi et al. 2008)
- Sensitivity studies of how fault properties of fault model setup influence simulated reservoir fluid flow. (Caine et al. 1996, Shipton et al. 2002, Harris et al. 2003, Odling et al. 2004, Lescoffit & Townsend 2005, Ottesen et al. 2005, Shipton et al. 2005, Manzocchi et al. 2008)

There are a number of algorithms used for calculating transmissibility multipliers representing the effect of flow across faults. Common for these is that the fault or fault zone is considered a homogenized interval at any given point on a "membrane" across which flow occurs between juxtaposed parts of the reservoir. This fits well into the existing standard modelling convention in which faults are represented as planes or surfaces along grid splits. The clay smear potential (CSP) (Bouvier et al. 1989), the shale gouge ratio (SGR) (Yielding et al. 1997) and the shale smear factor (SSF) (Lindsay et al. 1993) are all algorithms designed to give a factor of transmissibility for the

fault plane. They are based on the percentage of clay present locally in the faulted stratigraphic interval, thickness of the layers, amount of displacement and generally the probability of clay having been dragged or smeared into the fault zone.

- The CSP presented by Bouvier et al. (1989) calculates the probability of clay smears in sand-sand juxtaposition based on the amount of clay which is smeared from a single clay source layer at a certain distance from the bed. The relationship is defined as;

$$CSP = \sum \frac{(\text{Shale bed thickness})^2}{\text{Distance from source bed}}$$

Eq. 1.1 Fulljames et al. (1996); Yielding et al. (1997)

by Fulljames et al. (1996). The CSP was by Bouvier et al. (1989) calibrated against known sealing and non-sealing faults, and divided into high, medium and low probability of sealing. What exact number was considered as high or low depended on the data of the area in question. An example of this is that Jev et al. (1993) quoted a CSP of less than 15 as non-sealing and more than 30 as sealing, and Bentley and Barry (1991) used a CSP of more than 5 as sealing on a production time scale (Yielding et al. 1997).

- The shale smear factor, or SSF, was proposed by Lindsay et al. (1993) and expresses shale smear as a function of fault throw vs. shale layer thickness.

$$SSF = \frac{\text{Fault throw}}{\text{Shale layer thickness}}$$

Eq. 1.2 Lindsay et al. (1993); Yielding et al. (1997)

This simple relationship gives a number which relates to the probability of sealing or non-sealing conditions. Based on a study of 80 faults, Lindsay et al. (1993) concluded that with an SSF above 7, the shale smear might be incomplete. Smaller numbers mean higher probability of having continuous shale smears.

- The shale gouge ratio or SGR, is akin to the CSP and SSF in that it relates amount of shale/clay to displacement, but differs in method (see equations 1-1, 1-2 and 1-3), and in that it takes the sum of all shale which has passed a certain point of the fault and divides by throw. Using the sum of shale which has passed the point, means that the number we get is a fraction of one. Multiplied by

a hundred this comes out as percent shale vs. total rock volume for that window of the fault:

$$SGR = \frac{\Sigma\left(\text{Shale bed thickness}\right)}{\text{Fault throw}} \times 100\%$$

Eq. 1.3 Yielding et al. (1997)

Or alternatively, for models where zones are used in stead of shale bed thickness;

$$SGR = \frac{\Sigma\left[\left(\text{Zone thickness}\right) \times \left(\text{Zone clay fraction}\right)\right]}{\text{Fault throw}} \times 100\%$$

Eq. 1.4 Yielding et al. (1997)

Part of the decision of the cross-fault transmissibility of a fault, is based on to what degree permeable lithologies are juxtaposed. The aims of studies on juxtaposition are to help us understand and model to which degree the permeable lithologies are in contact across the fault (Knipe 1997), to improve modelling techniques of juxtaposition and quantifying the effect of juxtaposition of permeable layers on fluid flow (Clarke et al. 2005, Manzocchi et al. 2008).

The studies done on 3D architecture of faults and distributions of faults and geometries related to faulting, have mainly been done qualitatively, to be able to better predict the transmissibility of the fault (Harris et al. 2003) and to improve the general understanding the fluid-flow properties of faults (Caine et al. 1996, Shipton et al. 2002, Odling et al. 2004, Shipton et al. 2005), or quantitatively, to evaluate the impact the model setup has on flow (Ottesen et al. 2005, Lescoffit & Townsend 2005, Manzocchi et al. 2008).

The results of the quantitative studies often come in a form of a quantitative hierarchy of the degree of influence the various parameters employed in the model have fluid on flow. The resulting hierarchy of parameters varies little. Most studies conclude that the fault patterns and general geometries are very important, even more so than the fault-rock permeabilities (Lescoffit & Townsend 2005, Manzocchi et al. 2008).

As seismic scale faults in nature consist of 3D volumes of petrophysically altered host rock, the simplification of modelling them as 2D planes brings with it a loss of information on fault zone geometries and architecture which may be critical to the forecasting ability of the model. Representation of the fault core and damage zone is clearly oversimplified in present day models. As described in section 1.2, these parts of the reservoir may, and often do, contain deformation-bands,

sub-seismic folding, injection and dragging of elements into the fault zone, multiple minor faults or slip surfaces, high-perm lenses, sealing or non-sealing breccias, varying thickness fault zone and variations of the parameters along dip and strike. All of these commonly recognized geological features are in most cases compressed to a single parameter expressed as a transmissibility multiplier which can be mapped onto a fault surface.

Although the use of transmissibility multipliers, and in particular the SGR algorithm (Yielding, 2002), has proved to be a quite robust method of modelling faults, the method does not adequately account for the three dimensional nature of faults. The consequence of modelling faults as 2D units in stead of 3D is that

1:      the 3D-flow within the fault zone is lost (Tveranger et al. 2005) .

2:      Due to the complexity of fault zones and the necessity of using different algorithms for different scenarios, transmissibility and communication between non-juxtaposed lithologies is often modelled ad hoc, or based on production data, instead of explicitly including geological features in the fault zones.

3:      If the fault zone is extensive, modelling in 2D may lead to overestimation of in-place volumes as the tectonized volume inside the fault envelope is handled as an undeformed part of the reservoir.

A substantial amount of research has been done to improve on fault modelling within the framework of existing modelling conventions. But without addressing the oversimplification of fault representation in present day modelling software, geo-realistic representation of fault zone properties is not possible.

1.3.2 The next generation modelling technique

A logical next step for improving fault representation is to provide a method which allows fault zones to be included as separate grids in the model. Having achieved this, a wide range of object and pixel-based modelling methods developed for sedimentary facies modelling are at our disposal to populate the fault zone gird with properties and structures as seen in outcrop analogues, using a set of conditioning factors such as displacement gradient and strain distribution to structure the fault zone facies and petrophysical models.

An effort to provide a method as outlined above was initiated in 2004 by the Centre for Integrated Petroleum Research (CIPR) as the "Fault Facies Project" (Tveranger et al. 2004). The core of the method is to classify and handle tectonically deformed rocks as volumetrically expressed

"fault facies" for description purposes, pattern recognition, statistical handling and modelling. Local grid refinements (LGRs) are defined around faults and modified to constitute continuous grid which include the fault envelopes. The fault facies are distributed inside this grid using standard facies modelling tools and employing strain and displacement as conditioning factors. (Tveranger et al. 2005, Røe & Soleng 2006, Syversveen et al. 2006, Fredman et al. 2007, Cardozo et al. 2008, Fredman & Tveranger in prep., Fredman et al. accepted).

A comprehensive fault facie database is currently being compiled at CIPR, from which empirical data on fault facies and their petrophysical properties can be derived. As it expands, the database will provide increasingly accurate descriptions and statistics which can be utilised for modelling purposes.

This method of modelling is however, not entirely without challenges of its own.

- Scale related problems. Including fault zone grids in reservoir models requires additional grid cells, the number of which is related to both needed resolution and the number of faults present in the model. The higher the number of cells, the longer it will take to simulate. For it to be possible at all on a 32bit workstation, the LGRs need to be up-scaled to reduce the numbers of cells, which again simplifies the 3D structures we want to represent to begin with.

- The statistical grounds for defining petrophysics for each fault facie must be sound. The database currently being compiled is a work in progress at CIPR which essentially started from scratch. A comprehensive database providing high quality data for all types of faults and lithologies is not available at present.

2 Chapter 2 Fault facies modelling grids

2.1 Introduction:

Faults zones must be represented by volumetric grids for it to be possible to include and account for the three dimensional architecture of fault zones. An algorithm to create and include such grids in standard Irap RMS™ reservoir models was presented by Syversveen et al. (2006). It creates a volumetric LGR around the fault plane, and uses the throw of the fault to calculate strain distribution inside the fault envelope. This is further explained in sub-chapter 2.3.

The program running the fault zone grid – algorithm is Havana - Cuba Libre (see chapter 2.3). Fault data from RMS, including geometry and throw, are exported from RMS in the "RMS Pillar Format" (RPF). This format is converted by Havana to the "Pillar Fault Model" (PFM) format used by Havana. Using the fault plane as a centre, the user defines the width of the fault zone as number of cells distant from the plane in the Havana input-file (Appendix G). The fault cells within the predefined distance are stretched so that the cells of the hanging wall and footwall are at the same level on both sides of the fault (Figure 2.3.1).

The resulting fault zone grids are in standard Eclipse .grdecl format. These grids can then be imported back into RMS where they can be populated with fault facies and petrophysical properties. The finished Fault Facies grid is exported, again in .grdecl format, and merged in Havana with the original conventional grid to create the final product, a .grdecl file of the reservoir model where the fault planes, have been replaced by a 3D representation of the fault zones.

Three faulted reservoir models were used as base-models in this thesis and will be presented below (Chapter 2.2). The models are taken from Sæther (2006), and represent geometries mapped in outcrops of a Jurassic succession at Kilve on the Somerset Coast, UK. The model grids were originally generated in RMS version 7.4, and were remade with RMS 8.1 for this thesis, which was the latest version available fall 2007. RMS 9.0 and 9.1 no longer support the RPF file format export needed for performing fault zone gridding as outlined in Syversveen et al. (2006), but the problem is being addressed and will be solved in a later version of Havana (Røe, Pers. comm.).

2.2   The Input grids

Three models were chosen for the present work out of 8 original cases by Sæther (2006). The original labelling has been kept to ease comparison.

Case 3   –   a relay ramp

Case 4.1   –   a domino system with four faults, two of which are intersecting

Case 5   –   a simple synthetic graben

The geometries of the grids were recreated by creating constant-depth horizons at the depth used by Sæthre (2006), importing the fault- input data from the original models and recreating the faulted grids based on that. All of the faults were modelled as purely normal faults with no strike-slip component.

As with the grid-geometry for each case, the sedimentary facies model used by Sæther (2006) was kept. This is a northwards prograding shoreface succession ranging from upper shore face in the south, to offshore in the north (Figure 2.2.1).
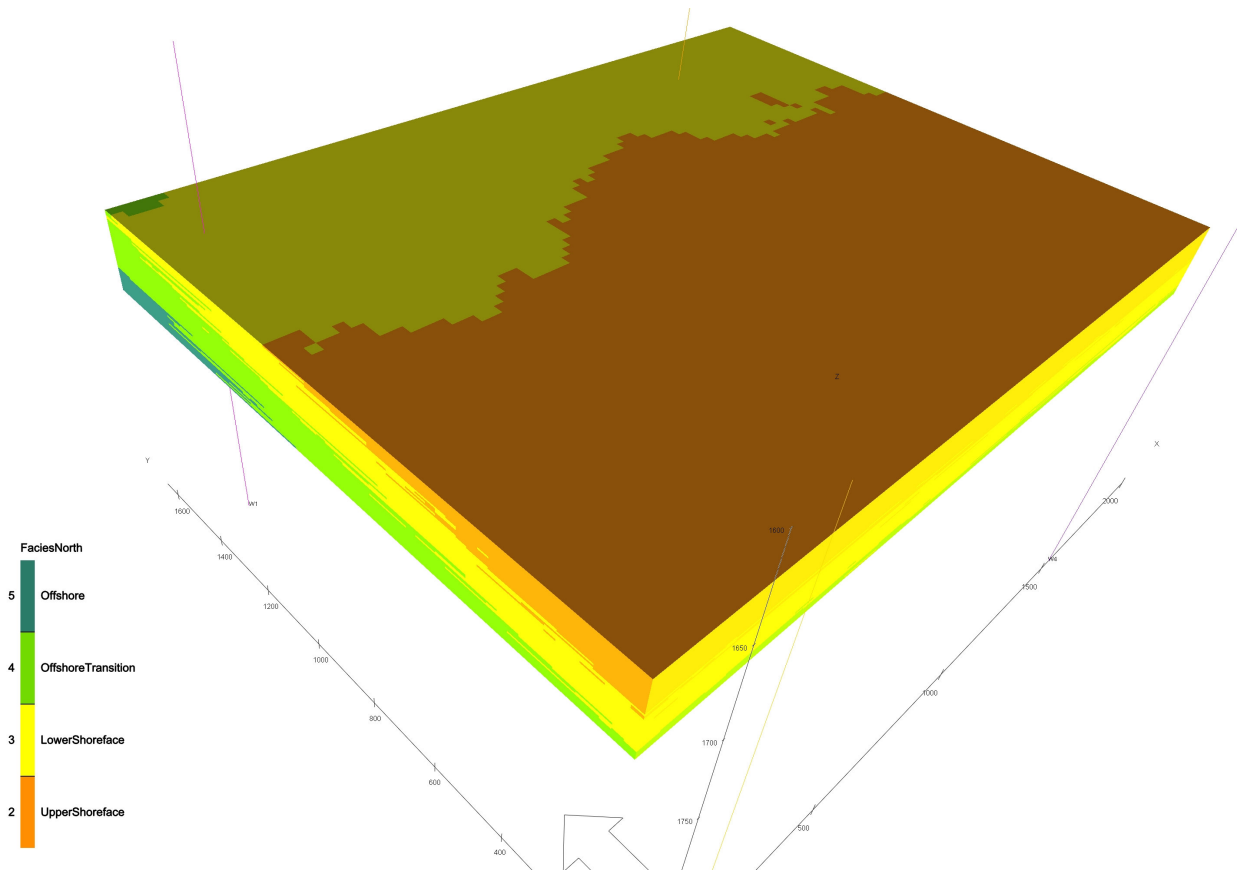

Figure 2.2.1   Northwards prograding shoreface to offshore sedimentary succession.

The petrophysical values for this succession are based on data from the SAIGUP project (chapter 3.2.1, Table 3.2-1, Manzocchi et al. 2008). The sedimentary and fault facies properties are treated in detail in Chapter 3.

The table below summarises some of the data on the pre-fault facies geo grids (Table 2.2-1).

Case	Grid dimensions (m)	Cell dimensions (m)	Number of cells	Volume	Fault throw	Grid rotation
Case 3	2000x1500x50	25x25x1	240000	150100648,29	0-58m	5º
Case 4.1	2000x1500x50	25x25x1	240000	148425993,15	2-25m	0º
Case 5	2000x1500x50	25x25x1	240000	148700020,5	15m	0º

Table 2.2-1

Case 3 is a relay-ramp type fault model, where the displacement goes from 0 to 58m. The dips of the faults vary between 59 and 70 degrees, and the grid is tilted down towards the south-southeast.
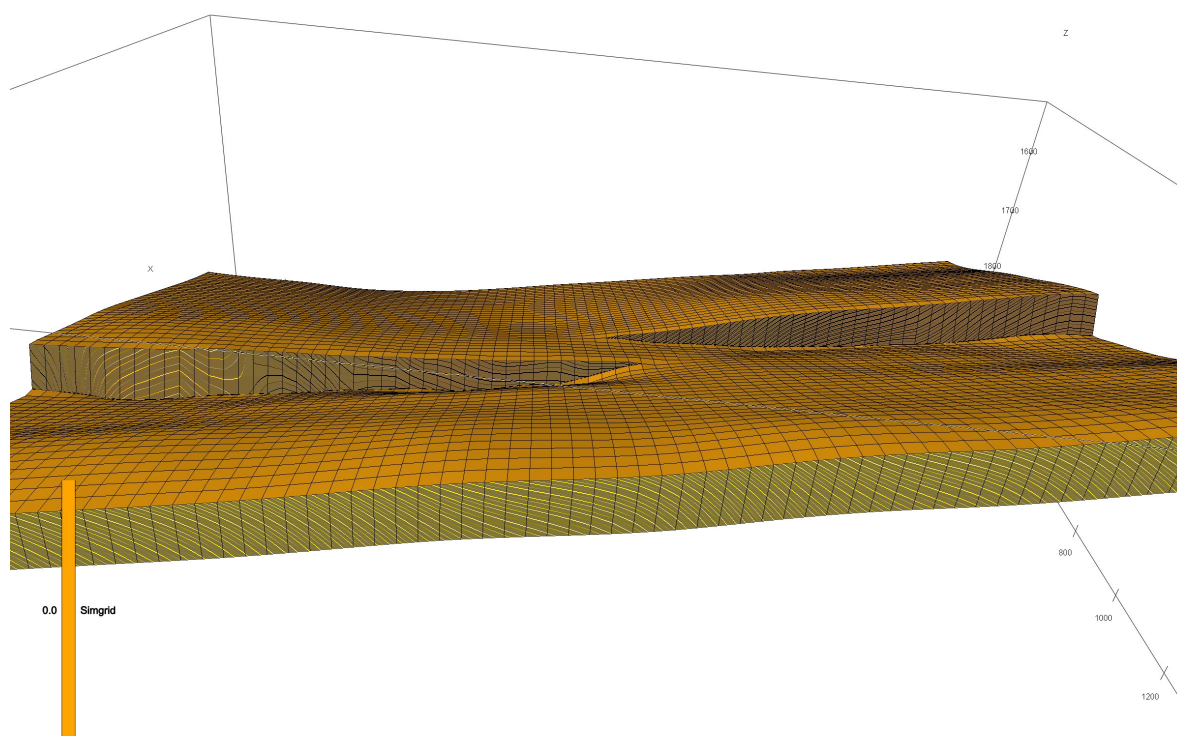
Figure 2.2.2   Case 3

Case 4.1 (Figure 2.2.3) contains four faults dipping southwards striking mainly east-west, forming a domino system. The two southernmost faults intersect. The faults dip between 46 and 71 degrees towards the south. The segments are slightly rotated down towards the north. Displacement varies from 2 to 25m.
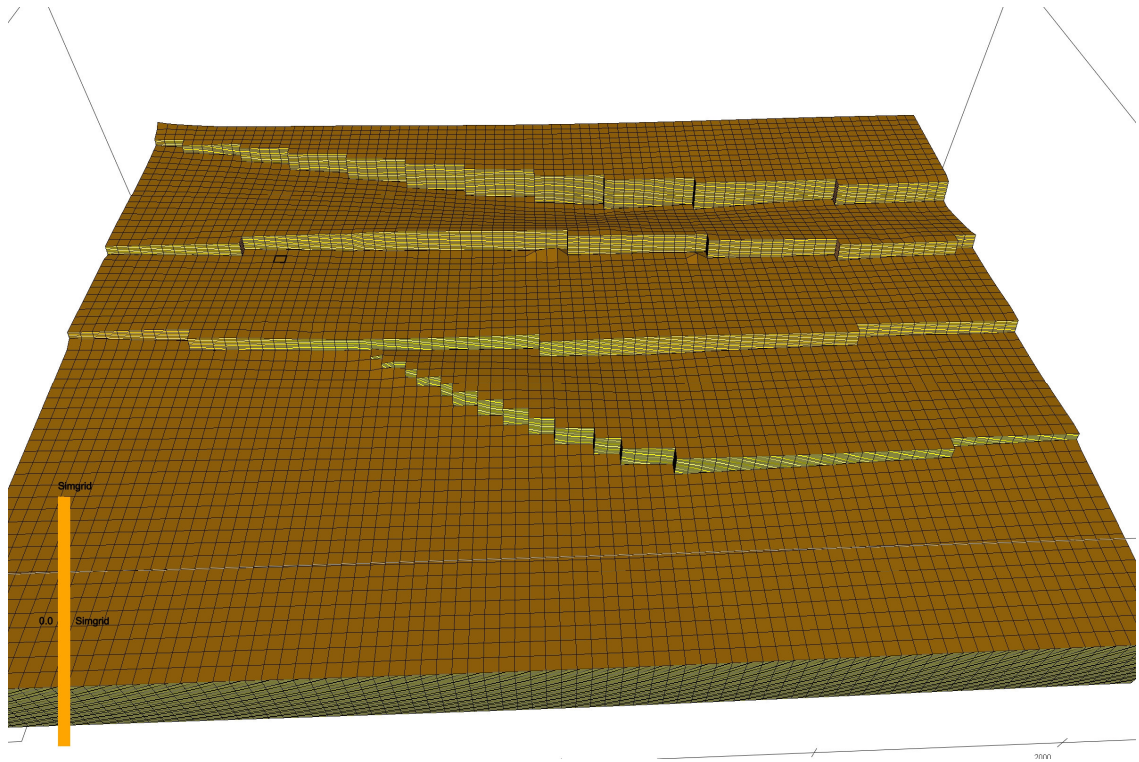
Figure 2.2.3   Case 4.1

Case 5 is a synthetic model containing two faults dipping 60 degrees towards each other creating a graben. The faults strike directly north-south and have a constant throw of 15 meters.
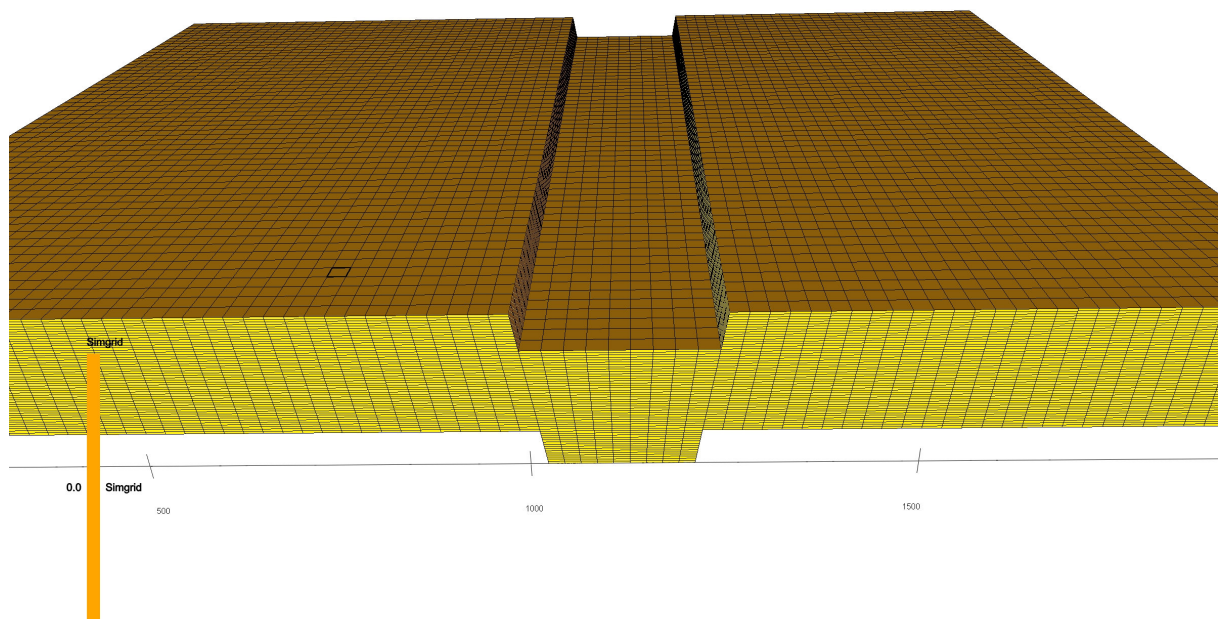
Figure 2.2.4   Case 5

2.3   Havana

The program used to calculate strain, displacement and to create the fault zone grids is Havana (Hollund et al. 2002). Havana is a fault modelling tool designed and maintained by the Norwegian Computing Centre (NR). Havana_Version 5.6 (known as Robusto) was employed. Versions 5.6.6 to 5.6.9 were developed in response to results from tests performed during the work on the present thesis. Originally a Unix-based program, it was ported to Windows by the Fault Facies project to ease the combined use and interaction of Havana and RMS (required by the fault facies workflows) on a single PC. These Windows versions of Havana are labelled "Cuba Libre".

The original function of Havana was to perform stochastic modelling of sub-seismic faults, model faults in the PFM format and do stochastic modelling of fault sealing properties. For the purpose of the Fault Facies project, the functionality of Havana has been extended to include several other uses. (Røe and Soleng 2006, Cardozo et al. in press):

- Creating volumetric fault zone grid (with which to replace the fault plane)
- Calculating 3D strain distribution
- Generating displacement fields
- To restore faulted grids, and deform it according to a displacement-curve
- Merging volumetric fault zones with conventional grids

Havana uses its own file format for input files, with .model as extension, where the user enters keywords readable by Havana. All the Havana files are found in Appendix E. The user input includes dimensions of the LGR's and the dimensions for the strain-calculation grid. As an example, some of the input for the LGRs dimensions are shown below:

```
GRID_REFINEMENT  FAULTS   1 25 1 3 \

        output/localgrid_nostrain.GRDECL \
```

The dimensions given are x, y and z refinement, plus the distance the refinement extends from the fault plane (in number of grid cells).

2.3.1 LGR creation

The creation of the volumetric representation of the fault zone, the LGR, is performed by Havana. The LGR is generated by extending the grid cells on each side of the fault in the opposite direction of fault movement, dividing the stretched cells to follow the imagined extension of the global grid, and optionally refining the cells in the resultant grid (Figure 2.3.1).
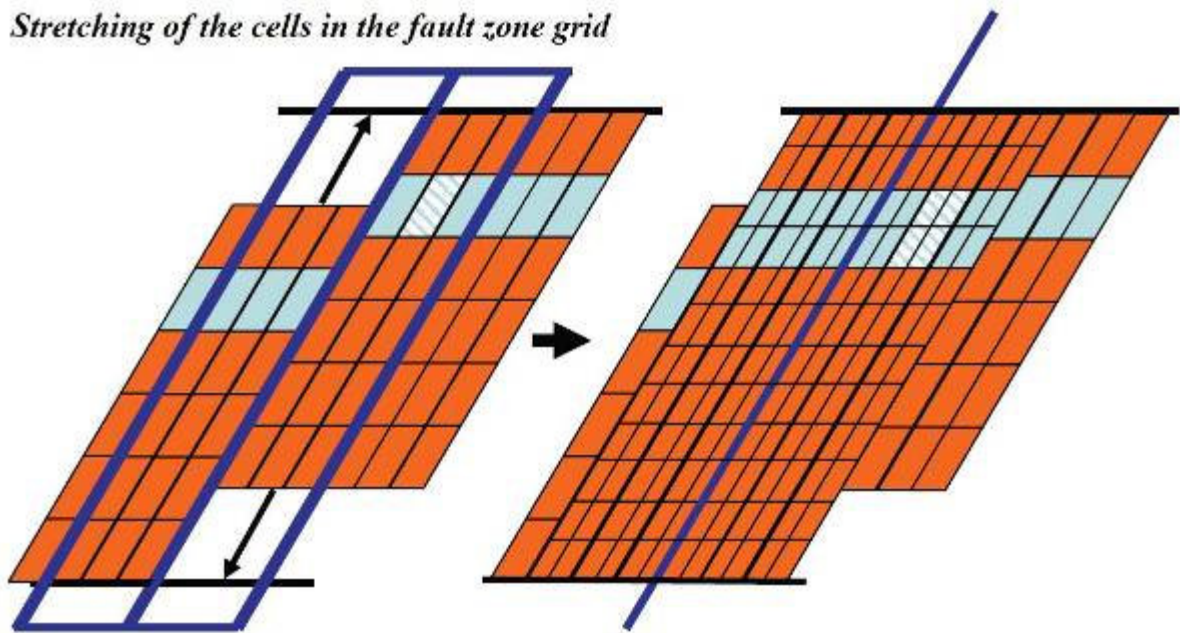
Figure 2.3.1

For the fault facies modelling method used in this thesis, Figure 2.3.1 can be somewhat misleading with regard to facies distribution, as the figure implies that the facies which remain in the grid after stretching are being kept. The sedimentary facies which remain after stretching are replaced by another set of facies which is re-sampled into the LGR grid from another grid created by Havana. The grid from which the sedimentary facies are re-sampled is created in Havana in two steps. First Havana restores the conventionally faulted grid its pre-faulted state, then it displaces the grid following a displacement function known as the Fault Product Distribution Factor (FPDF, Syversveen et al. 2006). This produces a folded grid as shown in Figure 2.3.2
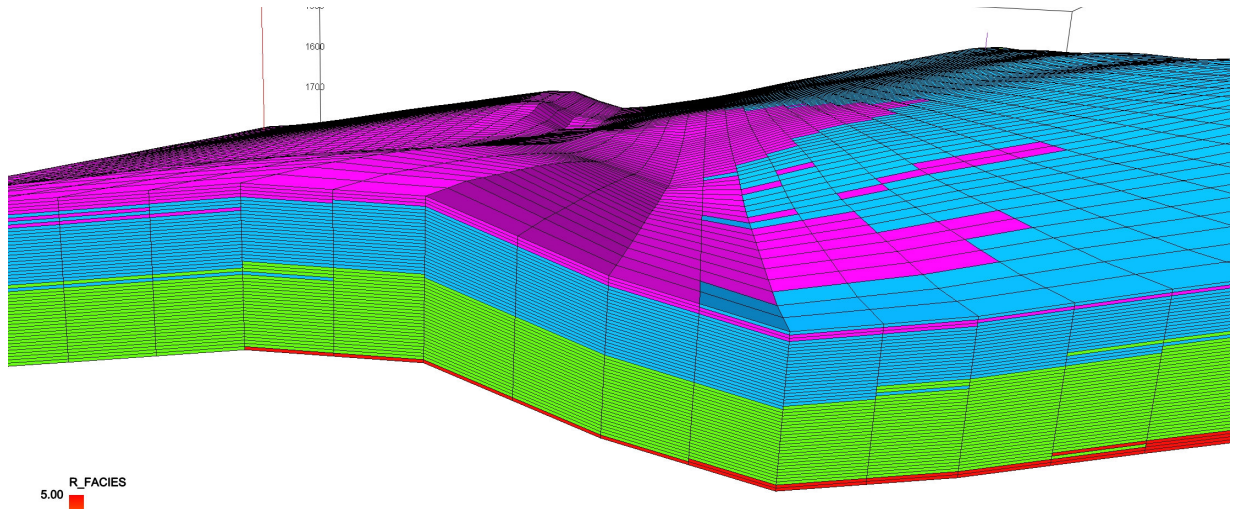
Figure 2.3.2   **Grid after FPDF displacement.**

This grid is used to place the sedimentary facies into the LGR, where they will act as a controlling parameter for the occurrence of fault facies originating from different strata. The workflow and result of re-sampling of the facies into the LGR will look like what is shown in Figure 2.3.3.

Faulted grid

Restored and displaced grid

Empty LGR
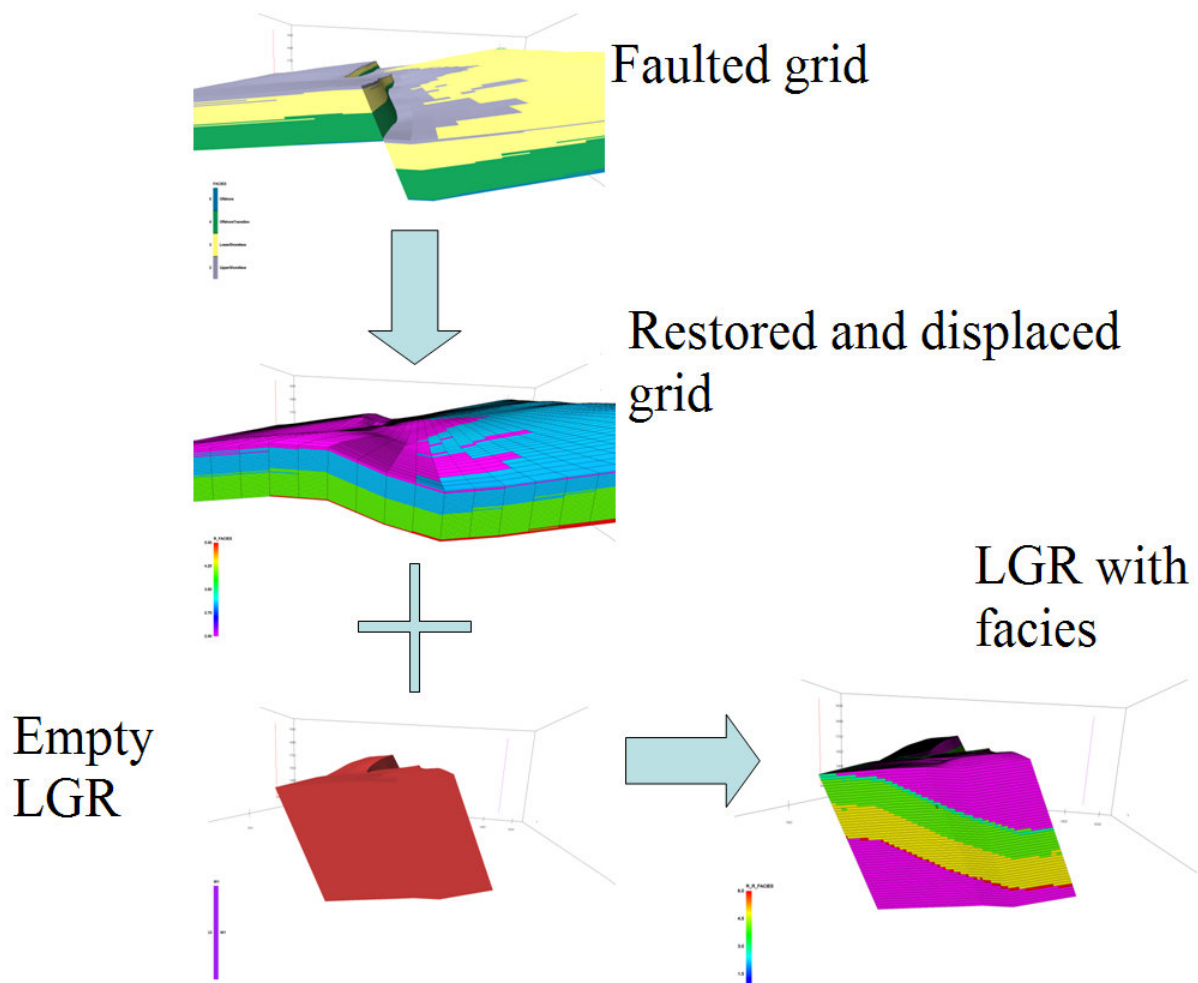
LGR with facies

Figure 2.3.3   **Workflow of LGR with sedimentary facies distributed following the FPDF function.**

2.3.2 Strain and displacement modelling

Strain is the degree of change in shape of a body, or the amount of extension or contraction a body has experienced. It is defined as new length minus old length divided by old length, or as the new length of an object (L1), divided by old length (L0) of the object, minus one.

$$e = \Delta L / L_0 = (L_1 / L_0) - 1$$

Eq. 2.1

In the modelling technique used in this thesis developed by the fault facies group, strain is used as a conditioning factor for the distribution of fault facies in the fault zone. The value of the strain in any given cell is dependant on the gradient of displacement across the fault, and the distance perpendicular from the fault plane.

Strain is computed in Havana – Cuba Libre. The program uses a method to calculate strain developed by NR in collaboration with CIPR (Cardozo et al. in press), which uses an algorithm based on "a simple fault displacement formula, and a numerical, volumetric computation of finite strain" (Cardozo et al. in press). The output from the calculation is given as stretch, which is the new length of deformed volume divided by the original length. This is the (L_1 / L_0) -part of the equation Eq. 2.1. To get the proper numbers for the strain, we simply subtract 1 after importing the parameter to RMS as a 3D parameter.
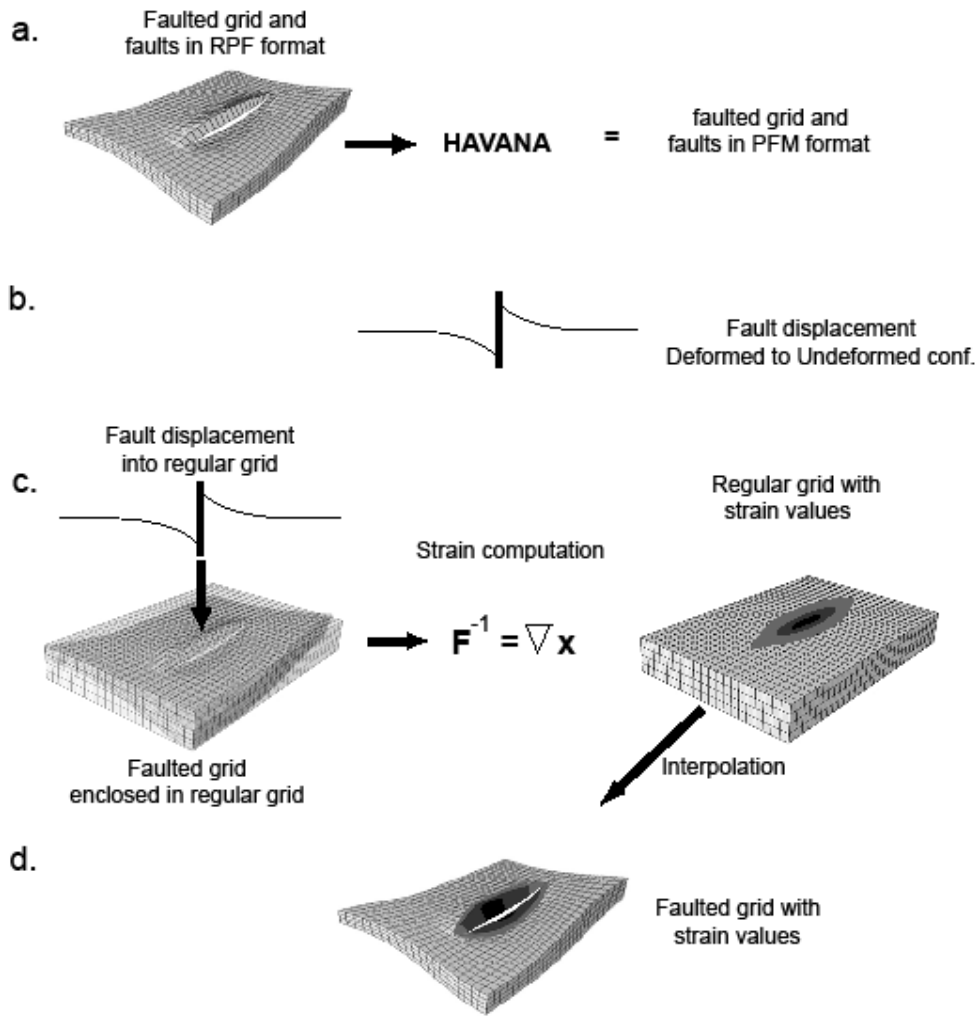
Figure 2.3.4 (Cardozo et al., in press)

The calculations starts with a faulted RMS grid and an RPF file describing the fault in 3D. Havana converts the 3D RPF description file to the program's own format, Parametric Fault Model Format (PFM) (Figure 2.3.4). It then assumes a displacement model across the fault describing how the magnitude of displacement decreases with increasing distance to the fault (Figure 2.3.5). The displacement model is built up of two fault pillars on the fault plane and a third one away from the fault, creating a triangle for each segment of the fault. The distance from the midpoint of the two pillars on the fault out to the third pillar is defined as the r_d. (Figure 2.3.6)
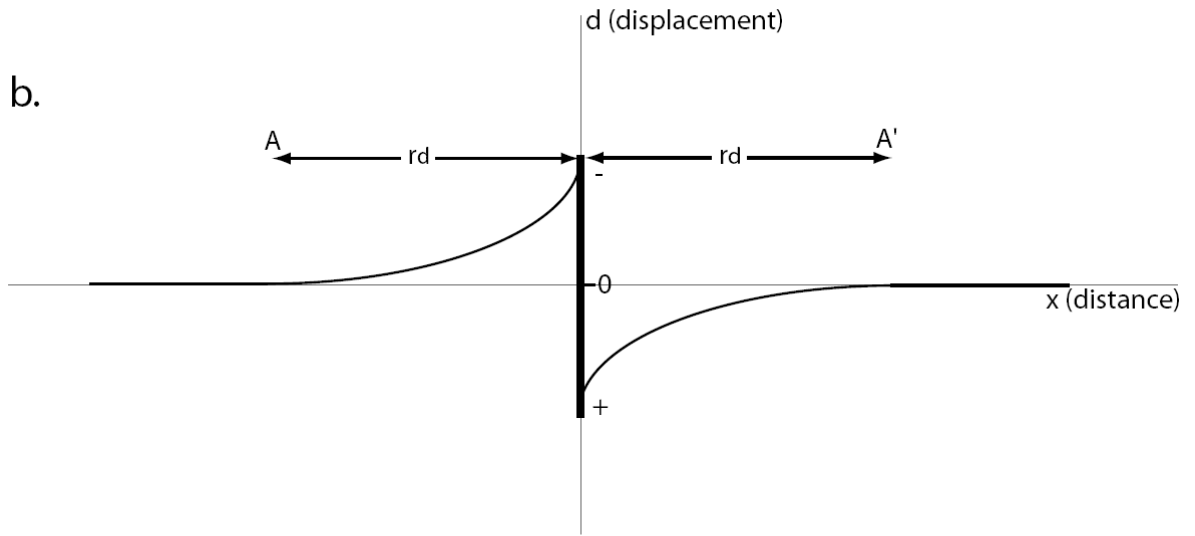
Figure 2.3.5 Cardozo et al., in press, Petroleum Geoscience
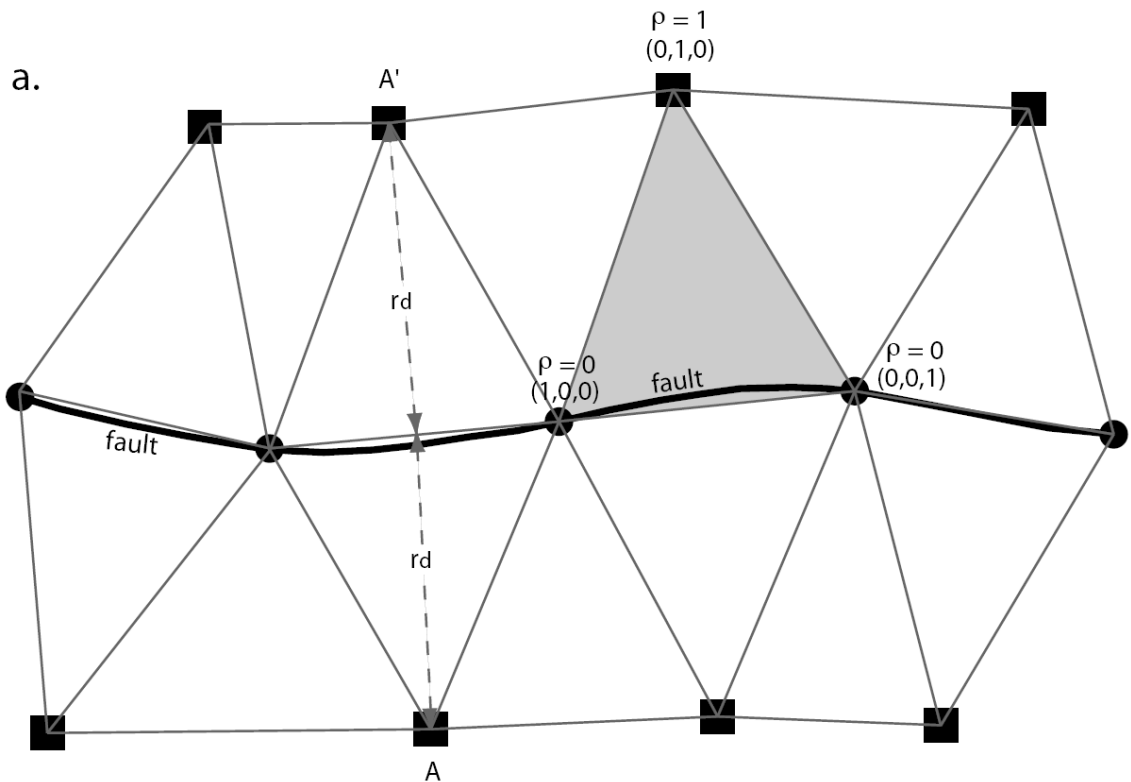
Figure 2.3.6   Cardozo et al., in press, Petroleum Geoscience

Inside the triangles the displacement (d) follows equation (2.3),

$$1-(\frac{|x|}{r_d})^2 Dc \quad 0 \triangleleft |x| < r_d$$

Eq. 2.2

D is the fault displacement, *c* is a constant indicating the proportion of fault displacement distributed in each fault block and r_d is the drag radius, which is how far away from the fault the displacement goes (Figure 2.3.6).

The displacement decreases from the midpoint of the fault pillars to the "far-field pillar" by equation (2.2).

$$d = (1 - \rho 1 \upsilon - \rho 2 \upsilon - \rho 3 \upsilon)$$

Eq. 2.3

where d is the displacement, ρ is a "displacement reduction coefficient" assigned to each pillar, ρ_n is the coefficient of displacement reduction of the fault pillar *n*, {υ, ν, ω} are the coordinates of a local system referenced to the pillars, (*Cardozo et al., in press, Petroleum Geoscience*)

This is consistent with outcrop and seismic data treated by different authors (Barnett et al. 1987, Stein et al. 1988, Walsh and Watterson 1989, Roberts and Yieldinig 1991).

The displacement model is applied to all faults in the reservoir modelling grid (Figure 2.3.4 b). The strain is computed numerically in a regular grid which surrounds the faulted reservoir modelling grid (Figure 2.3.4 c). Finally the strain is interpolated from the regular grid back to the faulted reservoir modelling grid (Figure 2.3.4 d) the result is a reservoir modelling grid with nodal strain values.

The r_d, drag radius, strongly influences the model as it decides how far out the strain and deformation reaches. The value of the r_d can be estimated based on empirical throw – damage-zone width ratios such as what is presented in Figure 6.1.1. The figure is a result of data gathering performed researchers at CIPR (Schueller et al. in prep). The form of the regression line through the point-cloud is as in the following equation (Eq. 2.4);

$$r_d = K * T \max^{0.5}$$

Eq. 2.4

r_d is the drag radius (Figure 2.3.6), K is a constant, Tmax is the maximum throw of the fault. K can be adjusted to change the r_d if needed, as the spread of damage-zone width is quite high for any given throw. Changing the rd is done by changing the number for the fault in question in a file called the Fpar.dat used as input in the Havana modelling run. There is one number for each fault, specifying the distance over which the strain will be distributed (Eq. 2.2). This means high r_d values will lead to a distribution of strain and displacement that goes very far from the plane, thereby "diluting" it, whereas low values for r_d will concentrate the strain and displacement closer to the

fault. As changing the r_d changes the extent of the drag, it influences the potential for interaction of faults, so if an interaction is wanted between two fault tips, the r_d needs to be such that the two strain and displacement fields overlap.

The data from the fault facies group used in this thesis, shown in Figure 6.1.1, exhibit a damage-zone width – fault throw relationship lower than what some other datasets show, such as that of Shipton & Cowie (2001), who describe faults from the Navaho sandstone, Utah, where the damage zone width is as high as 2.5 times the fault throw.

2.4 Fault facies modelling.

Using an LGR grid containing strain (Figure 2.4.1) and a regular grid containing the initial sedimentary facies (or "prior" facies) distribution in the position of the fault zone deformed to fit the displacement curve, from now on called "the restored grid" (Figure 2.4.2), are imported to RMS, and are used as the base to define a conditioning factor for stochastic modelling of the spatial distribution of fault process products inside the fault zone grid.
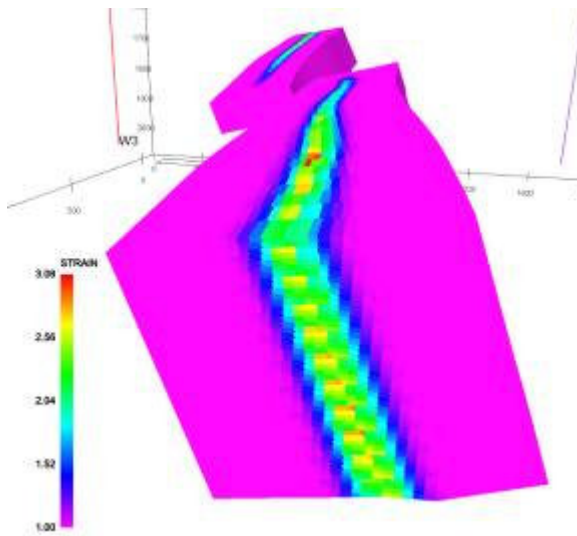
Figure 2.4.1   Strain representation   Figure 2.4.2   Restored Grid
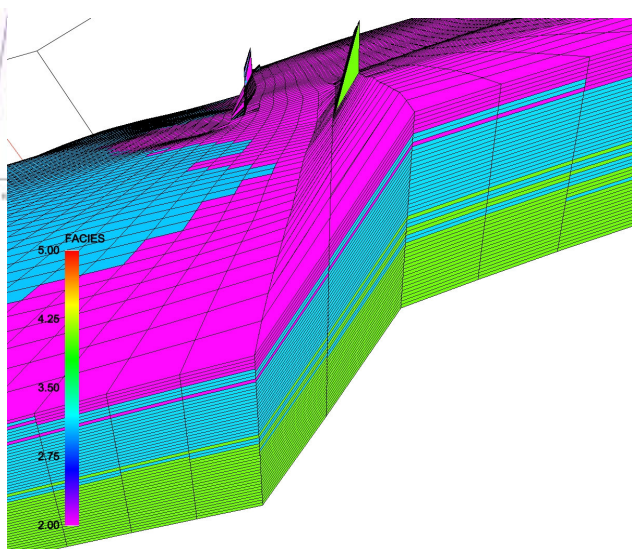
The strain values come as a continuous parameter with decreasing values away from the fault plane, which gives a possibility to model facies determined by proximity to the fault plane. The degree to which the deformed facies follow the displacement curve is determined by the resolution of the number of grid cells in the regular grid. The "prior" facies from the restored grid are re-sampled into the LGR grid, which allows us to assign a prior facies as well as a strain value for each cell in

the fault zone grid. Together these form the conditioning parameter for stochastic modelling of fault facies distributions inside the fault zone. Having provide facies distributions (Figure 2.4.3) these are used as input for the stochastic modelling of petrophysical property distributions.
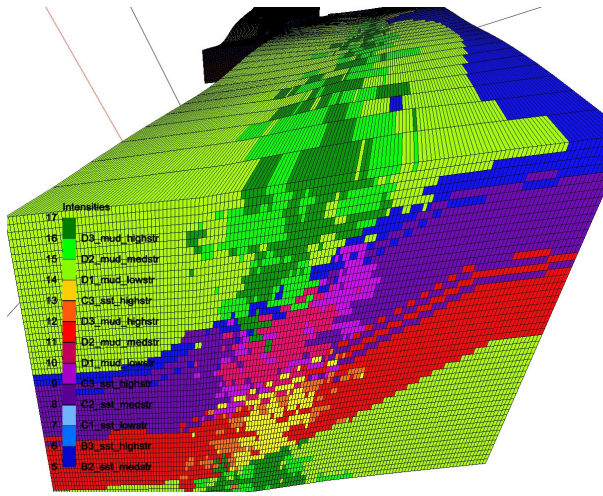
Figure 2.4.3   **Side view from case 3 showing the fault facies indicators.**

When the finished LGR with fault facies and petrophysics is in place, RMS can be used to up-scale the values to a coarser LGR, and then merge the coarser LGR with the regular grid. This yields a model where the fault planes of the conventional model have been replaced by fault zone grids populated by fault facies. The LGR grids used in this thesis have a refinement factor of 25 perpendicular to the fault plane for the fine LGRs (Figure 2.4.4) leading to grid cells being 1m wide perpendicular to the fault plane, and the up-scaled LGRs have a refinement of 5, compared to the regular grid (Figure 2.4.4, Table 2.4-1), making the cell width of the coarse LGRs 5 meters (perpendicular to the fault plane).
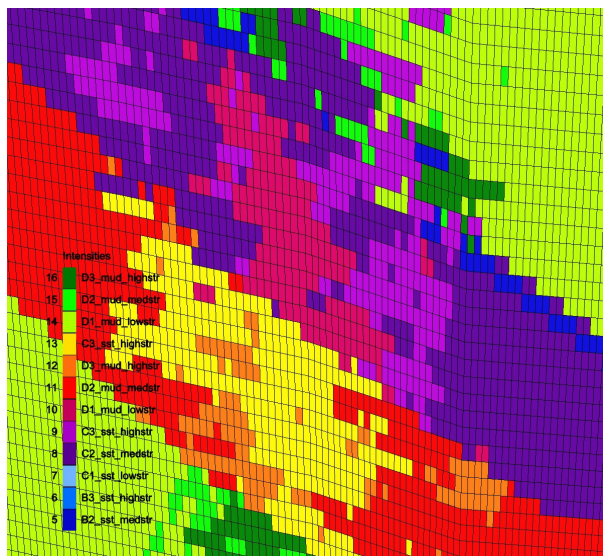
Figure 2.4.4a   **A grid refinement of 25**   **Figure 2.4.4b**   **A grid refinement of 5**
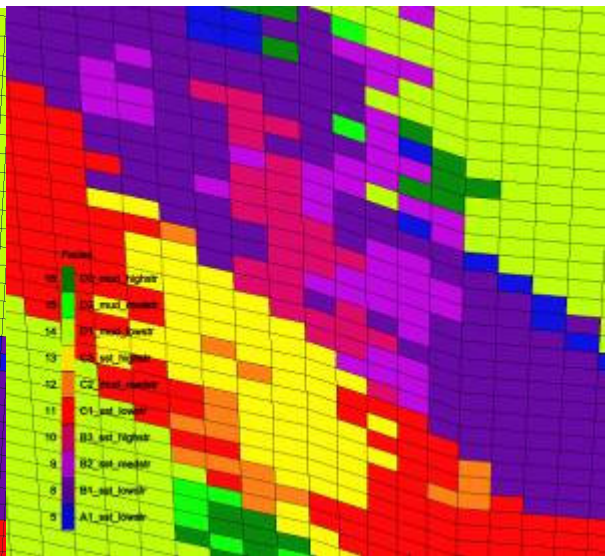
2.4.1 Fault Facies grid results

Summarised in the table below are the dimensions and cell numbers of the simulation-ready fault facies grids:

Case	Grid dimensions	Cell dimensions	Number of cells	Grid Refinement In X-Y-Z	Number of Cells in LGRs	Number of Cells Including LGRs
Case 3	2000x1500x50	25x25x1	240000	1x5x1	132000	372000
Case 4.1	2000x1500x50	25x25x1	240000	1X5x1	480250	720250
Case 5	2000x1500x50	25x25x1	240000	5x1x1	180000	420000

Table 2.4-1

Adding the LGR to the conventional grid increases the number of cells and the volume of the completed grid. The facies populating this added volume are given permeability and porosity values at, or close to zero, so as not to influence the simulation too much. For a realistic case the values used should be derived from the formation overlying and underlying the reservoir interval being modelled. The volumes of the grids pre and post LGR creation are shown in the table below. These are from the base cases where the LGR was set to extend 3 grid cells, 75m, from the fault plane on each side.

Case name	Without LGR: m^3	With LGR: m^3	Difference: m^3	Difference in %
Case 3	150100648,29	162993556,34	12892908,05	8,590
Case 4.1	148425993,15	165060327,69	16634334,54	10,077
Case 5	148700020,5	155961482,4	7261461,9	4,656

Table 2.4-2   Case volumes

2.5   Geomodelling workflow:

This chapter gives an overview of the fault facies workflow A more detailed explanation of the complete workflow is presented in Appendix E. The workflow used here is an adapted, and somewhat modified, version of the workflows developed by Syversveen et al. 2006, and Fredman et al. 2007(?). This workflow can be broken down to twelve steps:

1. Structural modelling and zone gridding.

2. Sedimentary facies and petrophysical modelling.

3. Fault facies gridding.

4. Re-sampling sedimentary facies into fault facies grid.

5. Restoring sedimentary facies in the fault facies grid.

6. Setting up fault product distribution factor (FPDF) or displacement model.

7. Applying FPDF to the restored facies for creating lithologic distribution parameter.

8. Applying FPDF to create shear strain parameter.

9. Applying the combination of lithologic distribution and shear strain parameters to create probability distribution of each fault facies.

10. Pixel-based stochastic modelling of fault facies.

11. Petrophysical modelling for fault facies.

12. Combining original grid with fault facies grid.

"…" this workflow forms the basis for the overall workflow in geo-model matrix study."

In my work with this workflow I have had to make a few adjustments to this setup. For example indicator modelling based on strain intensity has been used when distributing fault facies. This and other amendments made to the workflow setup are detailed below.

Generalised in the same pattern as above, the workflow used here is as follows:

General workflow:

1. Structural modelling and zone gridding.

2. Sedimentary facies and petrophysical modelling.

3.a Local Grid Refinement (LGR), restored grid and strain modelling by Havana.

3.b Restored grid Bug-Workaround when applicable.

4. Re-sampling sedimentary facies into fault facies grid from Havana restored grid.

5. Extracting the wanted facies from the re-sampled facies by use of IPL script.

6. Define and generate fault facies and distribute them using strain

7. Petrophysical modelling for fault facies.

8. Combining original grid with fault facies grid with Havana.

1. Building the structural model:

    The model was built reusing the input parameters from the RMS 7.4 models by Sæther (2006), and using the same setup for the generation of horizons, faults and grids. The fault models were not always easy to reproduce, as they originally included some manual editing, and could thus not be reproduced automatically. This is reflected in the following note to the modelling taken from RMS workflow description of Sæther (2006):

    "Create/Manually edit the fault network to be flat at some specified depth, and create a fault model to match the input data. This was impossible to do the automatic way, without having large errors introduced to the grid. "select all values for horizon" set to 1750 and 1765 , top of fault was a fairly good match, but had to be adjusted slightly." These adjustments were reconstructed manually for the present models, but some minor differences are to be expected. The finished fault models were exported using RPF format and transformed by Havana to PFM-format for further use in Havana.

Three grids were created.

The first, called *Prograding,* was directly loaded from the RMS 7.4 models, and is a simbox grid containing the prograding facies scheme used by Sæther (2006).

The second is the *Geogrid,* which is the test-grid used to recreate the geometry of the RMS 7.4 models in RMS 8.1.1, this is quality controlled (QC) to make sure there are no cells which may prove problematic in the further steps.

The third grid is called the *Simgrid* and is the grid in which the final facies scheme is modelled and which is the grid being exported to the "coarsegrid.grdecl" eclipse file. This coarsegrid.grdecl file is used as input to Havana.

2. Facies modelling:
   a. The facies model and petrophysical parameters for the Simgrid are also a recreation of model by Sæther (2006) using RMS 7.4. The petrophysical data were based on work done in the SAIGUP projec t (*Table 2.5-1 Sedimentary Facies, Manzocchi, T. et al. 2008)*,

3. Local Grid Refinement (LGR), restored grid and strain modelling by Havana:
   a. The Havana files ExpandLGR- and Restore- .model (see appendix???) are run in Havana to create the fault zone grid LGR and the restored grid which displaces the prior facies according to calculated displacement in the fault zone. The resulting grid is imported into RMS as a .grdecl-file.
   b. The bug workaround is performed where necessary. This means recreating the restored grid by creating surfaces from the top and bottom cell layers of the restoredgrid grid, and making a new zone in between the new top and bottom horizons.

4. The facies from the restored grid (or the recreated restored grid) are re-sampled into the LGR grid
5. Extracting the facies from the resampled facies by use of IPL script.:
   a. In the IPl script called "MakeFacies" (see appendix H), I have created one facies parameter for each of the "prior" facies used in the grid. For all my cases this is upper shoreface, shoreface, offshore transition and offshore. Each of these facies is modelled as 1 or 0, where the 1 value is where the facie is present.
6. Define and generate fault facies and distribute them using strain :
   a. Using an IPL script called "MakeIntensity", each "prior" facies is subdivided into a user defined number of fault facies originating from any given "prior" facies". Here each facies made in the "MakeFacies" has been subdivided into three strain categories (for simplicity sake just representing high, low and medium strain fault facies). Thus combining strain distribution with the re-sampled "prior" facies in the fault zone grid yields an intensity parameter for the distribution of each fault facies in the grid: Each cell in the fault zone grid has an assigned value for strain and "prior" facies. The

combination of the two gives what fault facies should replace the "prior" facies in any given cell. This pattern is however not used directly, but rather as an intensity parameter for stochastic facies modelling in order not to make the model too deterministic.

    b. The intensity parameters used in combination with "Facies: indicator simulation", lets us create as many distinct fault facies for each sedimentary facie as we like, allowing us to model zones of varying intensity of deformation as discrete elements.

7. Petrophysical modelling for fault facies

    a. Petrophysical parameters were assigned each of the fault-facies. This is described in (Chaper 3.2).

8. Combining original grid with fault facies grid with Havana.

    a. Using the Havana file "FaultFaciesMerge.model" I merge the LGR grid into the reservoir model grid. This gives us a merged grid with a local grid refinement replacing the fault plane which is to be flow simulated.

Notes and discussion on the workflow:

Note on step 5 and 6 in "General workflow":
The IPL scripts were originally created by NR, and have been adapted to suit the cases in question.

Note on step 6 in "General workflow":
a: The IPL script is made to connect a certain value range of strain to a certain type of facie, i.e. low or high strain facies. This should ideally be defined empirically following general trend data from field observations connecting certain fault facies to strain magnitudes. At the moment this is done subjectively, as exemplified by the distribution used is a simple division of the values of strain. Ongoing work at CIPR strives to establish a less subjective method for linking fault facies and strain magnitude. The way the IPL works now is that high strain values are taken directly from the strain values, the medium strain values are at a high at the mean values of the strain, and low strain is distributed as the inverse of the strain. The calculations look like this:

Low strain	N1intensity =	intN*(tmp1*p+1.0)
High strain	N3intensity =	intN*p
Medium strain	N2intensity =	intN*(tmp1*Abs(p-0.5)*2+1)

Table 2.5-2

P is the strain, tmp is a constant -1 and the intN is a constant 1 and just connects the intensity to N facie.

Examples of full IPL scripts are found in Appendix H.

In the IPL script, it is possible to include a maximum level of the intensity, based on the strain. This means setting all values above ## to exactly ##. This was initially done for the standard cases to remove of some artefacts from the Havana strain calculations which led to areas of unrealistic high strain. After this had been fixed in the latest Havana version, the cap was kept, part as an oversight, and part to force the high-strain core to be thicker than the strain actually implies. For cases with low displacement such as the models used in this thesis, this was necessary to get any high-strain facies at all in to the models. This is tampering with the input data to the models, but I saw it as acceptable for the present purpose as this thesis focuses on proof of concept than an actual evaluation of flow simulation of a reservoir. Further research will be likely to improve this implementation problem

b: When running the indicator-modelling job in RMS, the variogram ranges in x, y, z directions should be set to follow empirical relations on geometry of fault facies, such as thickness vs. fault throw, to improve the fault facies distribution.

Note on step 8 in "General workflow":

When simulating in ECLIPSE, it is necessary to keep the cell number in the grid at a reasonable low to reduce the simulation time. It is not possible however, to represent the strain in the localgrid satisfyingly if the grid is too coarse, so a fine grid with a high number of cells has been chosen for this step of the process. This grid needs to be subsequently up-scaled before performing flow simulation.

Workarounds:

Step 3b, Restored-grid error workaround:

As mentioned in chapter 6.1.2 the restoration of grids sometimes introduces an error to the grid. This is worked around by doing the following:

1: Stratigraphic Framework: create two new horizons, one above the existing top, called Restored_C and one belowthe existing Base, called Restored_A.

2: Parameter calculator on restored grid, "Depth=@Z" to make a depth realisation of the grid.

3: Create surface: make two new surfaces from the restored grid depth. This is done by using an index filter, filtering away first the bottom 49 layers, the the top 49. "Layer: Start: 1 Width: 1 Skip: 50 Range: 1-50", then "Layer: Start: 50 Width: 1 Skip: 50 Range: 1-50"

4: Create zone, Zones, Between Restored_C and Restored_A, using the depth surfaces created in pt.3.

5: Model grid: UpdateRestored. This is done to make the grid the same as the original RestoredGrid. Angles, X, Y and Z values from previous grid.

6: Then resample the facies from Restoredgrid to UpdateRestored. This must be i,j,k, not nearest node re-sampling.

7: then to get the restored facies to Localgrid, resample facies from UpdateRestored to localgrid, using nearest node re-sampling.

This effectively produces a smoothed out version of the restored grid, where the spikes created are reduced to a small bump in the grid.

Step 8, Cell number workaround:

The number of cells in Localgrid needs to be quite high to get the strain satisfyingly modelled. This leads to a too high number of cells to simulate in ECLIPSE, so the cells must be up-scaled before the merge of localgridfinal.grdecl and coarsegrid.grdecl

Method:

- Export coarsegrid to the same folder as ECLIPSE files are to be used in.

- Run ExpandLGR.model in HAVANA again to recreate localgrid.grdecl from the coarsegrid.GRDECL with a coarse grid refinement to reduce cellnumber.

- Import the coarser localgrid.GRDECL and rename the zone LocalgridCoarse

- Rescale the original Loalgrid data into the LocalgridCoarse

- Export LocalgridCoarse to localgridfinal.grdecl in appropriate folder

- Run HAVANA file faultfaciesmerge.model using up-scaled grid"

When upscaling the data from the finer LGR to the coarser poro was rescaled by "arithmetric mean", and permeabilities were up-scaled by "Diagonal Tensor".

3 Chapter 3 Petrophysical properties:

3.1 Introduction

The main aim of the present work is to test the practical use of the fault facies methodology and workflow. Keeping the number of facies low eases verification and quality control of modelling results. Petrophysical input to the fault facies model is also simplified, using synthetic data based on general trends, approximations and assumptions extracted and compiled from a number published and unpublished sources, and thus not linked to a single specific case or single comprehensive outcrop study. This choice is considered to be justifiable for conducting a proof of concept.

It should be noted that there are at present few datasets available giving petrophysical properties for specific fault facies. The reason for this is that although petrophysical properties have been described for a wide range of fault related features, these tend to emphasise properties of planar features (deformation bands, slip planes etc.) rather than volumetrically defined entities such as fault facies. Consequently, compilation of fault facies databases tailored for use with the method is still in the process of being compiled.

Correlation of strain to fault facies is also kept simple. Three "strain levels" are identified: low-strain, medium-strain and high-strain. Each fault facies is linked to the distribution of these three categories of strain: The low-strain facies include deformation bands and lenses; medium strain facies include breccias and cataclasites and the high strain facies include gauge and the more intensely deformed rock making up the fault slip plane and fault core area.

Although fault cores may contain lenses and breccias of higher permeability than that of the fault gouge, these are not considered as part of the high strain fault facies, as they are included in the lower strain facies. In effect, this means that the high strain facies, should not be regarded as the only fault core feature, but only as the most deformed parts of the fault core with the lowest permeabilities.

3.2 Facies petrophysics

3.2.1 Sedimentary petrophysics

The petrophysical properties of the sedimentary facies used here are based on Sæther (2006), which were derived from results from the SAIGUP project (Table 3.2-1, Manzocchi et al. 2008). Assigning petrophysical properties to the fault facies originating from these sedimentary facies is not straightforward, as a comprehensive database for fault facies properties is still in the process of being compiled. The properties used here are derived from general trends extracted from a database containing approximately 300 measurements of outcrop permeability inside and around fault envelopes (Tveranger et al. unpublished). Although this database is limited, it can be assumed that the database, derived from different localities and different depositional environments (Chile – Lower shoreface, Sinai – fluvial and shallow marine, Utah – aeolian dune and intradune), reflects a valid approximation of permeability decrease from host rock through various fault facies into the fault core, at least for the demonstrative purpose of this thesis. Petrophysical properties for the sedimentary facies and fault facies are listed in Table 3.2-1 and Table 3.2-2 respectively. Details on estimation of the petrophysical properties of the different fault facies are explained in detail below, and the values are given in Table 3.2-3.

Facie :	Porosity %	Perm X mD	Perm Y mD	Perm Z mD
Upper shoreface:	0,2	854,1	854,1	164
Lower shoreface:	0,15	90,02	90,02	1,65
Offshore transition	0,12	20,09	20,09	0
Offshore	0,02	0,06	0,06	0

Table 3.2-1 Sedimentary Facies (Manzocchi et al. 2008)

Unique Facie Nr.	Sedimentary Facies Type	Unique Facies Name
1	Upper shoreface	Upper shoreface
2	Lower shoreface	Lower shoreface
3	Offshore transition	Offshore transition
4	Offshore	Offshore

Unique Facie Nr.	Fault Facies Type	Unique Facies Name
5	Lowstrain upper shoreface	A1_sst_lowstr
6	Mediumstrain upper shoreface	A2_sst_medstr
7	Highstrain upper shoreface	A3_sst_medstr
8	Lowstrain lower shoreface	B1_sst_lowstr
9	Mediumstrain lower shoreface	B2_sst_medstr
10	Highstrain lower shoreface	B3_sst_medstr
11	Lowstrain offshore transition	C1_sst_lowstr
12	Mediumstrain offshore transition	C2_sst_medstr
13	Highstrain offshore transition	C3_sst_medstr
14	Lowstrain offshore	D1_mud_lowstr
15	Mediumstrain offshore	D2_mud_medstr
16	Highstrain offshore	D3_mud_highstr

Table 3.2-2 Fault Facies

3.2.2 Low- strain Fault Facies

The low-strain fault facies comprise the damage-zone which is modelled as consisting of lenses of host-rock and deformation bands. This is implemented as a single facies. Property variations are included in the petrophysical modelling.

Deformation bands:

Deformation bands are areas in permeable rocks where localized strain is expressed in the host-rock as a thin shear-zone. These tiny shear-zones can be viewed as micro-faults where the host rock doesn't fracture, but is deformed through small-scale semi-brittle deformation (Fossen and Bale 2007). Displacement is accommodated either by crushing of grains or rearrangement of the grains, creating several distinct types of deformation bands. *(*Figure 3.2.1*)* The deformation bands are most often compressive, creating reorganisation-, cataclastic- or framework phyllosilicate bands and shearplanes, but dilatation can also occur, in which case dilatational-bands are created.

The type of deformation bands created is dependant on burial depth and composition and type of the sediment. For example, both fine sands and sands containing some phyllosilicates are more prone to have reorganisation bands as the main type of deformation band whereas coarser and cleaner sands more often exhibit cataclastic bands, as larger grains crush more easily than smaller, and as the clay

minerals give less friction to the sand due to their cleavage and soft nature (Fossen et Gabrielsen 2005).
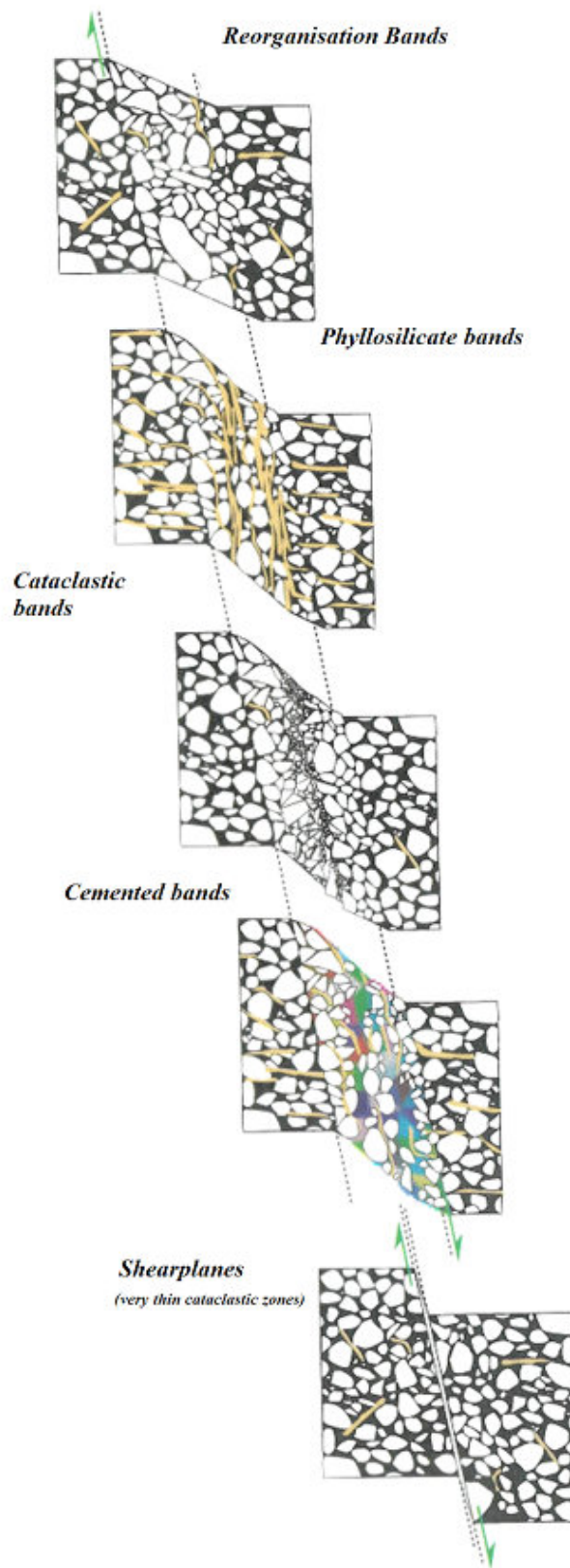

Figure 3.2.1

The different types of deformation bands: (Fossen and Gabrielsen 2005)

- **Reorganisation bands** are created through, as the name indicates, reorganising of grains by rolling and sliding within the band. Bands of this type generally don't influence flow significantly as the porosity reduction in them normally is quite small.

- **Phyllosilicate bands** are reorganisation bands containing phyllosilicates. These silicates will be oriented parallel to the slip plane and may hamper flow somewhat. Permeability of such bands is commonly reduced by three orders of magnitude.

- **Cataclastic bands** are created by crushing of grains, which gives a zone of angular larger clasts surrounded by fine material filling in the pore space. This deformation band type normally has quite a low permeability, due to the tight packing of the grains and infill of pores by finer materials. The permeability of such deformation bands can be down to less than 0.1mD (Appendix A).

- **Shearplanes** are deformation bands where the displacement has happened over a very thin zone of cataclastic deformation.

- **Cemented bands** are bands are just that, cemented. They can be very tight and have good potential to influence flow in a reservoir, however for quartz to be dissolved and cemented, a temperature of at least 120º Celsius is normally required, which, given normal geothermic gradients, means around 3000m burial depth.

The compressive deformation bands generally have lower porosity and permeability than the surrounding host-rock, and are therefore thought to constrain flow. Recent research has tried to establish to what extent this is true (Fossen and Bale 2007; Rotevatn et al. 2007). The results of these works indicate that the deformation bands have little effect on the flow unless several deformation bands are present very close to each other, in effect creating a thick cluster of bands acting as one.

In a case where flow needs to cross 100 deformation bands (db), a reduction of permeability of four orders of magnitude (from 1000 initial host rock perm to 0.1mD in the bands themselves) per band is needed to have a significant effect on the flow over a distance of 500 meters with the deformation bands logarithmically increasing in frequency the last 50meters towards the fault. Even then, with such a large drop in permeability, the effective flow is only cut down to approximately 1/3 of host-rock permeability as seen in Figure 3.2.2.
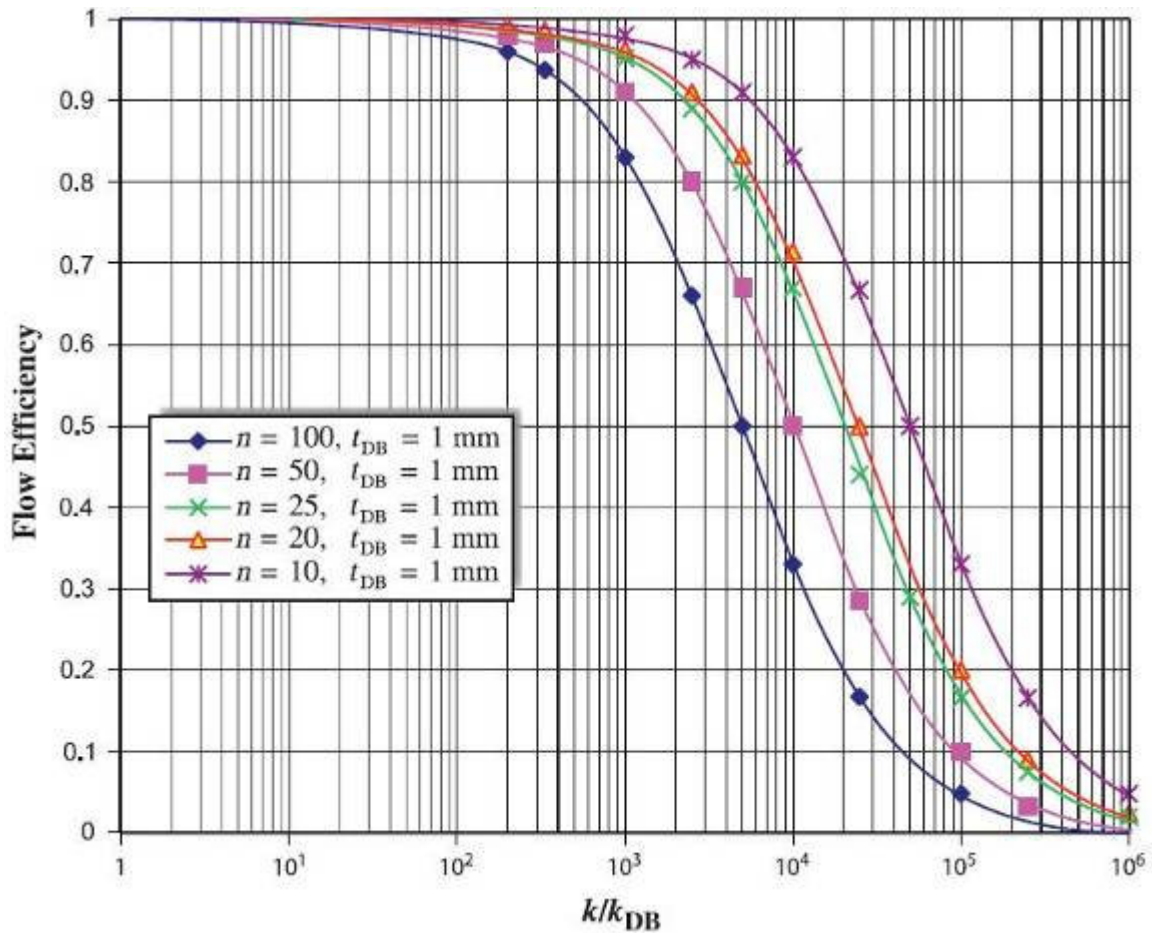
Figure 3.2.2 (Fossen, H. & Bale, A., 2007)   **Flow efficiency vs. reduction in permeability**

In Fossen and Bale (2007), the majority of deformation bands show a reduction of permeability between 0 and 4 orders of magnitude compared to the host rock. Only 5 samples exhibit a permeability reduction exceeding 4 orders of magnitude, and only one of these is not clustered.

In his PhD thesis, Rotevatn (2007) presented results from a fluid flow sensitivity study of the Arches relay ramp in Utah. The model included a pattern of mapped deformation bands which where implemented as contoured frequencies allowing bulk permeability properties for each cell in the model to be calculated using a host rock permeability of 1 D and running different scenarios where deformation band permeability was varied. The effect of clustering on scales smaller than grid resolution was not included, although the results by Fossen and Bale (2007) suggest this may cause additional decrease in permeability; the effect of multiple bands in cells was considered to equal the sum of individual bands. Rotevatn (2007) concludes that unless there are clusters present with at least a five order permeability reduction the effect on flow performance will be less than 1 order of magnitude. Deformation bands usually have between 3 and 4 orders of magnitude lower permeabilities than the host-rock, and only rarely 5 orders of magnitude, In addition to the

permeability of clusters averaging above the 4 orders of magnitude limit, the clusters are very variable in length, and are considered unlikely to make up continuous sheets of very low permeability.

Lenses:

Lenses are bodies of undeformed host-rock enclosed by deformed rock. The surrounding deformed rock may vary in thickness from very thin well defined "sheets" separating lenses, to thicker zones of deformed rock including variously fractured and brecciated parts of the host rock. Commonly lenses exhibit internal trends of deformation ranging from an undeformed central part to a fractured and brecciated rim. The length-thickness ratio of lenses is normally between 9:1 and 12.5:1, Semshaug et al. in prep, Lindanger et al. 2003 and Lindanger et al. 2007.

The lenses in the cases modelled here have for simplicity been incorporated into the low-strain fault facies together with the deformation bands. Based on the permeability database by Tveranger et al. (unpublished), an average reduction of permeability in the lenses is chosen to be around 1 order of magnitude. I see the choice of including the lenses into the low-strain facies as valid as the petrophysical parameters would have been equal for the two, as both facies have the same host rock petrophysical values, and both are reduced by 1 order of magnitude.

Permeability:

Based on this, it can be assumed that the overall permeability of the low-strain facies in the present work will be somewhere in the region of 1 order of magnitude lower than that of the host-rock, taking into account the lenses which are normally around 1 order of magnitude lower than that of the host-rock, and the low probability of continuous sheets of very low permeability deformation band clusters. Directional variation in permeability is dealt with in chapter 3.2.3.

3.2.3 Medium strain Fault Facies

The data by Tveranger et al. (unpublished), suggest that brecciated lens permeabilities exhibit 1-2 orders of magnitude lower permeability than the host rock. These data only give the permeability of the lenses themselves, and do not include fractures and deformation bands which may occur inside them. Consequently some general assumptions need to be made to provide an average permeability value for the brecciated facies in the medium-strain zones.

The assumptions are as follows:

1. The areas of brecciated rock generally have a higher density of deformation bands than the low-strain facies.
2. The breccias themselves are often quite closely packed.
3. The flow restricting higher-strain deformation-bands and brecciated areas combined, make for a fault zone of lowered permeability perpendicular to the fault plane.

Based on these assumptions I conclude upon a permeability reduction of approximately *2 orders of magnitude*, with a σ (standard deviation) of 0.5 orders of magnitude appears reasonable.

3.2.4 High strain Fault Facies

For the high strain facies, few permeability measurements are available in the database supplied by Tveranger et al. (unpublished). This means that the standard permeability reduction used here is given with a rather large uncertainty, but since the available samples appear to be quite consistently in the area of 2-3 orders of magnitude lower than host rock, faulting an estimate of 2.5 orders of magnitude reduction seems reasonable. This is supported by the findings of Antonelli et al. (1994), and Shipton et al. (2002), dealing with fault permeabilities.

Based on this, I have chosen to set the fault plane and fault gauge permeabilities to have 2,5 orders of magnitude lower permeability than the host rock in a fault plane parallel horizontal and vertical direction.

3.2.5 Directional variations of permeability

Perpendicular vs. parallel

In the data used by Sæther (2006), the permeability were considered isotropic parallel and perpendicular to the fault plane. When modelling the fault facies we need to take into account the anisotropy, as the fault plane perpendicular permeability, and distribution of it, is the paramount parameter for flow across the fault.

The permeability measurements from The Tayeba Mines (Figure 3.2.3) and Wadi El Khaboba (Figure 3.2.4) in Sinai Tveranger et al. (unpublished) show a clear difference in permeability between the perpendicular and parallel measurements, where the mean permeability is

between 0.5 and 1 order of magnitude lower in the perpendicular direction. The mean values of Wadi El Khaboba are 589,51 and 59,43, and in the Tayeba Mines 511,09 and 173,72 .

Assuming these data reflect a more general trend, a factor of 0.25 to give a 0.75 order of magnitude lower permeability for the perpendicular flow than for the parallel, which is estimated from the regression line through the datapoints. I chose to make a visual estimate rather than calculate one, as the amount of available datapoints with permeability measured along two axes was very limited (Appendix C).
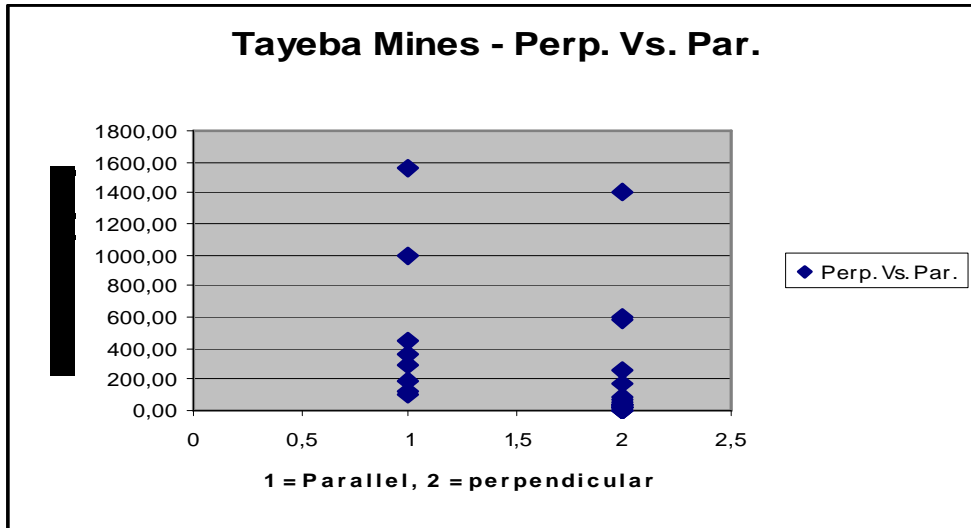

**Figure 3.2.3 Tayeba Mines (Tveranger et al. 2008)**
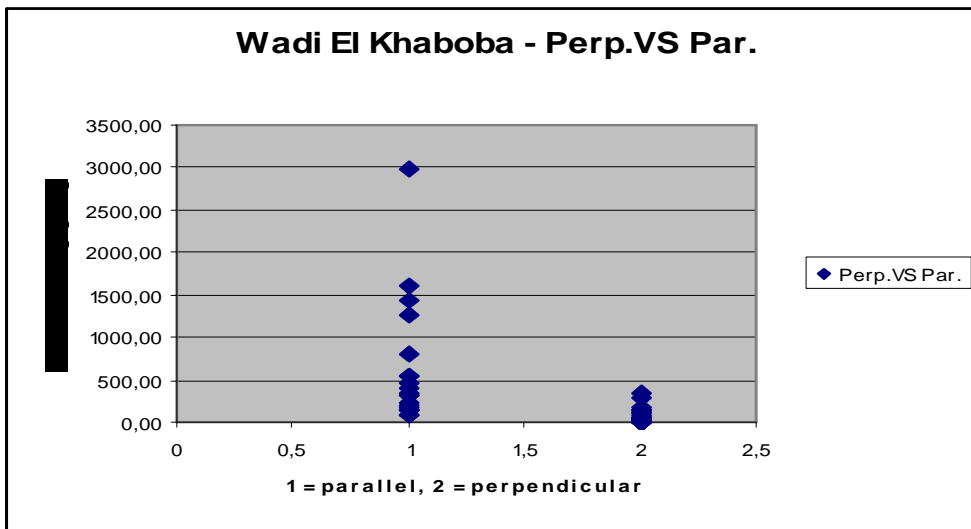
Figure 3.2.4 Wadi El Khaboba (Tveranger et al. 2008)

Horizontal vs. vertical

The permeability anisotropy created due to the lozenge geometry of deformation band (Figure 1.2.3, Parnell et al. 2004, Fossen & Bale 2007) distribution leads to a small drop in permeability from fault-plane-parallel slip-normal to fault-plane-parallel slip-parallel (from now on referred to as vertical). If no values for sedimentary vertical permeability are available, a calculation can be made based on the average drop in permeability from horizontal to vertical measured by Tveranger et al. (unpublished) (Appendix A). The average horizontal vs. vertical measurements from the Entrada sandstone, of Utah, USA, show that the vertical permeabilities are 75,36%, 31,72% and 27,41% of the parallel permeability, giving an average drop from the three locations of 44,83% from horizontal to "vertical", plane parallel. (Figure 3.2.5, Appendix A petroplots_FF) Based on this one can multiply the plane parallel value with a factor of 0.45 to get the average permeability drop for the cases where there were no data beforehand. It should however, be noted that this permeability drop is based on a rather small dataset which is part of a work in-progress, the fault facies database, and that the measurements were made on aeolian sandstones rather than shallow marine deposits which are used in this thesis.
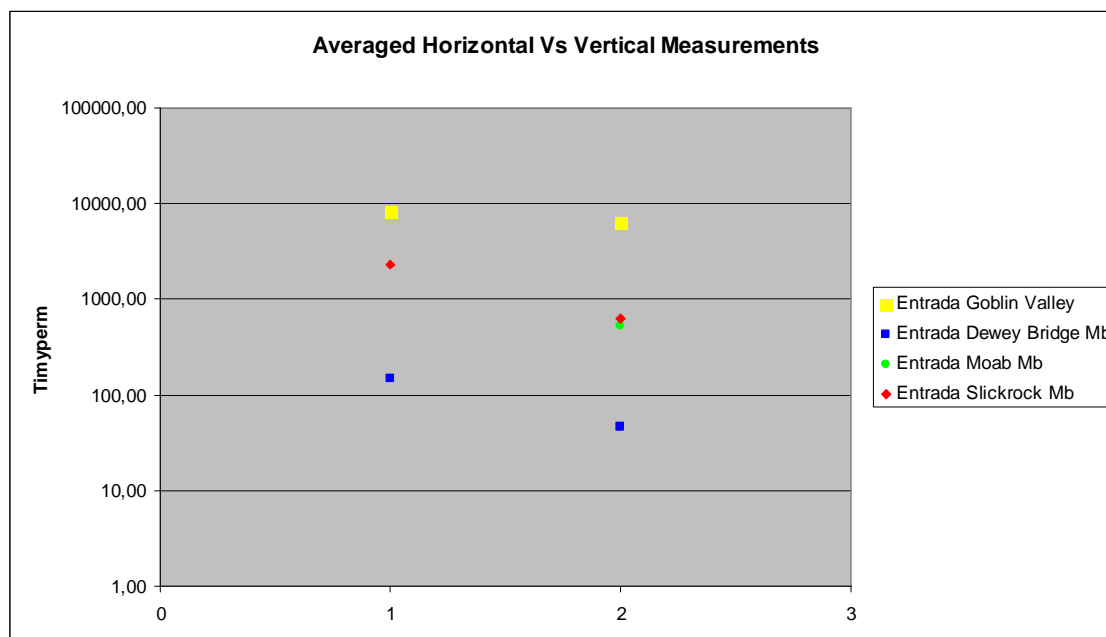

Figure 3.2.5   Tveranger et al. 2008   1 = horizontal, 2 = perpendicular

3.2.6 The Fault facies data table (Appendix D)

In the input data used by Sæther (2006) the vertical permeability was only specified for the upper and lower shoreface facies. The offshore transition z-permeability was calculated by using the

ratio offshore transition/lower shoreface permeability, subsequently multiplied with the vertical lower shoreface fault facie value, like this: ((20.09/90.0)*C# vertical). Offshore z values were kept at 0. The porosity drop for the facies is not based on hard facts, as I was unable to find general trends for porosity drop. I chose the values based on the assumption that porosity only is reduced slightly during faulting.

The factors used for calculating the numbers in Table 3.2-3 are as follows:

Parallel: (X*0,1/0,01/0,005)

Perpendicular: (parallel value*0.25)

Vertical: (Z*0,1/0,01/0,005) (except for C1 as described in the above text)

All in all, this gives a permeability and porosity distribution as follows:

	Initial perm	PORO	PERM # (parallel)	PERM # (perpendicular)	PERM # (vertical)
A1	**X** - 854,1mD **Z** - 164,0mD	0,2	85,41 $\pm 2\sigma$	21,35 $\pm 2\sigma$	16,40 $\pm 2\sigma$
A2		0,15	8,54 $\pm 2\sigma$	2,14 $\pm 2\sigma$	1,64 $\pm 2\sigma$
A3		0,15	4,27 $\pm 2\sigma$	1,07 $\pm 2\sigma$	0,82 $\pm 2\sigma$
B1	**X** - 90,0mD **Z** - 1,65mD	0,15	9,0 $\pm 2\sigma$	2,25 $\pm 2\sigma$	0,17 $\pm 2\sigma$
B2		0,12	0,9 $\pm 2\sigma$	0,23 $\pm 2\sigma$	0,02 $\pm 2\sigma$
B3		0,10	0,45 $\pm 2\sigma$	0,11 $\pm 2\sigma$	0,01 $\pm 2\sigma$
C1	**X** - 20,9mD **Z** – 0 mD	0,12	2,09 $\pm 2\sigma$	0,52 $\pm 2\sigma$	0,04 $\pm 2\sigma$
C2		0,12	0,21 $\pm 2\sigma$	0,05 $\pm 2\sigma$	0,0 $\pm 2\sigma$
C3		0,10	0,10 $\pm 2\sigma$	0,03 $\pm 2\sigma$	0,0 $\pm 2\sigma$
D1	**X** - 0,06mD **Z** – 0 mD	0,02	0,01 $\pm 2\sigma$	0,0 $\pm 2\sigma$	0,0 $\pm 2\sigma$
D2		0,02	0,0 $\pm 2\sigma$	0,0 $\pm 2\sigma$	0,0 $\pm 2\sigma$
D3		0,02	0,0 $\pm 2\sigma$	0,0 $\pm 2\sigma$	0,0 $\pm 2\sigma$

Table 3.2-3

4   Chapter 4 – Simulation

4.1   Simulation setup

Fluid flow simulations on the conventional faulted grids made by Sæther (2006) were originally performed using "FlowSim" in Irap RMS 7.4. Simulating the fault facies grids however, was not possible as Flowsim does not handle LGRs. Because of this we have had to simulate the fault facies grids in ECLIPSE, which has lead to some of the simulation parameters which were default in RMS being slightly altered.
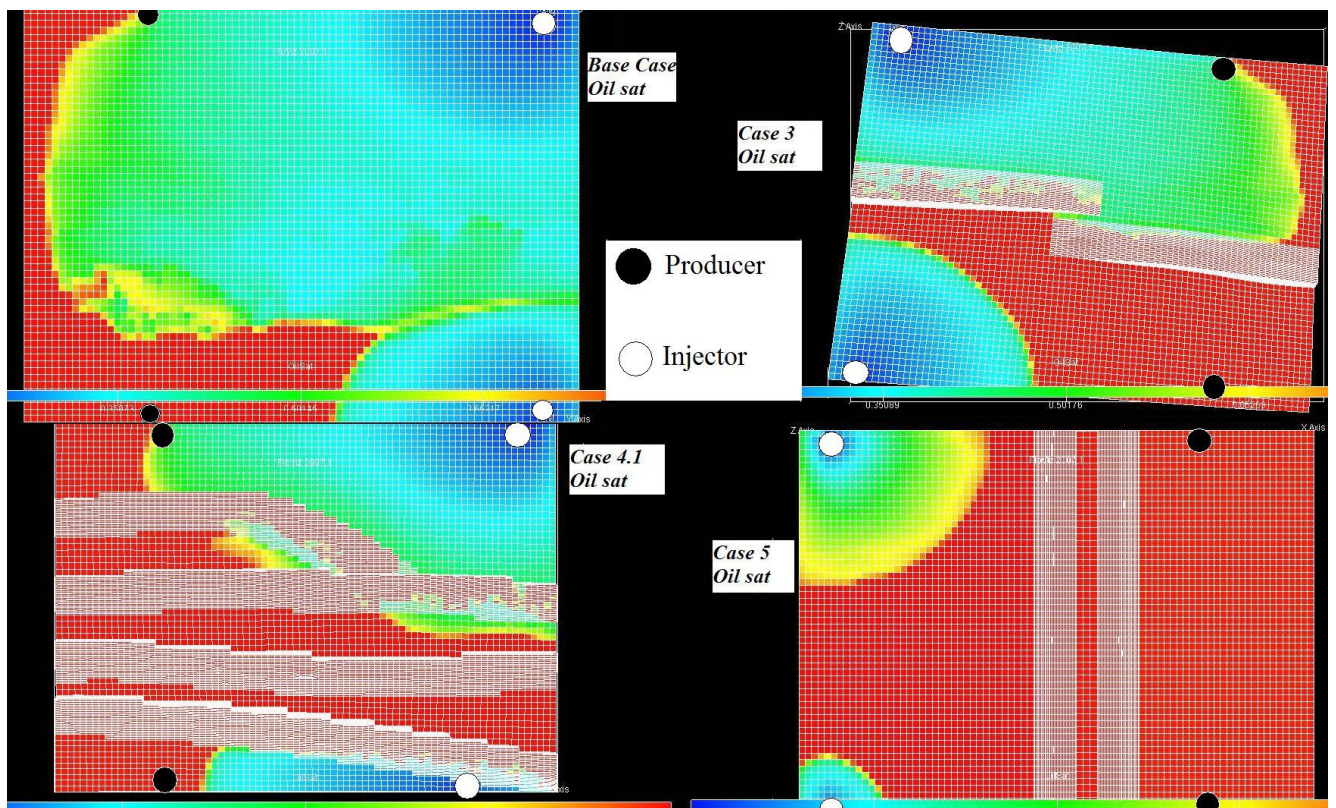
Figure 4.1.1   Figure showing the well-placement for all the cases.

4.1.1 The data:

When simulating in RMS, changing PVT data for water were used, and oil PVT was kept constant, oil viscosity was kept at 0.628 and water at 0.432. Water doesn't change volume by pressure (at least not more than 4% or so), whereas oil does. Using the numbers from the "conventional model" dataset by Sæther (2006) might therefore have produced strange results in ECLIPSE, and so were changed. The PVT for water was kept constant, and changing PVT data for oil were included. The

oil viscosity was also changed, following a general data table created by Muhammad Fachri (PhD. Student at CIPR). Both the original simulation parameters used by Sæther (2006) in the previous phase of the project and the data used for this part have been included as appendixes (Appendixes F and G respectively). Other than that, the data used for the oil the Eclipse data file was kept as close to those used in the RMS flowsim simulations as possible. Oil water contact was set at 2000m to keep the reservoir completely oil filled. Oil density was set to 800 rho, water at 1100 rho, reference depth was set at 300 bar 1740m as this was an average of the different models, BHP was set to 50 bar for the producers and 550 for the injectors. Well spacing was 1425 and 1450m (1433.3m on average) except for case 4.1 where the wells had to be set closer due to coming in contact with the LGR when LGR width was 75m. This was mainly done to save simulation time as the simulations take a lot longer if the wells are placed within an LGR.

Reference depth	Reference pressure	Oil water contact	Oil Visc.	Water Visc.	Oil kg/m^3	Water kg/m3	BHP Producer	PHP Injector	Well spacing
1740m	300 bar	2000 m	0,628	0,42	800 rho	1100 rho	50	550	1433 m

Table 4.1-1

4.1.2 Number of simulations and different scenarios:

Simulations were set up to run 5 realizations for each model with the standard sedimentological and fault facies petrophysical values. Additional scenarios added in order to investigate how changing the various parameters would impact reservoir flow. This was performed after having seen that the faults were practically sealing with the standard values and given simulation time (2 years). The different scenarios and number of realizations run for each model setup are tabulated below:

	Case 3	Case 4.1	Case 5	Base case
Standard 75m Case	4 real[1]	5 real	5 real.	N/A
Standard changed well-config.	1 real	1 real	1 real	N/A
High permeability	1 real	0	0	N/A
Softer strain conditioning	1 real	0	1 real	N/A
Softer strain conditioning high permeability	0	0	1 real	N/A
Alt 1 50m	1 real	5 real	0	N/A
Alt 2 25m-Standard	1 real	N/A	1 real	N/A

| 25m changed well-config. | 1 real | N/A | 1 real | N/A |

Table 4.1-2 [2]

By "softer" strain conditioning, it is meant that the cap (workflow step 6) which was put on strain in the IPL scripts for improved visualization and inclusion of high-strain facies, is set high or removed, so as to produce only thin medium and thin or non-existent high strain facies.

The difference between the standard scenario and the 50 and 25m scenario is the thickness of the fault zone. The standard cases have a fault zone extending 3 grid cells from the fault plane making the whole zone 150m wide, the fault zone for the 25m scenario extends 1 grid cell out on each side of the fault plane in stead of 3 and for the 50m scenario 2 cells. This gives a total fault zone thickness of 50 and 100 meters for the 25 and 50m scenarios.

For the changed well-configuration scenarios, the configuration of the two pairs of injector and producer wells was changed 90 degrees by swapping of a diagonally opposite producer-injector pair of wells.

Simulation time

The simulation-time of the different cases varied substantially, ranging from under 2 hours to more than 12 hours for the longest simulations. The variation in simulation-time from case to case (Table 4.1-3) did not seem to depend on number of cells in the grid, but rather how complex the flow-path was from injector to producer. I have been unable to find out why there was such a large variation in simulation time internally for each case.

Case name	Number of cells	Simulation time
Base Case, no faults	*240000*	*t < 1 hour*
Case 3 – Relay Ramp	372000	From 2 – 12 hours
Case 4.1 – Domino system	720250	From 1.5 – 7 hours
Case 5 – Graben	420000	From 1.5 – 2.5 hours

Table 4.1-3

4.2 Flow-defining parameters

Many factors influence flow across the faults in the simulation, the most obvious of which is the fault zone permeabilities. This is the easiest factor to control, and is quick to change similar to the SGR of the 2D transmissibility multiplicator modelling technique. In addition to this there are other factors influencing the fluid flow, which may be critical for the communication across faults:

Factors influencing fluid flow:
-             Fault zone permeability
-             The conditioning of facies to strain.
-             The Rd value
-             Restored grid generation technique
-             Distribution of indicators
-             Thickness of fault zone
-             Havana artefacts

Table 4.2-1

-     **The strain conditioning**: When creating the intensity parameters to which we connect the indicators (the fault facies), we choose the range of strain which each intensity indicator facies will encompass. This is normalized for each intensity indicator in the IPL job creating the intensity values and an artificial maximum level of strain is set both to remove any values which stand out and to increase the thickness of the high strain facies. Since the value of the intensity is normalized, the lower this value is set, the thicker the high-strain zone will be. If the value of strain varies greatly along strike, such as if a fault dies out within the grid, this will relatively lessen the strain intensity of the lower-strain areas, and thereby effectively remove some of the high-strain volumes, and possibly increase flow unduly. Inversely, if this is a problem and is taken into account by lowering the maximum value in the IPL script, we thicken the zone of high-strain across the whole fault increasing the amount of high-strain facies generated and greatly reducing the chances of flow across the fault, along substantial lengths of the fault. This is therefore a parameter it is important to balance, and is a parameter which it is difficult to predict the influence of without more extensive testing.

-     The R_d used when strain modelling (explained in chapter 2.3.2) is also a parameter which can be critical. The Rd defines how far away from the fault-plane the deformation extends, and

influences how fast the strain values drop when moving away from the fault. This may restrain the high-strain facies to a very thin or a very thick area, which changes the probability of a sealing fault.

- The **restored grid generation-technique**, which is the technique by which sedimentary facies are being included into the fault zone, is important. If the sedimentary facies are being folded into the fault as they are at present, the volume of original facies is too high, leading to erroneous estimates of fault zone permeabilities. A routine for controlling this volume need to be implemented.

- The **variograms** set when defining geometry for the intensity indicators can influence flow greatly. The range the indicators are given when setting up the variograms in the indicator simulation job in the modelling tool (RMS) influences the probability of having continuous sheets of low or high-permeability fault facies. Having large sheets of low permeability will reduce the probability of across-fault flow significantly.

- **Fault zone thickness:** Assuming the same petrophysical values for the fault zone, the thicker the fault zone is, the lower the cross-fault flow will be. Especially modelling the fault facies as I have done, having no zero-strain facie in the LGR, makes the width of the LGR's important for fluid flow. Using an extra zero-strain facie would diminish the importance of fault zone thickness.

- With the version of **Havana** currently used, the dip of the fault also has a possible effect on the flow. The strain created in Havana gets a discontinuous look if the dip is too low, and the facies indicators modelled on the strain thereby inherit the same discontinuity. This affects the facies distribution, and decreases the probability of a continuous sheet of low-perm facie occurring, thereby possibly creating a flow pathway.

4.3 Qualitative simulation analysis

When doing the primary flow simulations, the points of reference available were the results of the simulations by Sæther (2006) on conventional models (Figure 4.3.1).


Base case - Oil sat. end flow sim.

Case 3 - Oil sat. end flow sim.

Case 4.1 - Oil sat. end flow sim.

Case 5 - Oil sat. end flow sim.
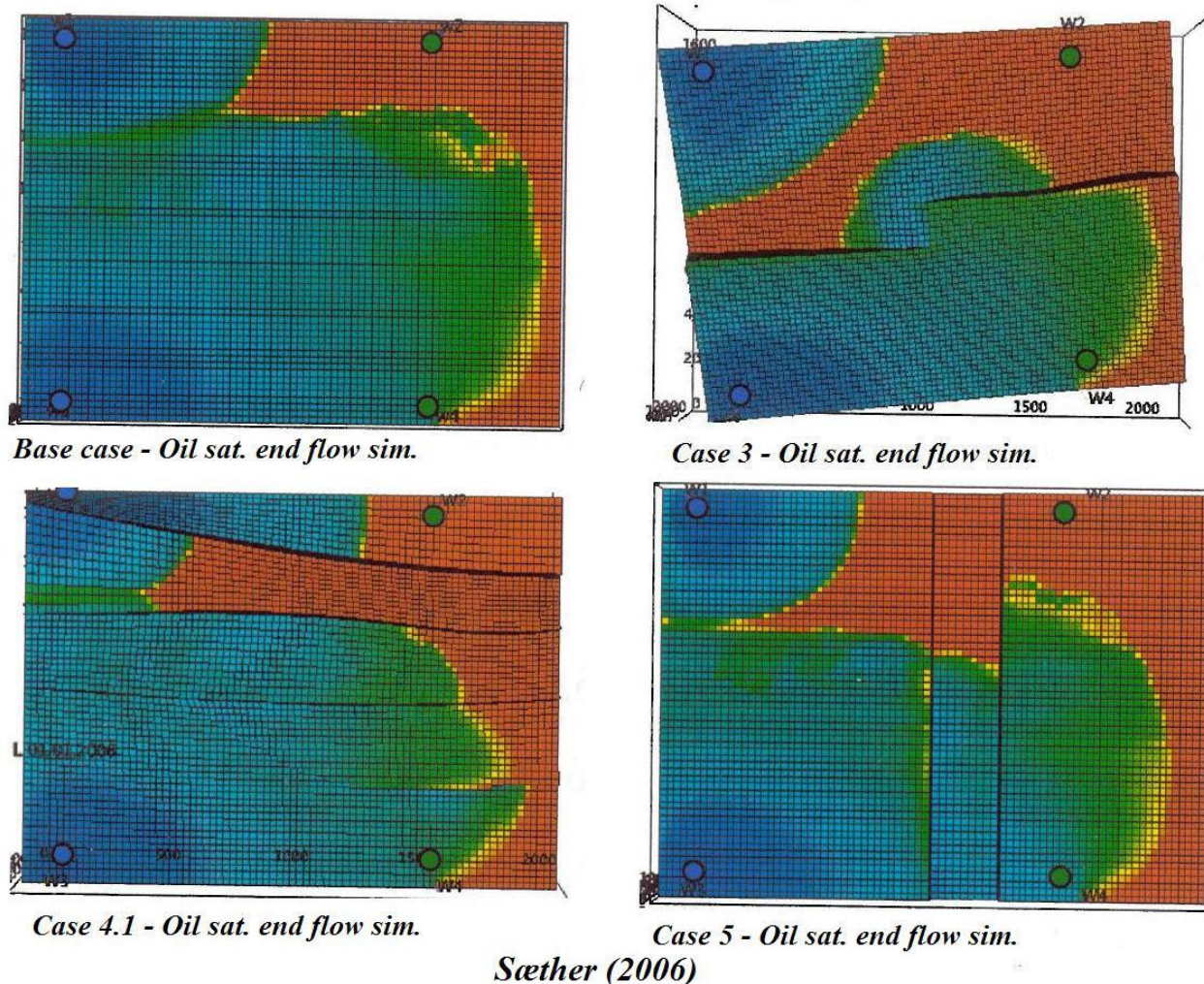
Sæther (2006)

Figure 4.3.1   Case flow simulation results, Sæther(2006). Red indicates high oil saturation, blue indicates low.

The results from the Eclipse runs with faults were inconsistent with Sæther's cases in that the faults in my cases had lower transmissibility. Even though streamlines and visual inspection of the RMS grid showed that there was communication across the faults, with low-strain areas of high perm connecting over thin bridges of more than 2 mD permeability in the facies A2-A3 and B2-B3 (Figure 4.3.2), it was not enough to have pressure communication across the faults with the chosen simulation scenarios (Figure 4.3.3, Figure 4.3.3 and Figure 4.3.4). The streamlines of RMS (Figure 5.3.1) were found to be faulty when used to predict flow-patterns across LGR's. When creating streamlines, RMS calculates the flow-paths based on the petrophysical parameters from the global grid, stretched to fill the LGR's extra volumes around the fault, and does not include the

petrophysics of the LGR. Because of this the use of streamlines in RMS was discontinued for the purpose of this work. The simulation showed that most of the faults were practically sealing and caused compartmentalization of the reservoirs where possible, as seen in Figure 4.3.4 which shows the oil saturation of all the cases at the end of 2 years production time.

Figure 4.3.2   Visual inspection 2-500mD fault plane perpendicular permeability.
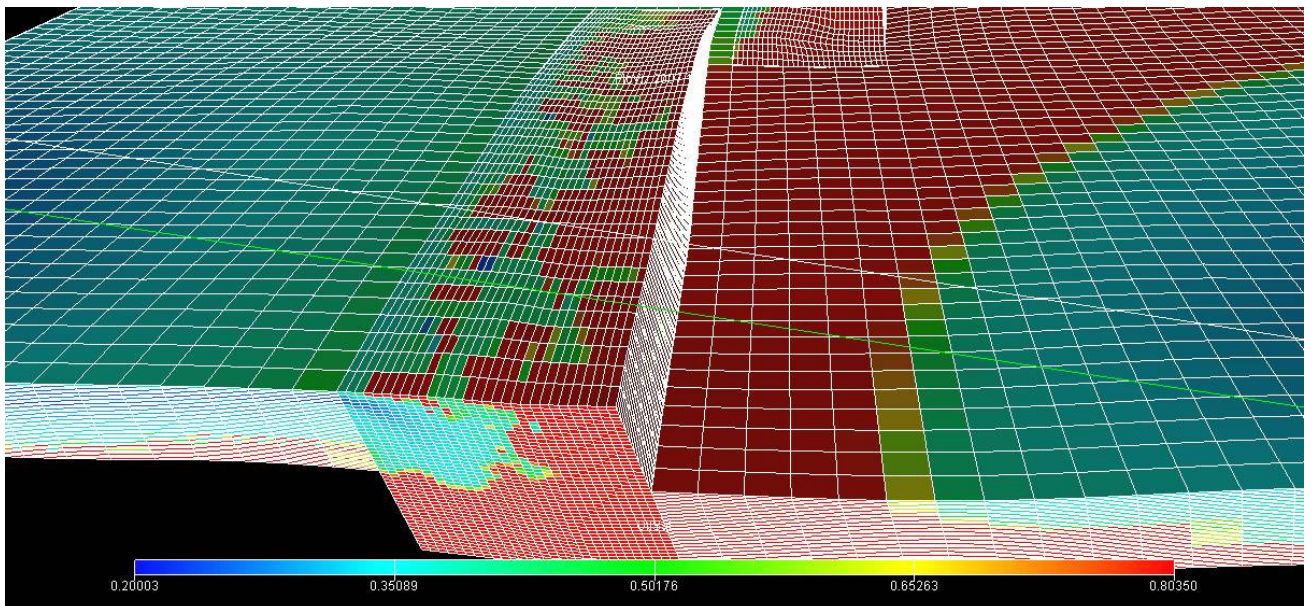

Figure 4.3.3   Flow simulation of case 3, standard scenario. Colder coloured areas indicate higher water content, whereas warmer indicate higher oil content.
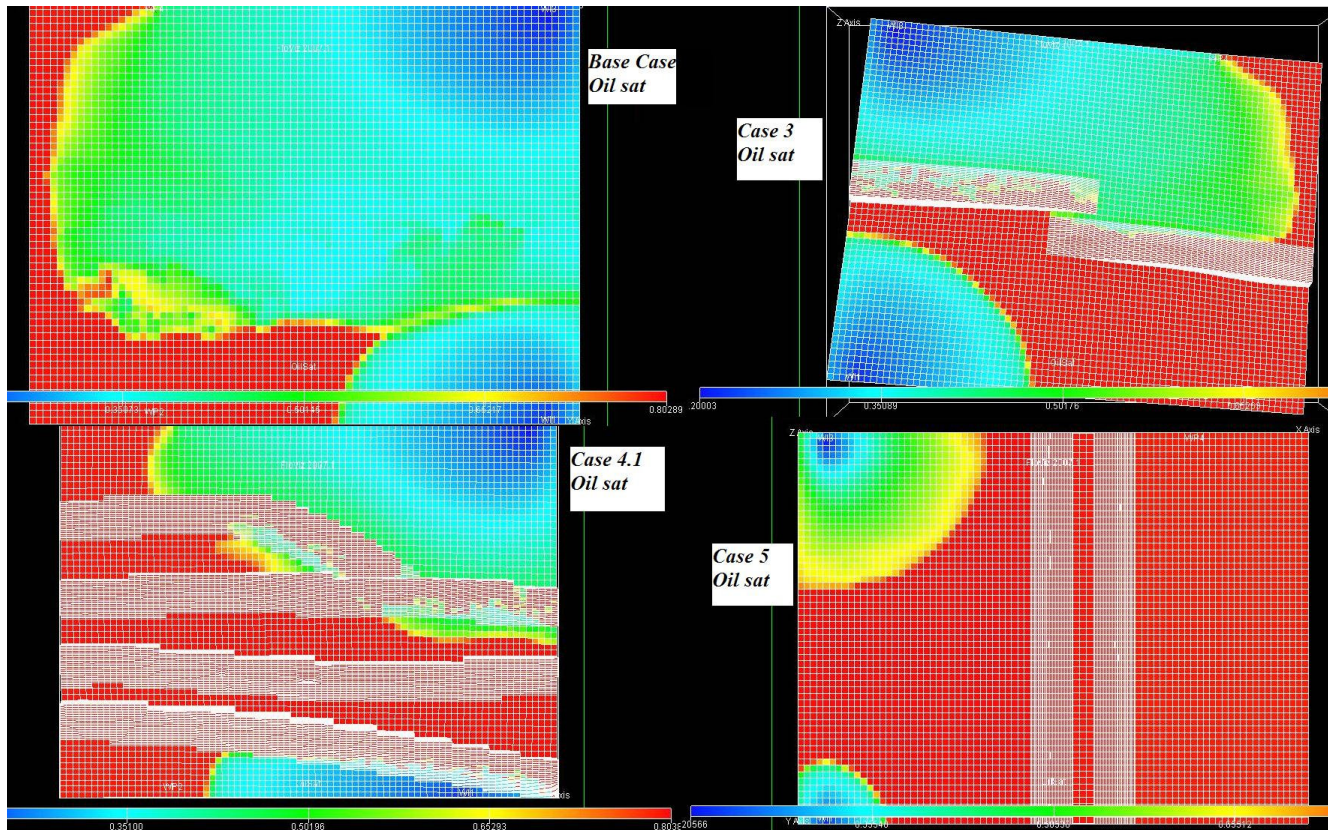
Figure 4.3.4   Base Case, Case 3, Case 4.1 and Case 5, oil saturation at end of flow simulation, 2 years. Colouring is the same as above.

To better be able to compare the results of my models to those created by Sæther (2006), the low cross-fault transmissibility of the fault zones had to be revised. The main parameters I wanted to look into were the strain conditioning, the permeabilities and the fault zone thickness.

When first choosing the values for the permeability table, the values were calculated entirely based on the data from the Fault Facies Group, and the assumption that they could be used as average values for the each facie. As noted in the facies description, some of the data showed a range of up to 2 orders of magnitude in the variability of the facies. This variability was not well taken into account in the RMS petrophysical modelling as I was unable to get the proper amount of skewness into the model, and I left the petrophysical distributions more or less normally distributed, as shown in Figure 4.3.5, showing the distribution for the C1 facie, low strain offshore transition.

Data: final_PERMY, localgrid
Facies: 1 of 12: C1_sst_lowstr

166232 observations (0 undef), Min = 0, Max = 1.569
Mean = 0.53994, St.dev. = 0.26485, Skewness = 0.094912
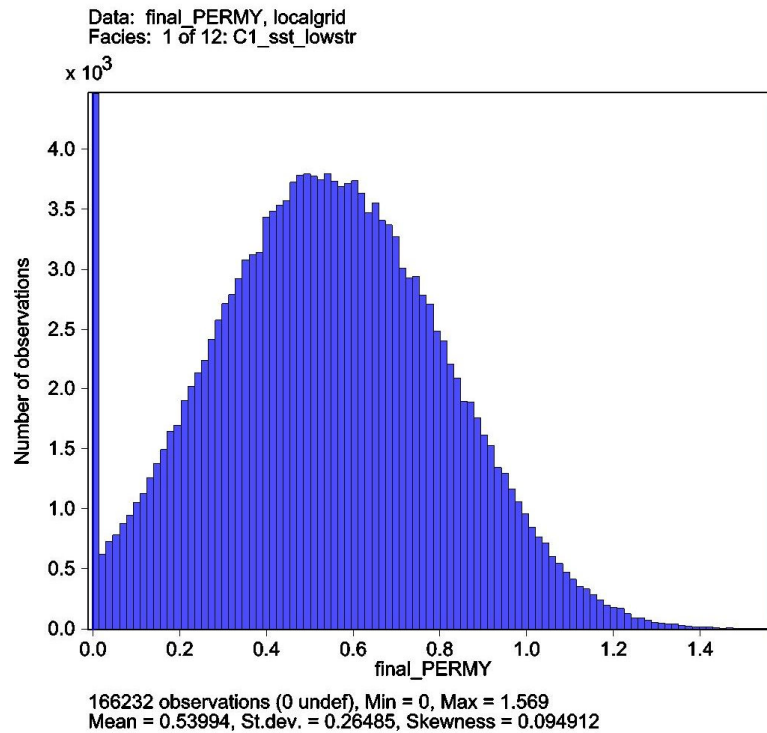
Figure 4.3.5

The problem with this, is that it excluded the effect of the tremendous variability in permeability over a short distance along the fault, as seen in field data by Tveranger et al. (unpublished) (Appendix C, frequency diagrams) and discussed by Manzocchi et al. 2008 (which again refers to Flodin et al. 2001), and means that the average values chosen could be too low to correctly represent flow. However, since no hard data on reservoir flow was available for comparison beyond another synthetic model, it can not be evaluated whether the values chosen were too low or just right. Some conclusion can be made however. With a fault zone as thick as used for the standard models, the permeabilities chosen did not allow significant cross-fault flow. The overall transmissibility of the faults is much lower than that found using the transmissibility multiplier method based on SSF and SGR values, as were used in the previous module of the fault facies study (Sæther M.Sc. 2006).

The fault zone width was set at 3 grid cells thickness to keep artefacts generated by Havana from becoming too large, as discussed in chapter 6.1.2 under Strain. As this was a rather large width compared to the displacement of the models, it may have impaired flow too much.

Setting a cap for the strain parameter will influence flow significantly as it controls the amount of high and medium strain facies. Increasing or removing the cap reduces the amount of high strain facies, thus increasing permeability across the fault.

4.3.1 Changing the permeabilities

Increasing the cross-fault transmissibility was tried in the hopes that it would give a more comparable flow and show us what factors had the most influence on flow, thus allowing a better comparison of the differences between the conventional 2D-fault models and the fault facies models.

An easy way of doing this is through a changing the permeabilities. The permeabilities of the fault-zone facies were changed substantially to get a model which rendered results closer to that of the previous synthetic models made by Sæther (2006). Although the values were substantially changed the maximum changes were not much above 1 order of magnitude, and still within what was considered geologically reasonable.

	Initial perm	PORO	PERM # (Parallel) (X*0,1/0,01/0,005)	PERM # (Perpendicular) (parallel*0.25)	PERM # (Vertical) (Z*0,1/0,001/0,005) or ((20,9/90)*C#)
A1	**X** – 854,1mD **Z** - 164,0mD	0,2	$85,41 \pm 2\sigma$	$21,35 \pm 2\sigma$	$16,40 \pm 2\sigma$
A2		0,15	$8,54 \pm 2\sigma$	$2,14 \pm 2\sigma$	$1,64 \pm 2\sigma$
A3		0,15	$4,27 \pm 2\sigma$	$1,07 \pm 2\sigma$	$0,82 \pm 2\sigma$
B1	**X** - 90,0mD **Z** - 1,65mD	0,15	$9,0 \pm 2\sigma$	$2,25 \pm 2\sigma$	$0,17 \pm 2\sigma$
B2		0,12	$0,9 \pm 2\sigma$	$0,23 \pm 2\sigma$	$0,02 \pm 2\sigma$
B3		0,10	$0,45 \pm 2\sigma$	$0,11 \pm 2\sigma$	$0,01 \pm 2\sigma$
C1	**X** - 20,9mD **Z** – 0 mD	0,12	$2,09 \pm 2\sigma$	$0,52 \pm 2\sigma$	$0,04 \pm 2\sigma$
C2		0,12	$0,21 \pm 2\sigma$	$0,05 \pm 2\sigma$	$0,00 \pm 2\sigma$
C3		0,10	$0,10 \pm 2\sigma$	$0,03 \pm 2\sigma$	$0,00 \pm 2\sigma$
D1	**X** - 0,06mD **Z** – 0 mD	0,02	$0,01 \pm 2\sigma$	$0,0 \pm 2\sigma$	$0,0 \pm 2\sigma$
D2		0,02	$0,0 \pm 2\sigma$	$0,0 \pm 2\sigma$	$0,0 \pm 2\sigma$
D3		0,02	$0,0 \pm 2\sigma$	$0,0 \pm 2\sigma$	$0,0 \pm 2\sigma$

**Table 4.3-1   The standard Fault Facie permeability table**

Better communication across the faults was obtained when increasing the fault-perpendicular and parallel flow for the upper shoreface (facie A) and lower shoreface (facie B) facies. The parameters of main importance which were changed were perpendicular flow for A and B facies from 2.14 and

1.07 to 20 and 2 for A, and 0.23 and 0.11 to 2 and 1 for B. In Table 4.3.2.changes are highlighted in turquoise.

	Initial perm	PORO	PERM # (parallel) (X*0,1/0,01/0,005)	PERM # (perpendicular) (parallel*0.25)	PERM # (vertical) (Z*0,1/0,001/0,005) or ((20,9/90)*C#)
A1	**X** – 854,1mD **Z** - 164,0mD	0,2	85,41 ± 2σ	21,35 ± 2σ	16,40 ± 2σ
A2		0,15	50,0 ± 2σ	20,0 ± 2σ	1,64 ± 2σ
A3		0,15	10,0 ± 2σ	2,0 ± 2σ	0,82 ± 2σ
B1	**X** - 90,0mD **Z** - 1,65mD	0,15	20,0 ± 2σ	4,5 ± 2σ	0,17 ± 2σ
B2		0,12	10,0 ± 2σ	2,0 ± 2σ	0,02 ± 2σ
B3		0,10	5,0 ± 2σ	1,0 ± 2σ	0,01 ± 2σ
C1	**X** - 20,9mD **Z** – 0 mD	0,12	2,09 ± 2σ	0,52 ± 2σ	0,04 ± 2σ
C2		0,12	0,21 ± 2σ	0,05 ± 2σ	0,00 ± 2σ
C3		0,10	0,10 ± 2σ	0,03 ± 2σ	0,00 ± 2σ
D1	**X** - 0,06mD **Z** – 0 mD	0,02	0,01 ± 2σ	0,0 ± 2σ	0,0 ± 2σ
D2		0,02	0,0 ± 2σ	0,0 ± 2σ	0,0 ± 2σ
D3		0,02	0,0 ± 2σ	0,0 ± 2σ	0,0 ± 2σ

Table 4.3-2

However, as seen in Figure 4.3.6, this change was not large enough to change the flow simulation results significantly.

Case 3 - High Perm. flow   *Case 3 - Standard Perm. flow*
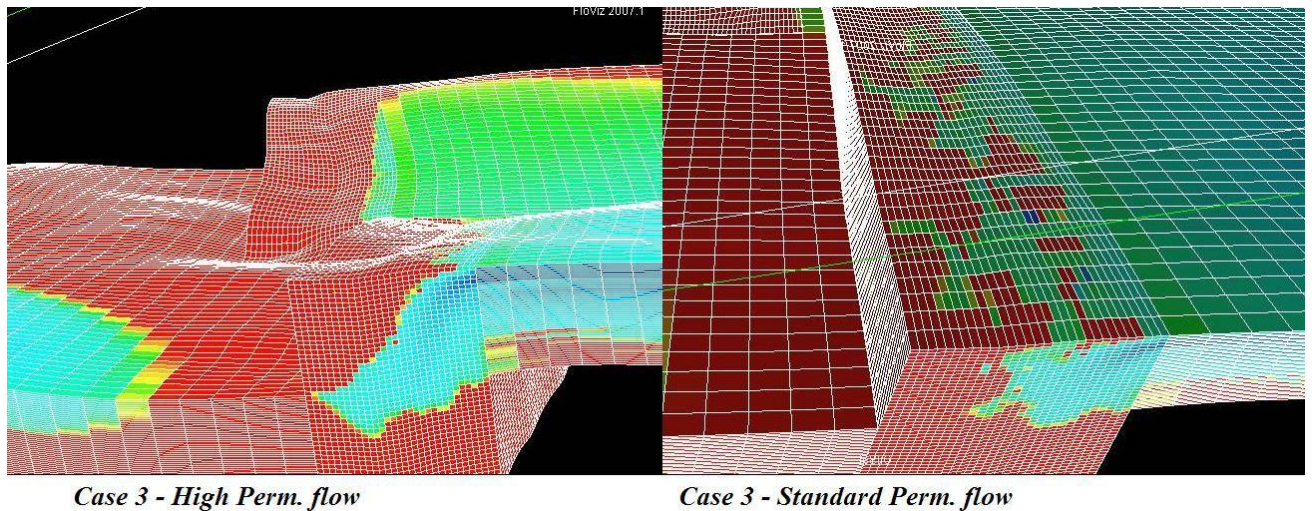
Figure 4.3.6   Variation in flow between the two scenarios.

4.3.2 Changing LGR width

The initial width of the fault zones was chosen without much consideration to how realistic the width was, as the primary object was to get the modelling procedure to work. When simulation on the grids was successful, the probability of having the fault thicknesses modelled was evaluated. Based on data from Tveranger et al. (unpublished) and the fault core thickness vs. throw diagram (Figure 6.1.5), the thickness was set to be only one grid cell, i.e. 25 meters, for all three models rather than the initial 75. For case 4.1, simulation was done on a 50 meter LGR, as creating a 25m LGR was impossible for that case due to problems with the strain generation (Chapter 5.1, Strain, Figure 5.1.5). This was also done for case 3 for comparison.

The result of changing the width of the LGR was indeed better cross-fault flow, as seen in Figure 4.3.7.
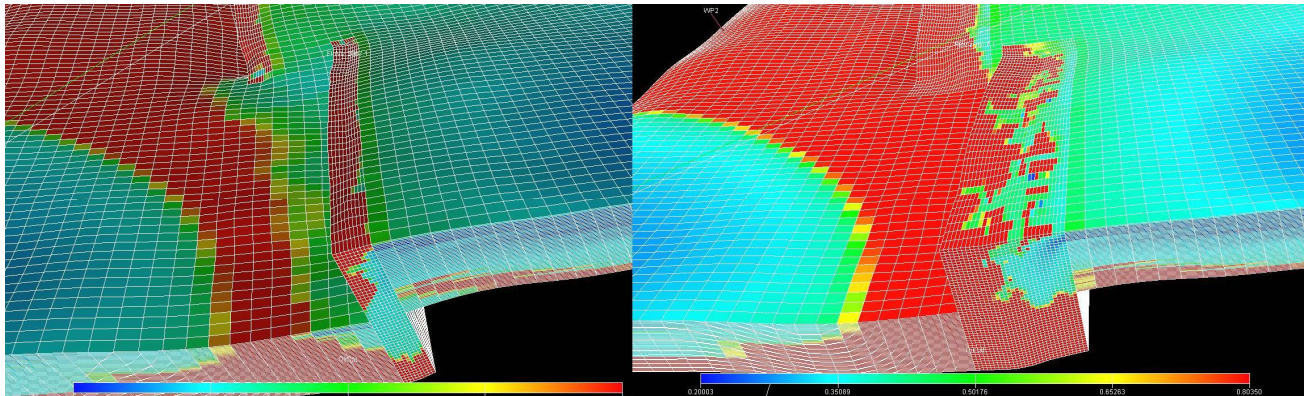

Figure 4.3.7　　**Case 3 - 25m fault zone vs. 75m fault zone**

4.3.3 Changing Strain conditioning

As previously explained the cap on the strain value, set in the IPL at step 6 in the workflow, reduces the overall fault transmissibility. The result of removing the cap on strain was less high-strain facies in the fault zone, which increased the cross-fault transmissibility somewhat, as seen in Figure 4.3.8.

Strain cap set to 0.21   **Strain cap set to 1**
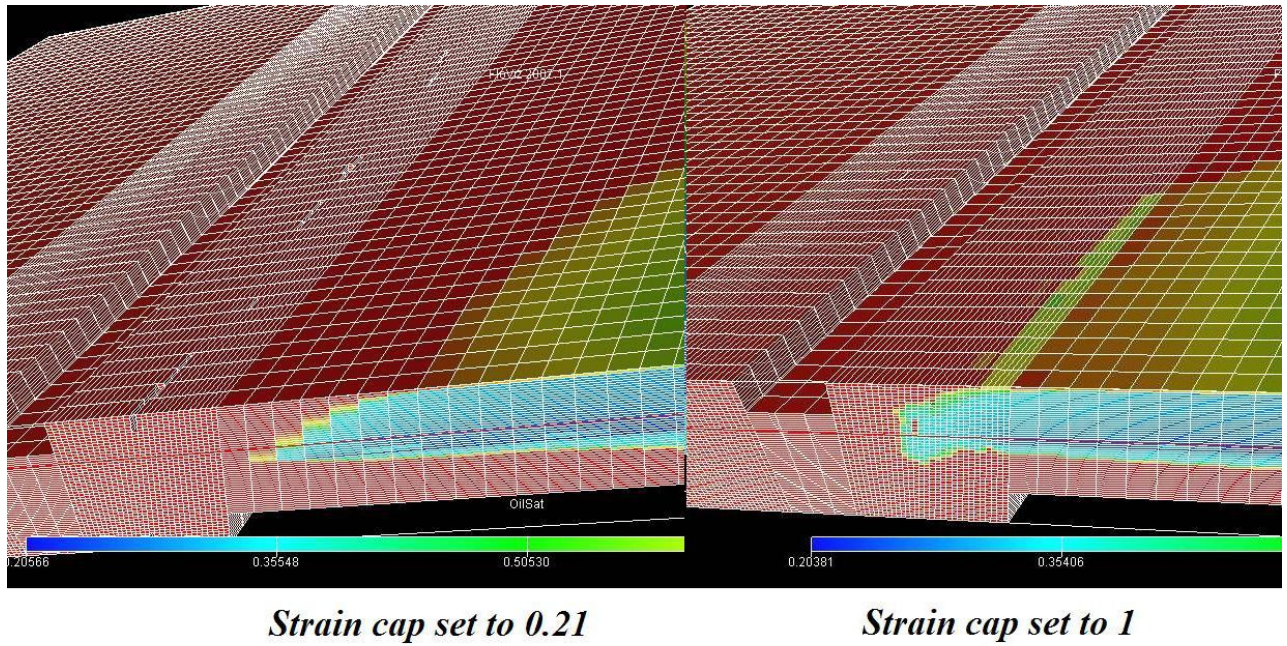
Figure 4.3.8   Case 5   Hard strain conditioning vs. Soft strain conditioning

4.3.4 Combining soft strain and high permeability

In a further attempt to increase the cross fault flow, I combined setting the cap on strain close to the maximum calculated strain, greatly reducing the amount of high strain facies, as in sub-chapter 4.3.3, and increasing the permeability as in sub-chapter 4.3.1. This greatly reduced the fault sealing effect, as seen in Figure 4.3.9.


Standard Perm., strain cap set to 0.21   **High perm., strain cap set to 1**
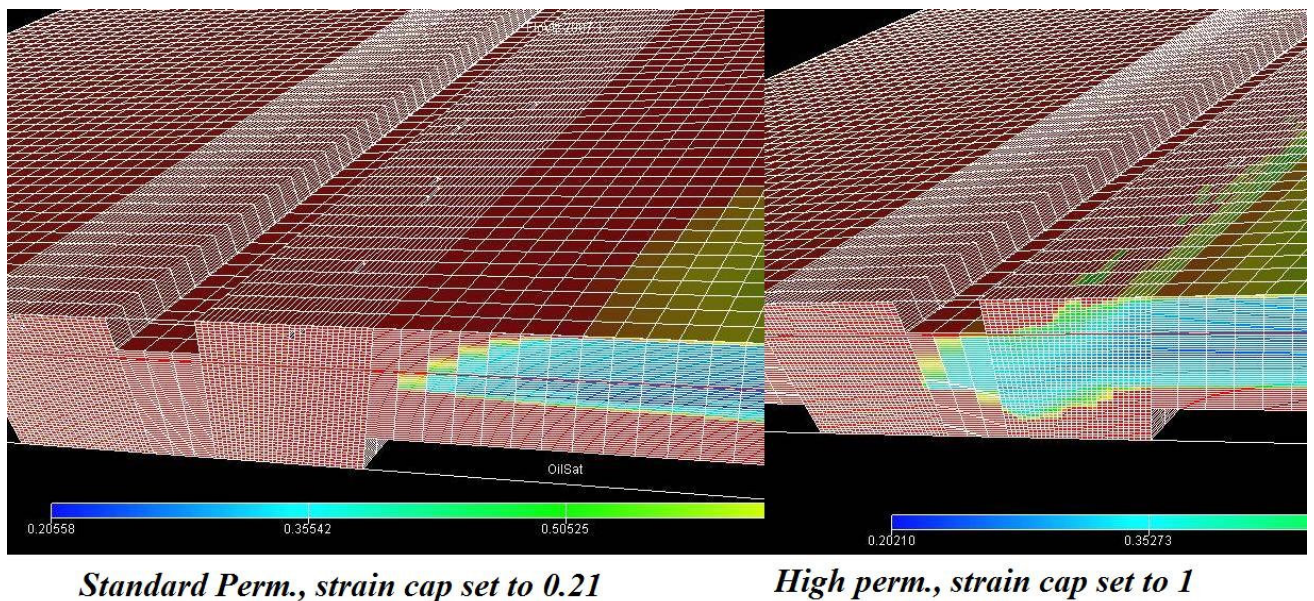
Figure 4.3.9   Case 5, standard scenario vs. high perm, soft strain.

4.4 Simulation results and quantitative simulation analysis

The simulation results from the different scenarios were, as expected, quite variable in both total production and in behaviour over time. Complete sets of production profiles and summaries for all the cases and realisations are found in Appendix J – "Flow sim results, Eclipse résumé and visuals"

The stochastic modelling of fault facies and permeabilities only had a minor impact on the total production after ended simulation as seen in Figure 4.4.1. The maximum variation in production was seen in the relay ramp case, case 3, where the difference from largest to smallest value was 8.32 %. For case 4.1 and 5 the difference was 0.45 % and 1.44 % respectively. The stochastic variation was naturally also reflected in the recovery factor of the cases, where the difference was 2.76 %, 1.92 % and 1.43 % for case 3, 4.1 and 5 respectively.
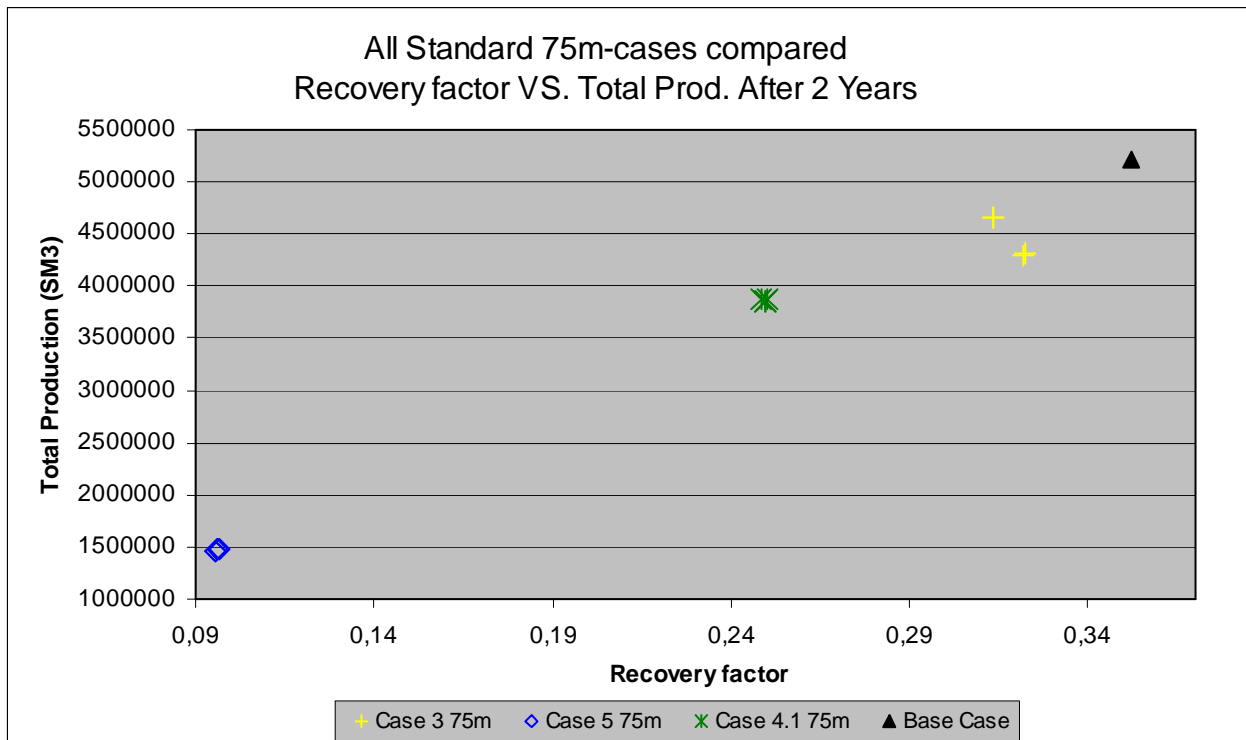

Figure 4.4.1 **Recovery factor vs. total production for the standard cases with 75 meter LGR width.**
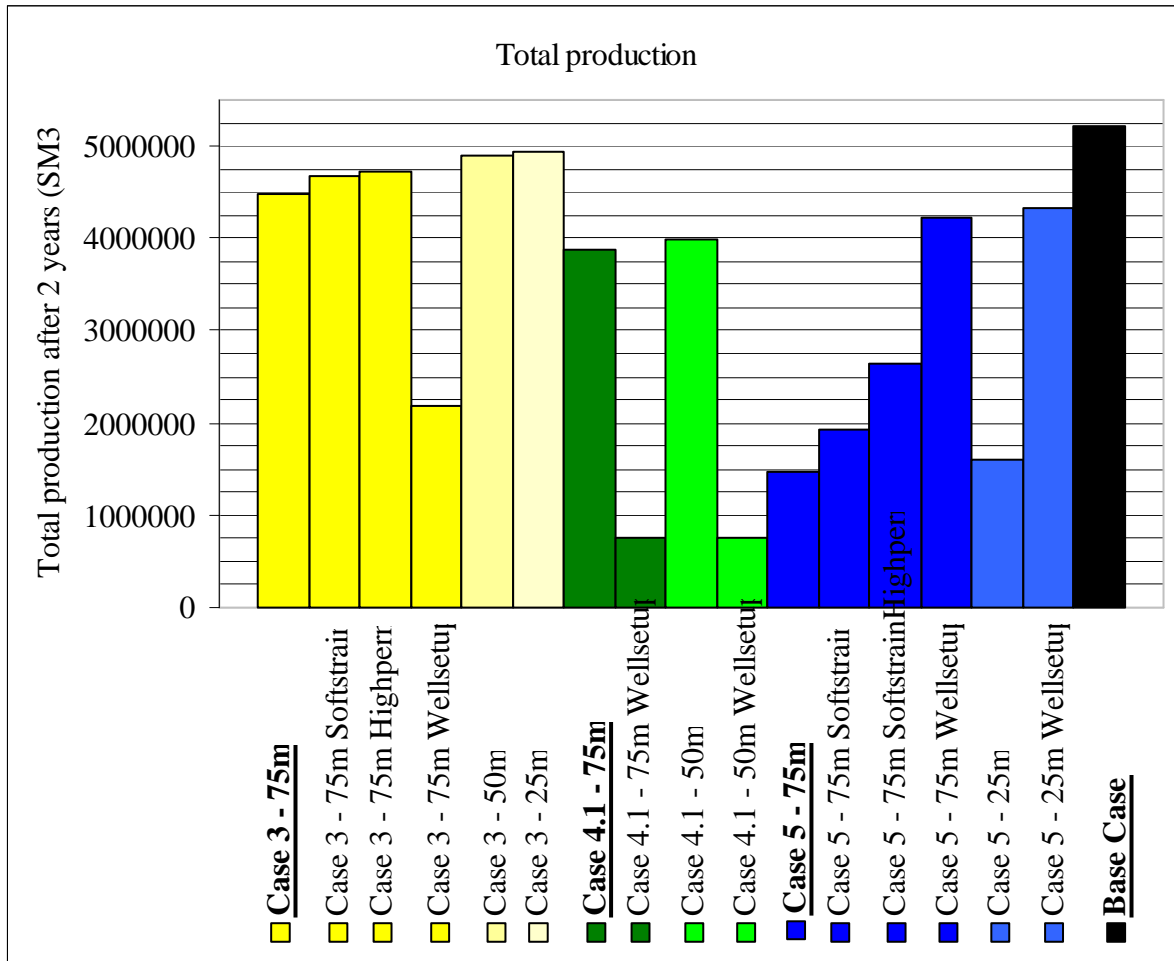
Figure 4.4.2   Total production (Sm^3) at end of 2 year simulation (average value for multiple realisations).

The effect an increase in permeability, a softening of strain or a decrease of width of the fault zone has on total production varies depending on the fault setup (Figure 4.4.2). The relative effect of the different scenarios is listed in Table 4.4-1.

For the relay case, Case 3, the different scenarios giving an increase in cross-fault transmissibility only increase the total production slightly (Table 4.4-1). This is only to be expected as there is free pressure communication across the relay ramp, diminishing the importance of the faults when producing and injecting on both sides of the faults.

When changing well setup to inject on one side of the faults and produce on the other, the total produced volume drops to below half. This is due to the sedimentary succession prograding north with progressively lower permeabilities.

For Case 4.1, the domino fault system, an increase in production is again observed going from thicker to thinner fault zone width. However the change is less pronounced than it was for Case 3, due to the fact that it is a more complex fault system with more faults obstructing flow.

When changing the well placement for case 4.1 we see a tremendous drop in total produced volume. This is because the combination number of faults and fault permeability completely seals

the producer wells from the injector wells, thus only producing what is present in the compartment being produced from.

The graben model, Case 5, is from the start being produced across the faults, with producers on one side and injectors on the other. This means that the different scenarios with higher cross-fault transmissibility have a greater effect relative to the other two cases. Changing the well configuration for this case leads to production and injection wells on both sides of the graben, leading to a greatly increased total production.

When creating multiple stochastic realisations, one can assume that the effect on total production and recovery factor will be more pronounced on a model with a thinner fault zone than a with wide zone, as it would take less for a high permeability conduit to occur as a consequence of connected low-strain facies. Comparing the variation of the case 4.1 50m and 75m scenarios shows a maximum variation of 1.9% for the 75m scenario and 0.2% for the 50m scenario, and generally a larger spread as seen in Figure 4.4.3, which is not consistent with the hypothesis.
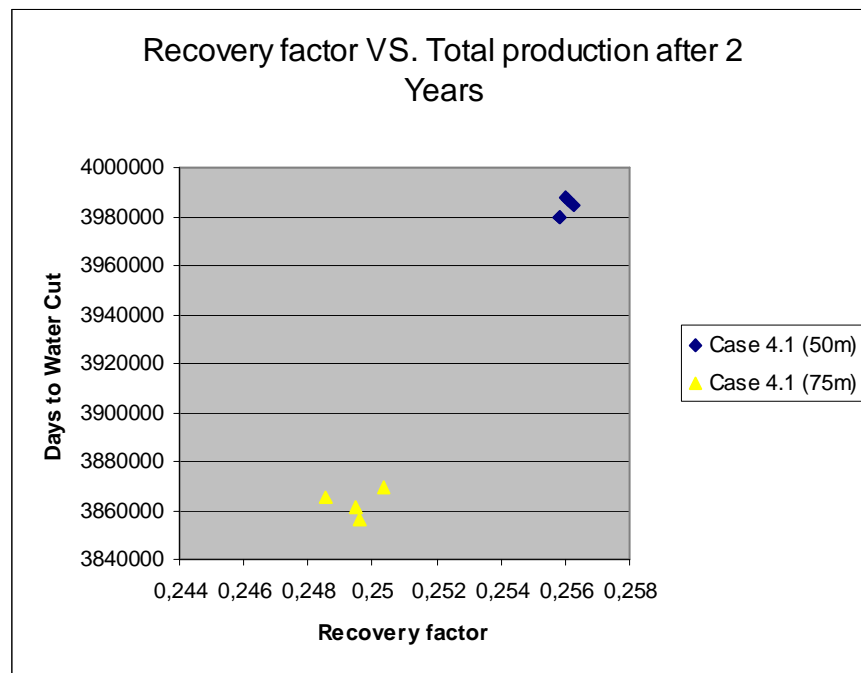

Figure 4.4.3

Unfortunately I only simulated one realisation for each of the lowest fault zone width scenario and so did not get to check the hypothesis for this, but this is something which may be looked into in the future.

Comparing the simulation results of this thesis (Figure 4.4.4) to those produced by Sæther (2006) (Figure 4.4.5), we see that there are only two cases which are similar, the base case and case 3.

When simulating the base case in Eclipse, a slightly lower recovery factor is seen compared to that of the simulation by Sæther (2006). Based on inspection of the figures it is seen that the difference in recovery is 2.23% between the two. As this model is exactly the same for both simulations, the difference seen must be due to the slightly different oil viscosity and water PVT data used for the Eclipse simulations compared to the RMS flowsim simulations (mentioned in chapter 4.1.1). All the cases of this thesis were simulated using the exact same numbers, and it is therefore reasonable to presume that the 2.23% difference is a difference existing from the start in all three cases.

The value of recovery factor for case 3, seen in Figure 4.4.4 is almost the same as the recovery factor obtained by Sæther for the same model. Case 4.1 has a significantly lower recovery factor, but sees water cut after approximately the same the time. Case 4.1's recovery is greatly influenced by fault geometry. The water being injected does not flood the compartments as the faults are relatively tight, in effect allowing nearly only the volume outside the fault compartments to be produced. The reason why both case 3 and 4.1 show water cut at approximately the same time is because both for case 3 and 4.1 the production is parallel to the faults, thus being controlled by stratigraphy more than the faults.

For the standard well setup scenarios, Case 5 does not see water cut at all, and has a maximum recovery factor of 17.35%.

This indicates the same as previously mentioned; that the faults have only little effect on flow when a relay flow pathway such as a relay ramp is present. For the other two cases where the faults either have to be crossed or compartmentalize the reservoir, the faults total cross-fault transmissibility play a major role on both the total production and recovery factor.
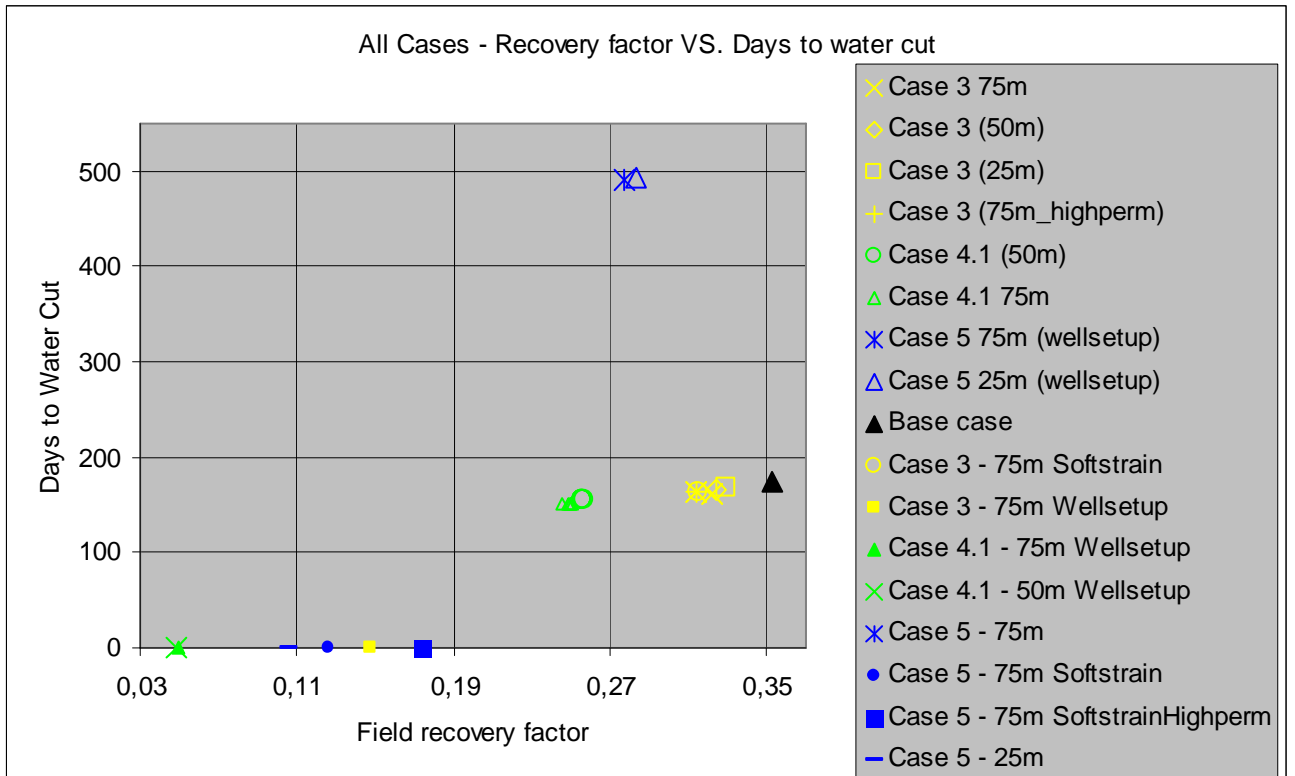
Figure 4.4.4 **Cross plot of days to water cut vs. recovery factor for all scenarios.**
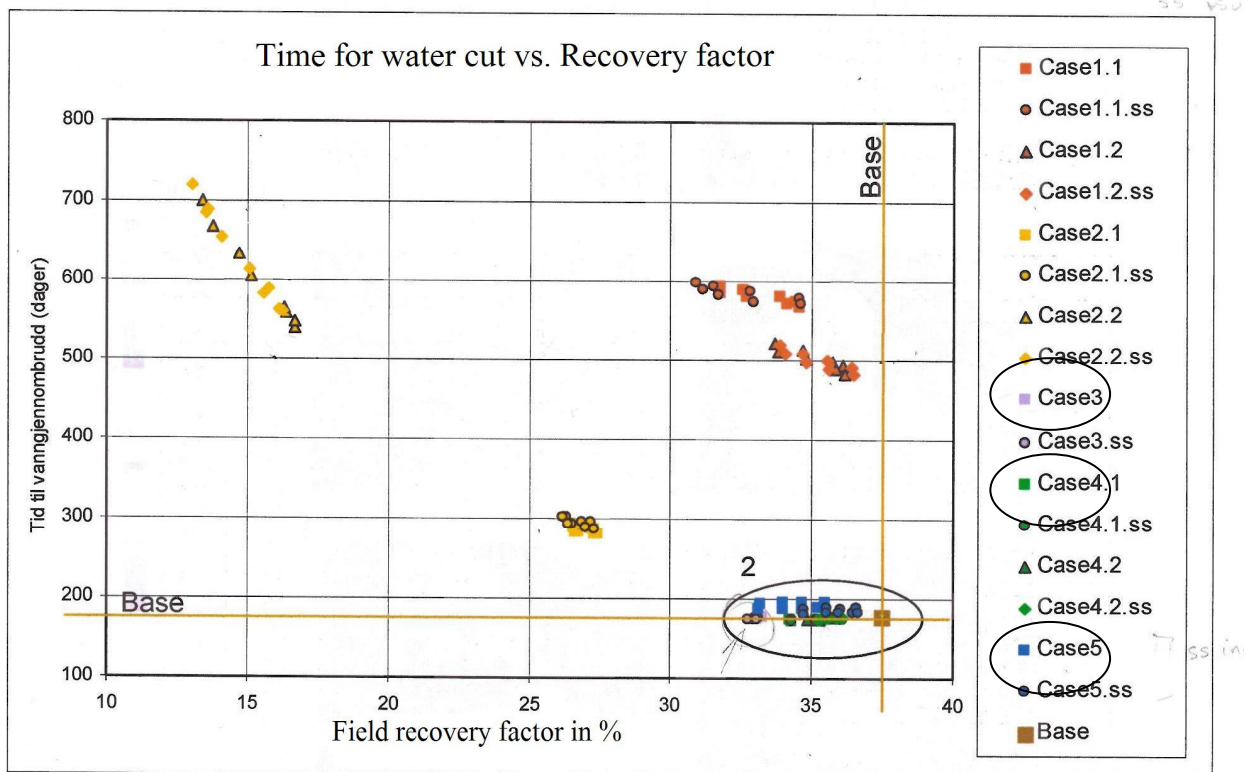

Figure 4.4.5 **The days to water cut vs. recovery factor from Sæther (2006)**

The simulation of these additional models constitutes a minor sensitivity study of the faults. Regrettably only one realisation was done for each of the alternative scenarios, and the full range of scenarios was not simulated on all the cases, but even so, it is fair to say that a general trend is apparent. The simulations are most comprehensive for case 3 and 5 where most of the changes were performed. The table below sums up the average effect in % decrease and increase of total oil production at the end of a two years production time, relative to the base and standard cases using the permeability described in the tables Table 3.2-1 and Table 3.2-3, and an LGR width of 3 cells, or 75 meters.

|	Changed Permeability	Changed LGR Width		Changed Strain Conditioning	Changed Strain Conditioning and Permeability	Changed Well Setup	
Case 3 vs. base case	-9.38%	50m -5.98%	25m -5.35%	-10.3%	N/A	-57.88%	
Case 4.1 vs. base case	N/A	50m -23.53%		N/A	N/A	75m -85.4%	50m -85.6%
Case 5 vs. base case	N/A	25m -69.13%		-62.94%	-49.09%	75m -18.76%	25m -16.78%
Case 3 vs. standard case	+5.31%	25m +9.99%	50m +9.26%	+4.24%	N/A	-51.05%	
Case 4.1 vs. standard case	N/A	50m +3.04%		N/A	N/A	75m -80.3%	50m -80.6%
Case 5 vs. standard case	N/A	25m +9.60%		+31.59%	+80.71%	75m +188.39%	25m +195.42%

Table 4.4-1   **Case total production in % increase or decrease from base case and standard cases production**

5   Chapter 5   Beta-testing

As the programs were being developed during the course of the work on my assignment, a number of bugs and errors where identified while working on it. Part of my assignment was to beta-test the program, that is, to report problems and bugs to the developers. I have added a few examples of this to give an impression of the progress that has been made during the last year.

5.1   Strain

Firstly some problems with the generation of strain will be presented. The strain generated by Havana, is supposed to follow a smooth logarithmic curve away from the fault plane, thus giving a smooth and quick fall in strain from maximum at the fault plane, to a minimum strain furthest away from the fault plane. The example in Figure 5.1.1 is from model 2.1, which I stopped developing at Havana CubaLibre version 5.6.6. :
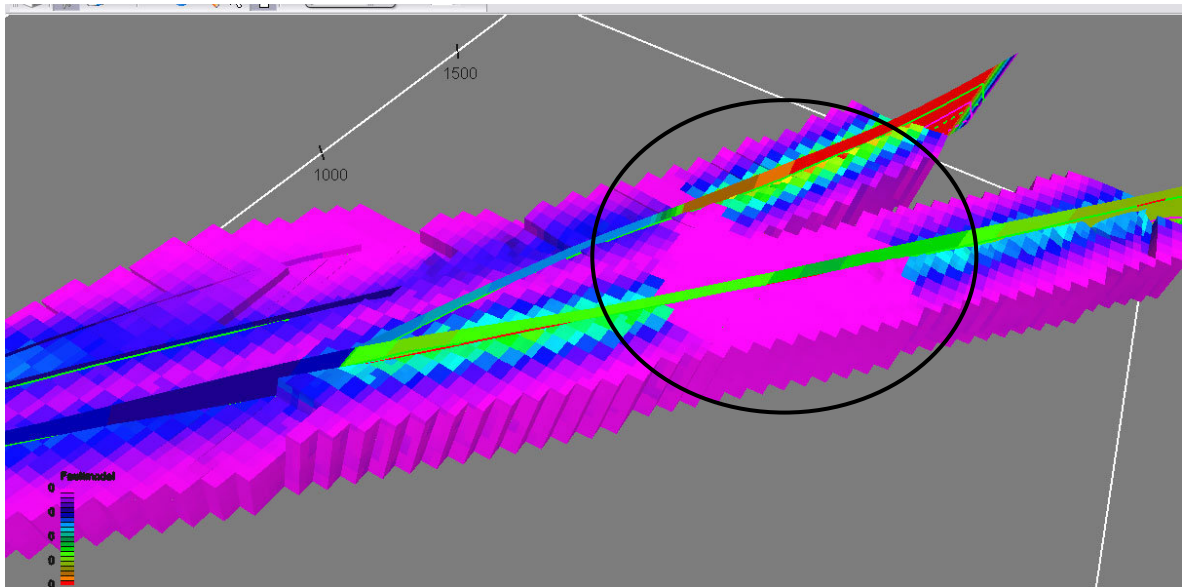
Figure 5.1.1   Showing 4 faults with surrounding LGRs. The figure is from Case 2.1, a case where further development of the model was discontinued.

As is clearly visible here strain is lacking in two areas in the middle of the model. These are areas where the strain should have been continuous. In addition to this lack-of-strain problem, we have also had cases where the strain generation has given ludicrously high values in restricted areas. Whenever I encountered problems such as these, I have tried changing the parameters to better allow

the program to run. When that has proven useless I have sent the necessary information to NR by way of ftp transfer, and awaited the following software update. This has been a fairly good way of working for the project, as it has allowed the geoscientists discovering the problems to directly influence the software development to best suit the needs of the fault facies group.

Another strain problem is getting a strain discontinuity in the vertical direction when modelling strain on inclined faults or in thin fault zones. It seemed that both the smaller the angle of the fault and the thinner the fault zone, the more difficult it was for Havana to calculate strain. The strain on such faults gains a cyclic appearance where it grows and wanes in the fault throw parallel direction as seen in the figure below. This leads to "concretions" of higher strain along the fault plane, where it ideally should be continuous.

"Good" strain vs. "bad" strain
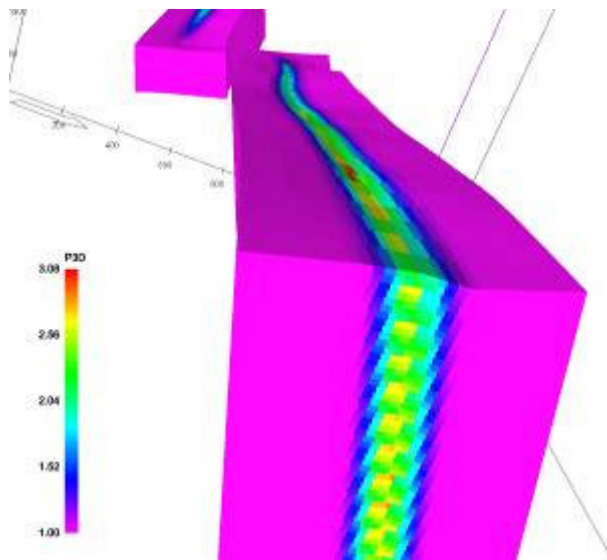
Figure 5.1.2
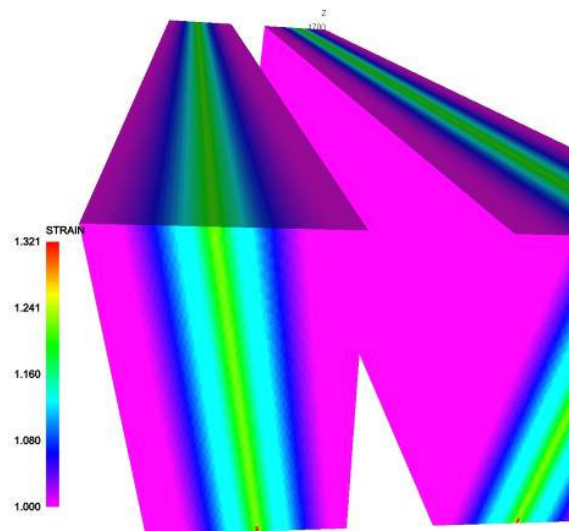
Figure 5.1.3

The two figures above are the LGR's from the relay-structure case and the graben case (cases 3 and 5 in RMS projects.

Figure 5.1.4 shows the strain in the domino fault system case, case 4.1, where I have used an LGR of 50m on each side of the fault plane and where the inclination of the faults is between 45 and 67 degrees.
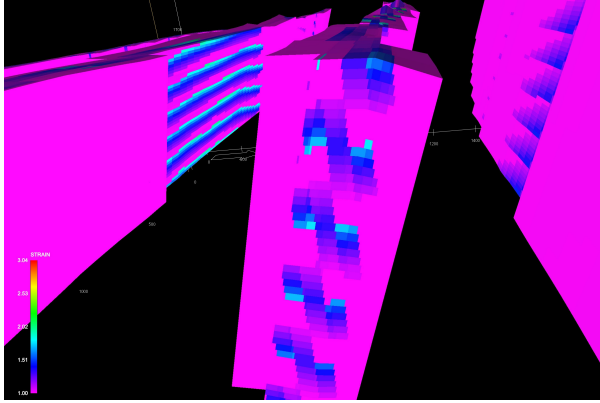
Figure 5.1.4   strain artefact as seen in case 4.1

When the LGR of case 4.1 was set to 25 meters on each side, the resulting strain was even worse as seen in Figure 5.1.5, rendering simulation impossible.
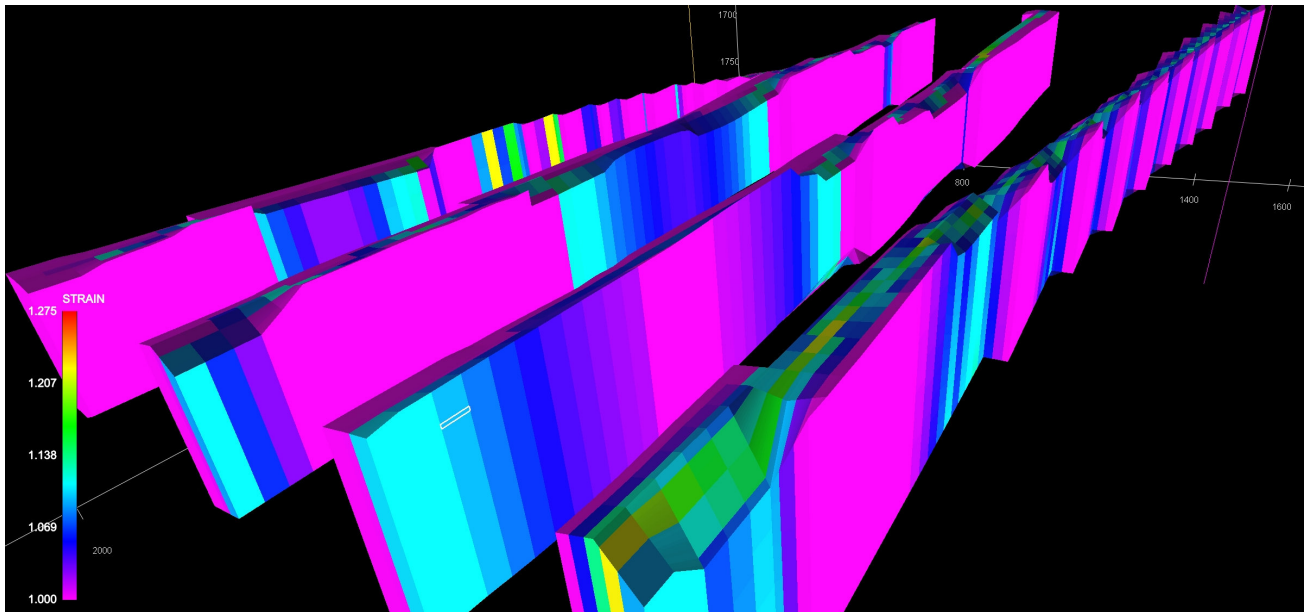
Figure 5.1.5   Case 4.1 25m LGR

To test if it was the low inclination or the thin fault zone LGR that lead to an extreme result on the strain error, I tried to straighten up the LGR by making a vertical fault model as a replacement for the original, and to create an LGR based on a combination of both. The strain from the vertical LGR was then resampled as nearest-node to get the improved strain to the inclined LGR grid. This test was an attempted workaround to the strain problem, hoping that if the angle of the faults alone was the decisive factor I could overcome the problem. Unfortunately, this method did not give any useful results.

5.2   Grid restoration problems.

The Restorgrid.model file returns some faulty results in certain cases. Some cells at the fault boundaries get stretched quite substantially, deforming the grid and displacing the facies they contain. No final solution has been found to this problem, but a fairly good workaround is in place, as explained in chapter 2.2 and 2.5, and it can be seen in detail in the RMS models Case3 and Case4.1. In Case5 no workaround was needed, as it is a very simple model. Seen underneath here is the stretched cells poking out of the restored grid from Case 4.1 :
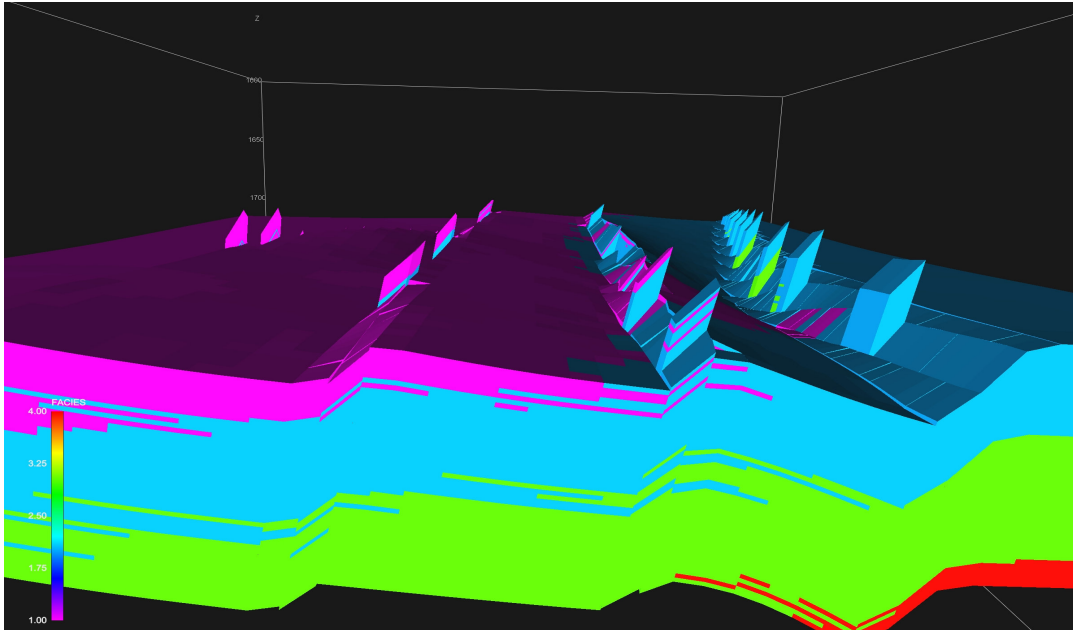
Figure 5.2.1   spikes in the grid as result of artefact from Havana

After the workaround the grid looks like this :
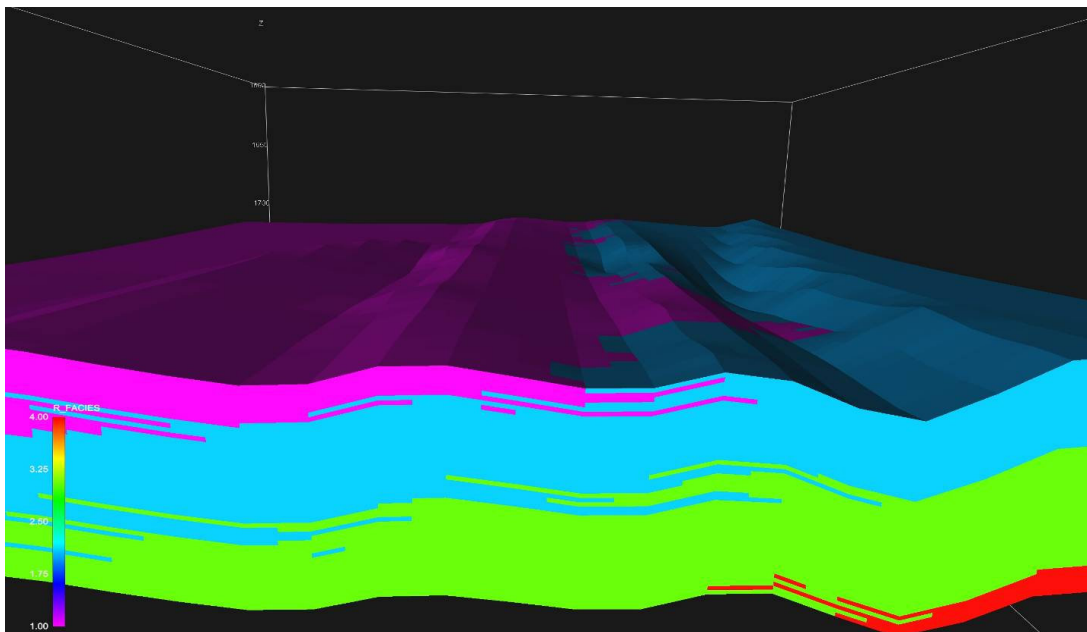
Figure 5.2.2   case 4.1 after grid-spike workaround

Although some of the geometry is lost during the workaround, it is a best practice until the problem has been resolved.

5.3 Flow problems in RMS

RMS cannot predict flow on a grid with an LGR present, so this has to be done in ECLIPSE, however it is possible to run a flow pattern simulation using the RMS function Streamlines, to see how the flow generally will behave. This unfortunately, doesn't work properly in RMS either. The streamlines ignore the fault facies permeabilities, and follow the permeability of stretched original facies. This renders RMS unsuitable for fluid flow and streamline simulation of fault facies grids until RMS gains support for LGR's. The image underneath (Figure 5.3.1shows streamlines ignoring the permeability variations of the LGR. The pink areas are areas of between 0 and 1 mD permeability (Colour scale inverted).
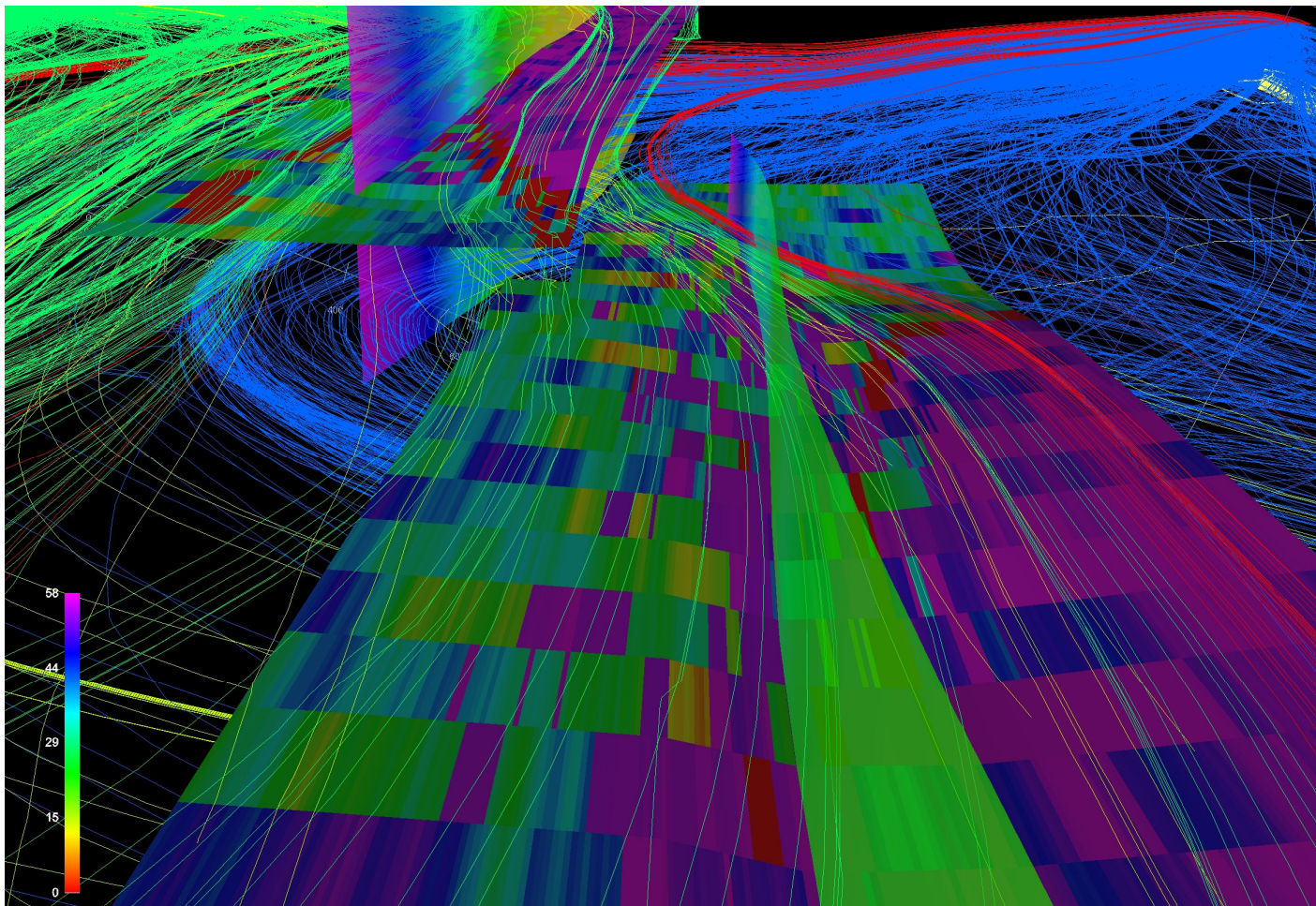

Figure 5.3.1   **Streamlines on case 3, crossing unhindered through 0 porosity areas.**

5.4 Eclipse – Havana incompatibility

For Havana 5.6.9 the output merged-grid file Havana gives after merging the conventional grid with the LGRs contains a keyword called AMALGAM. This keyword is included to get all the LGR amalgamations of the grid ready to simulate in Eclipse. For Havana 5.6.9 this keyword gives its output as a one line string of data for each amalgamated LGR group. The problem with this is that Eclipse cannot read lines of more than 80 signs, so that if the amalgamation contains more than 7 or so LGRs, Eclipse is unable to read them. This has been rectified in the Havana versions following 5.6.9.

Eclipse doesn't understand the keyword FACIES, so the merged grids had to be produced without facies parameters to be able to simulate on it. This was done by exporting the localgrid (localgridfinal.grdecl) and the simgrid (coarsegrid.grdecl) without facies to the appropriate folder. Unless this is done, one will have to manually edit the mergedgrid.GRDECL file by removing the facies data. If the faults are not straight, or crosscut the grids obliquely, this is a lot of lines to remove, so as a best-practice this should be done in the export of the simulation grids.

When using Eclipse to simulate a reservoir with LGR's, a keyword called AMALGAM must be included in the merging operation. This is done in the "*FaultFaciesMerge.model*" file. This keyword makes Havana group and amalgamate all LGR's which are in contact, making them ready for simulation.

Any LGR in Eclipse must have a rectangular shape. This means the large, amalgamated LGR's, which are not perfectly rectangular or which are not grid-parallel, will be built up of several minor LGR's (from now on referred to as LGR segments or simply segments). To keep the number of LGR segments in any grid as low as possible; the individual segments are made as large as possible while still maintaining rectangular shape. This means that any amalgamated LGR is made up of smaller and larger rectangular pieces, where the number of cells in each of these building blocks will vary accordingly. When simulating in Eclipse, the amount of memory used at any given step of the calculations has to be predefined, as Eclipse is unable to figure out for itself how much memory it needs for each operation (it uses static memory allocation). The user puts the maximum number of cells for any LGR in the grid, and the total number of LGR segments in the grid, into the Eclipse runfile. When Eclipse checks how much memory it needs, the number of LGR segments is multiplied with the maximum number of cells for a single LGR segment, which gives the worst-case scenario of memory usage. The problem with this is that if the simulation grid contains a few large LGR segments and a lot of small ones, the amount of required memory for the program is greatly

exaggerated compared to what is actually used in the calculations. This may lead to memory requirements higher than what's available.

5.5   Regarding Rd and grid cell size

The lowest possible Rd value on the faults was 30. Values of 7, 15 and 22 returned erroneous results in the restored grid. This is probably because the Rd value cannot be less than 1 cell width, which is 25 meters. Until we can make the grid a lot finer while still being able to flow simulate on it, this is the effective limiting factor of how narrow we can make the fault zone. Although this is not strictly a bug I chose to put it in this chapter as it is a problem at the moment, but which will be resolved with further development of computer hardware.

6   Discussion

6.1   Technical discussion

6.1.1 Discussion on the use of Havana

When using the empirical relationships from Figure 6.1.1 on the models used in this thesis, the r_d value is suggested to be lower than 25 m for all cases. Defining r_d values in this manner yielded unsatisfactory modelling grids because the grid cell dimension is larger than the minimum area over which the displacement is distributed. To avoid this scale problem and observing both the substantial spread in damage zone width/ throw, r_d is set higher than 25 m for the present models. This is done by editing the r_d values in the fpar.dat file (Appendix E – RMS cases/…/input), following Eq. 2.4, to fit the desired displacement distribution.
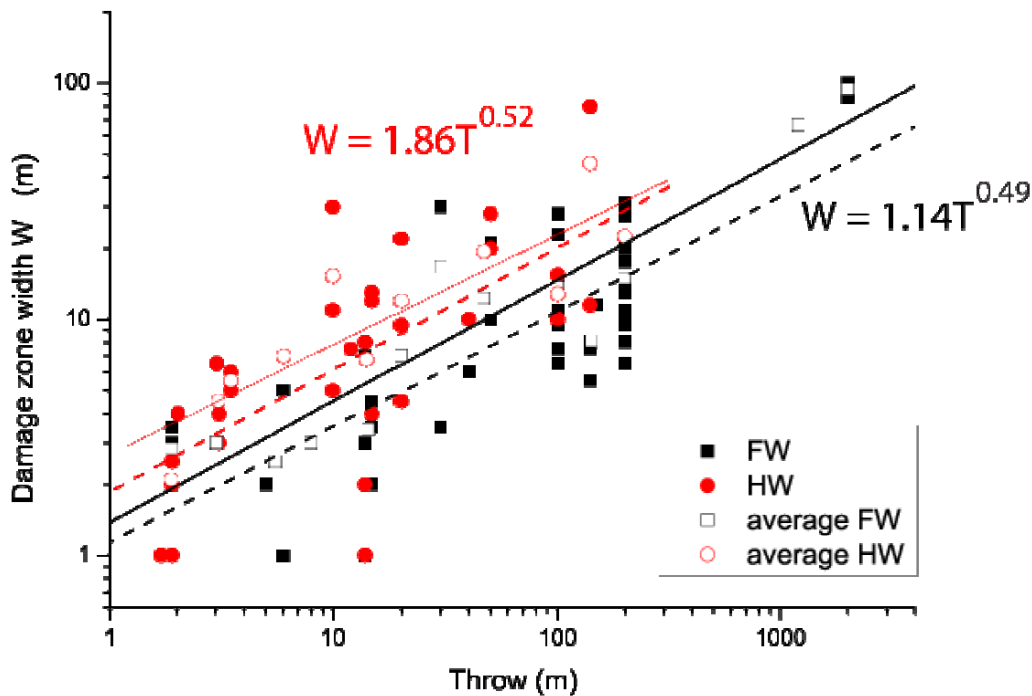

Figure 6.1.1 Damage zone width/throw relationships. Schueller et al. in prep

The r_d defines how far the influence of a given fault extends from the main fault plane. However, if the r_d is larger than the width of the LGR fault zone grid, it is the extent of the LGR

which defines the reach of the strain. This means that the low-strain facies will be distributed around the medium and high-strain facies and fill the rest of the LGR box, which will give a low-strain distribution geometry which is not entirely in accordance with natural distribution of low-strain facies. For my cases, the r_d has, for the most part, been lower than the width of the LGR grid, but nevertheless the LGR is here filled completely with fault facies. This was done to for reasons of expediency and to simplify modelling, as getting a fourth "zero-strain" facie into the IPL scripting in RMS, although turned out to be. For my "standard" cases, this means that the low-strain facie extends 3 grid cells, or 75 meters, away from the fault plane. For the additional cases the LGR, and thus the low-strain facie, extends from 25 to 75 meters, or 1 to 3 grid cells, from the fault plane, depending on the realisation.

For the standard cases 3 and 4, this keeps the damage zone width within 2.5 times fault throw as suggested by Shipton & Cowie (REF), but exaggerates the width for case 5.. In spite of knowing this, I have chosen to give all standard-cases the same LGR width, and rather supplement with additional simulations with thinner fault zones. This is done to make sure the strain and displacement is modelled in the same way for each standard-case, as the strain calculations become unstable when the LGR width gets too low. Doing this somewhat reduces the effect of the r_d, as it removes details from the transition from low-strain facie to zero-strain facie, but the distribution of the higher strain, and presumably most important, fault elements still follows the r_d as it should.

As modelling low-strain facies in this way is not completely correct, I see this as a point of improvement to the workflow, where as many extra facies as is mathematically possible (and practical), and geologically desirable should be included, and where the lowest strain facie should ideally be a zero strain facie surrounding the other facies so as not to get a box-distribution of the low-strain facies. The reason why a zero strain facie should be included is that the transition from low-strain to zero-strain is not in the form of a perfect plane surface. The transition is gradual, and amount of deformation bands etc. may change depending on the facie. *(The extent of the grid refinement is decided in the ExpandedLGR.model file on the line "*`GRID_REFINEMENT    FAULTS    1`
`25 1 3 \`*")*

Additionally, when modelling the fault facies like this, one should make sure the fault facies follow a geometrical distribution consistent with empirical values from field studies, so that for example fault cores of abnormal thickness are not modelled.

For this thesis however, as it is more of a proof of concept type assignment than a geological model, too thick volumes of fault core and breccia have been used to illustrate the idea better, and to minimize bug-problems.

6.1.2 Points of improvement:

Facies filling the LGRs

As strain varies along-strike of a fault, increasing where two faults meet, decrease as displacement varies along-strike, the box representation of the low strain fault facies in this thesis, having a low-strain facie which completely fills the LGR, is incorrect. It prevents the lowest strain fault facies from following the strain as it grows or wanes depending on throw, and forces it too extend too far from the fault plane when strain is not high enough to fill the LGR. If a fourth, zero-strain facie is included or the number of active facies is reduced to two keeping the one occupying the lowest strain area as the original facies, this source of error will be greatly lessened, if not removed completely. This could be implemented in a set of standard IPL scripts for fault facies modelling in RMS.

Volume

Both when generating the restored grid configuration and when re-sampling facies from the restored grid into the fault zone grid, to capture the displacement of facies inside the fault zone, some mismatches between the original un-faulted reservoir volume inside the fault zone and the resulting volume of the faulted reservoir rock inside the fault zone grid may occur. However, as RMS can not read data from the final merged models properly, I have not been able to quantify possible volumetric deviations. Qualitatively, upon visual inspection of the grid such as the side-view example of case 5 shown in Figure 6.1.2, the volumes seem fairly comparable. Assuming the ratio of gained to lost is approximately the same for the rest of the model a possible error can be presumed to be insignificant (keeping in mind that the extra volumes (in red in Figure 6.1.2) added to the LGR grids are populated by a default impermeable mud).
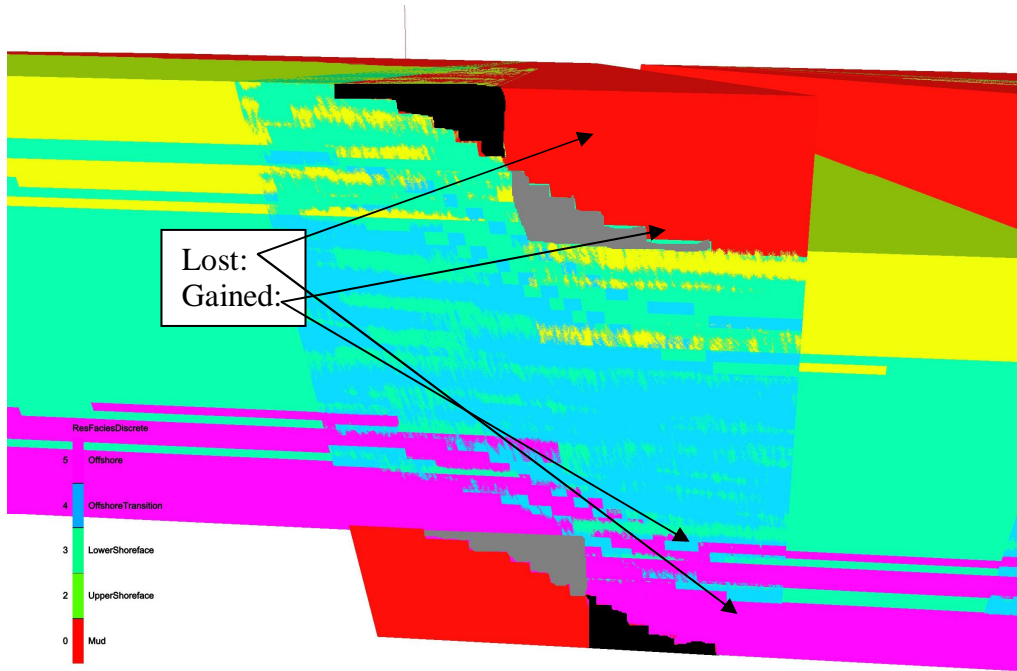
Figure 6.1.2   Case 5, conventional grid with LGR superimposed.

In models with higher throw however, the volume gained is significantly larger than that which is lost, as there is no volumetric constraint in the algorithm restoring and displacing the grid. Figure 6.1.3 shows a fault with a larger displacement, where the original facies have been distributed following a displacement curve in the same way as in my models. The displacement has been performed without constraining the volume of the facies to the original volume of the facies, thus increasing the volume significantly and introducing an error. The original volume from before displacement approximately filled the red box. It is easy to see that the new volume, which is seen between the black lines, is a lot larger than the original.
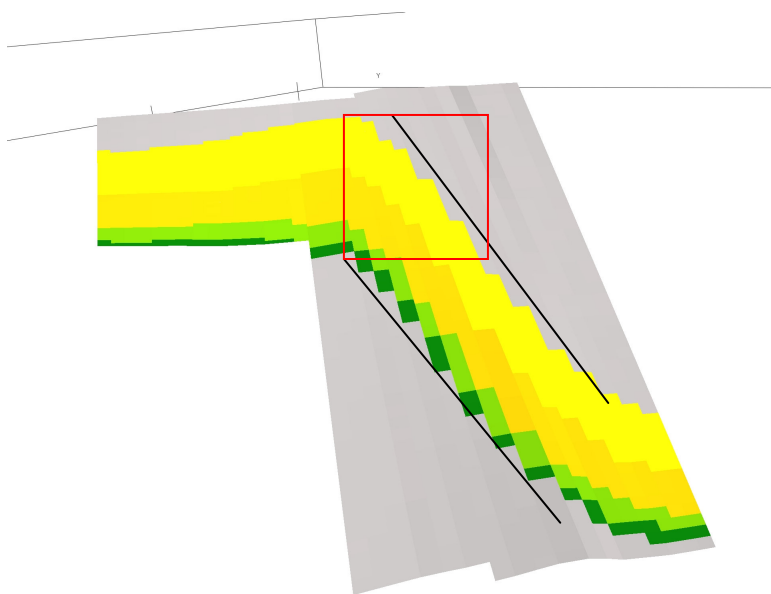
Figure 6.1.3

This problem is being looked into by Muhammad Fachri at CIPR, and a possible solution will be presented in his upcoming paper (Fachri et al. in prep). The method deals with the problem by using user-defined displacement curves (the displacement curve of the above example can also be used) for displacing the sedimentary facies along the grid pillars. By this method, the reservoir thickness in the fault zone grid is kept the same, and thereby the volume is maintained. The result of applying this method is called the lithologic distribution parameter (LDP) (Figure 6.1.4). Figure 6.1.3 and Figure 6.1.4 are from the same fault, just shown from different angles and with different areas removed by filtering, however displacement is the same and the figures are from the same general area of the fault.

Figure 6.1.4   Fachri et al. in prep.

The LPD method keeps true to the data trends from the data recorded by the group, presented in Figure 6.1.1 and gives a significantly better representation of the fault-zone facies distribution. It is also more compatible with the fault core thickness data seen in Figure 6.1.5, as it distributes more of the displacement in a thinner zone. The facies of Figure 6.1.4 are used in the same way as the re-sampled facies from the current fault facies re-sampling method, as a constraint on the occurrence of individual fault facies. A drawback of this approach is that it requires cell thickness to vary across the fault, which may cause problems when dealing with complex geometries: The corner-point grids currently used for modelling require each grid line in X and Y direction to extend across the model.

Furthermore, cell dimensions for LGR grids can not be differentiated in terms of size. In order to work on complex geometries this scheme would require an extremely high number of cells. This method may however work flawlessly on complex cases if unstructured grids were used.
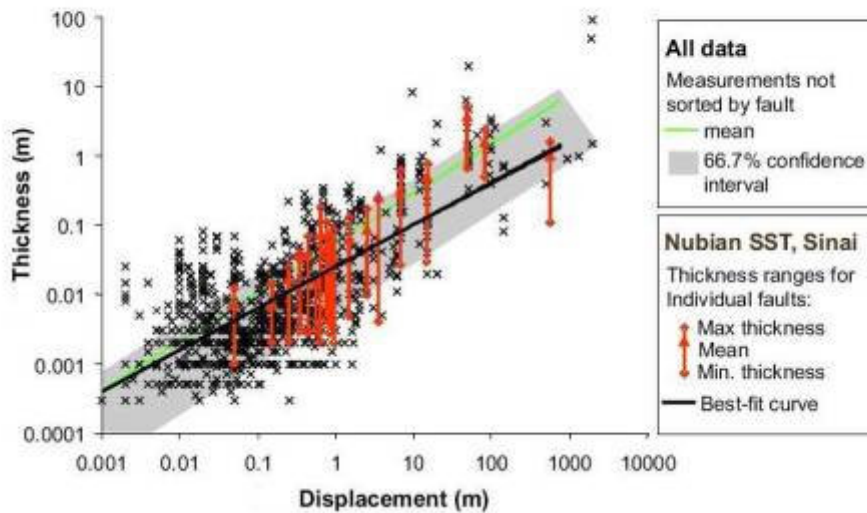
Figure 6.1.5 Quote Fault Facies Final Report: "Summary plot of literature data and Fault Facies project data, from Skar et al.(manuscript). The plot shows the mean trend line for displacement on faults and their related core thickness of the entire dataset of 823 faults, as well as the best fit curve for the Fault Facies project data of Sinai. Note the differences in the two trend lines, and the uncertainty range in the dataset."

Strain

When modelling the strain at the grid scale of the models in this thesis, the strain will in most cases be slightly discontinuous in the vertical direction if the fault is inclined. By discontinuous I mean it gets a cyclic heightening and lessening of strain values as seen in the figure below (Figure 6.1.6) :
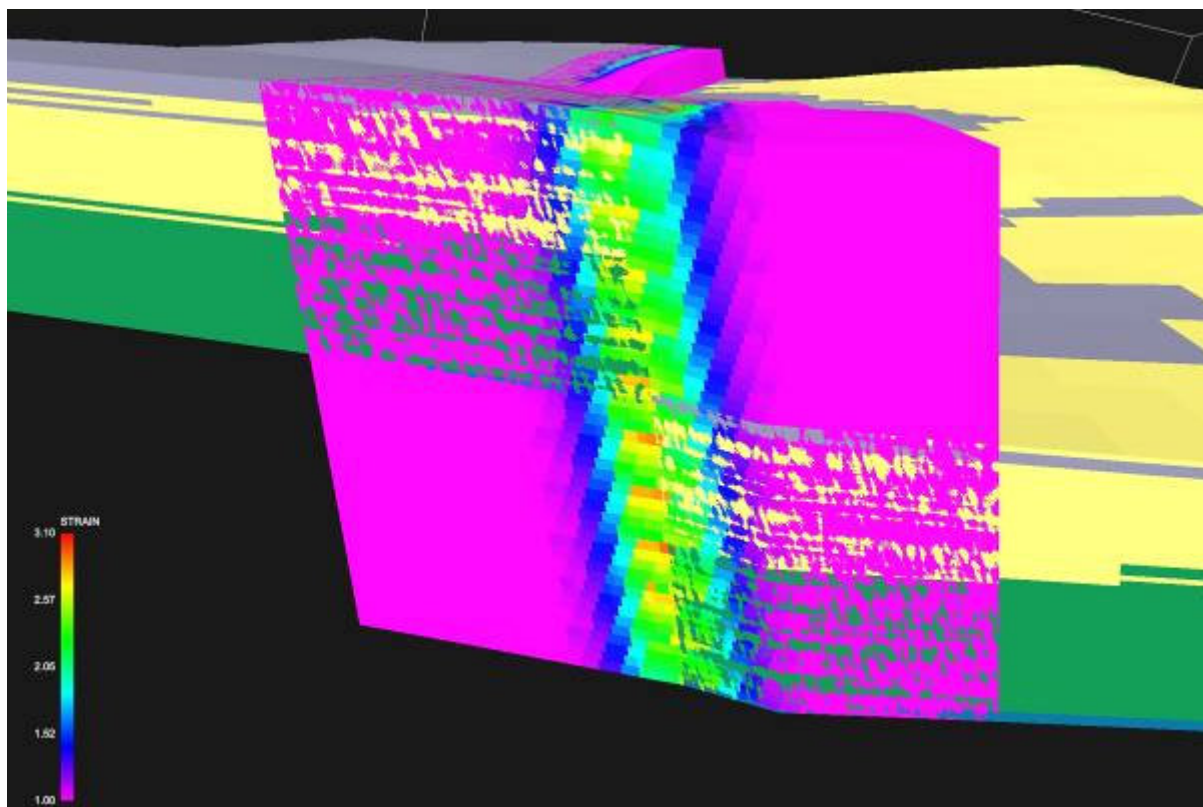
Figure 6.1.6   Strain varying with depth.

This artefact arises due to problems with computing strain in a regular grid of discrete size, and is most prominent on inclined faults. It becomes less pronounced when decreasing the cell size and heightening the resolution of the LGR grid, and may be of little importance in few years as the speed at which computing power is evolving. The error can be somewhat corrected by putting a cut-off, or conditioning filter, on the strain (e.g. "if strain>## then strain=##"). This only attenuates the highest strain values, and thus relatively augments the lower ones. Filtering values may introduce a source of error in the modelling, but for our purpose it works well as the vertical variation due to the error is negligible away from the fault plane, and as we are more concerned with relative strain distributions, not the absolute values. It gives a better distribution and visualisation of strain, making the distribution more even in the thin high-strain area. Nevertheless, this artefact means there is a problem with the algorithm and it should be fixed.

The width of the LGRs should ideally closely follow empirical relationships of fault throw vs. damage zone width (i.e. Figure 6.1.1), but for this to be feasible the strain algorithm used in Havana needs to be improved to handle thin LGRs and low displacements. Presently, thin LGRs give erroneous strain results when using Havana.

Displacement

The algorithm which calculates displacement distorts the regular grid, to give us the "restored grid" with the displaced facies, has a bug to it at the moment. Some of the grid cells in the immediate vicinity of the fault plane are elongated vertically, displacing the cells above and beneath creating spikes jutting out of the grid (Figure 6.1.7). Values inside the elongated grids are correct, but the shape of the cells is distorted. This problem emerges due to a problem with curved fault pillars in Havana. Havana normally uses straight fault pillars, so if the pillars are curved, some nodes of cells very close to the fault plane may be erroneously taken to be hanging wall/footwall cells of the wrong "polarity".
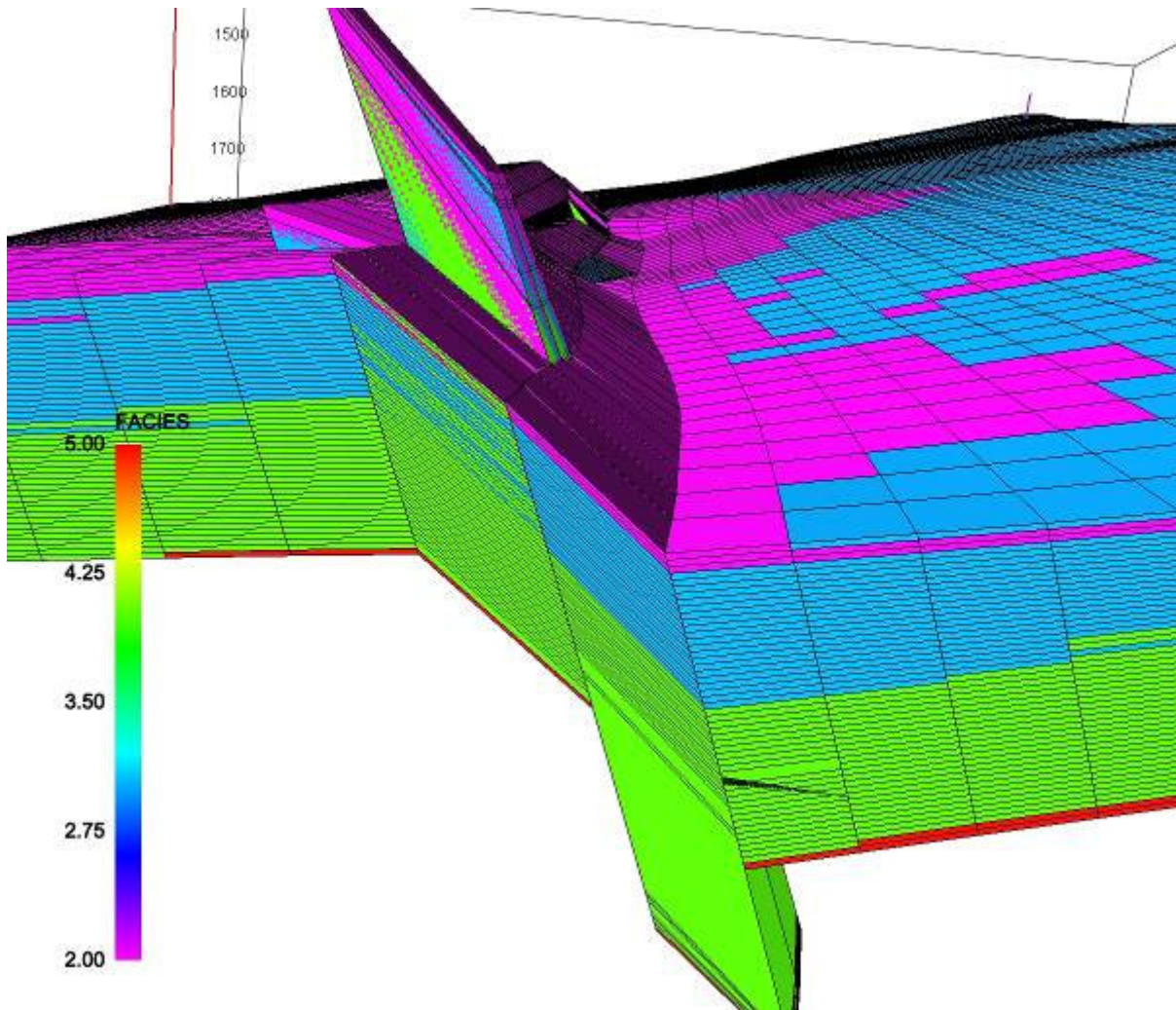
Figure 6.1.7

This changes the flow conditions in the area, and needs to be remedied. Current a fairly good workaround is in place to deal with this problem. The case project in RMS includes several zones, and using different zones and a bit of a data-transfer in-between the zones allows us to overcome the cell-spikes. The workaround includes making a new zone called the "updated restored grid" which is based on horizons made from the "restored grid" which has the error. Then re-sampling the facies

from the "restored grid" to the "updated" one through ijk re-sampling, and then using the re-sampled facies from the "updated restored grid" to resample the facies to the LGR grid (further explained in Chapter 2.5, General workflow:). This works quite well, but is not ideal, as the displacement is slightly averaged out.

6.2   General discussion

Making programs which are capable of generating fault facies is not a trivial task. As little research has been done on 3D fault models previously, little is known about the sensitivity of the technique or how it performs in practise. Tveranger et al. started work on creating a fault facies workflow, usable by the industry, in 20045at CIPR and it has been a continuous effort including the present work. Albeit the projects phase one is complete, it can be said to still be an ongoing project as phase two is in the making, and as it is far from streamlined enough to be used commercially as of today.

Facies probability distribution

The method for distributing the intensities, by use of IPL scripting and in a sense crossplotting sedimentary facies to strain, is complicated and not user friendly. It should be possible to create an addon to RMS which lets the user define values of distribution percentile in a graphic display, possibly following the model of the "Facies probability function…" of "Data analysis" in RMS. This should not altogether replace strain modelling, but should be used together with a strain calculation, where the strain could be used as input for a default distribution in the module. This could be done by having an RMS module where meters from the fault, and percent probability of occurrence of facie could be the X and Y scale. Each facie would be represented as a continuous line following the percent of that facie at any given point. These lines should be possible to alter manually in the same way it is possible in the "Facies probability function…" in RMS. The way it is done in RMS for the Facies probability function is illustrated in Figure 6.2.1.

Data: final_PERMX, localgrid
Facies: 12 of 12: A1_sst_lowstr, A2_sst_medstr...
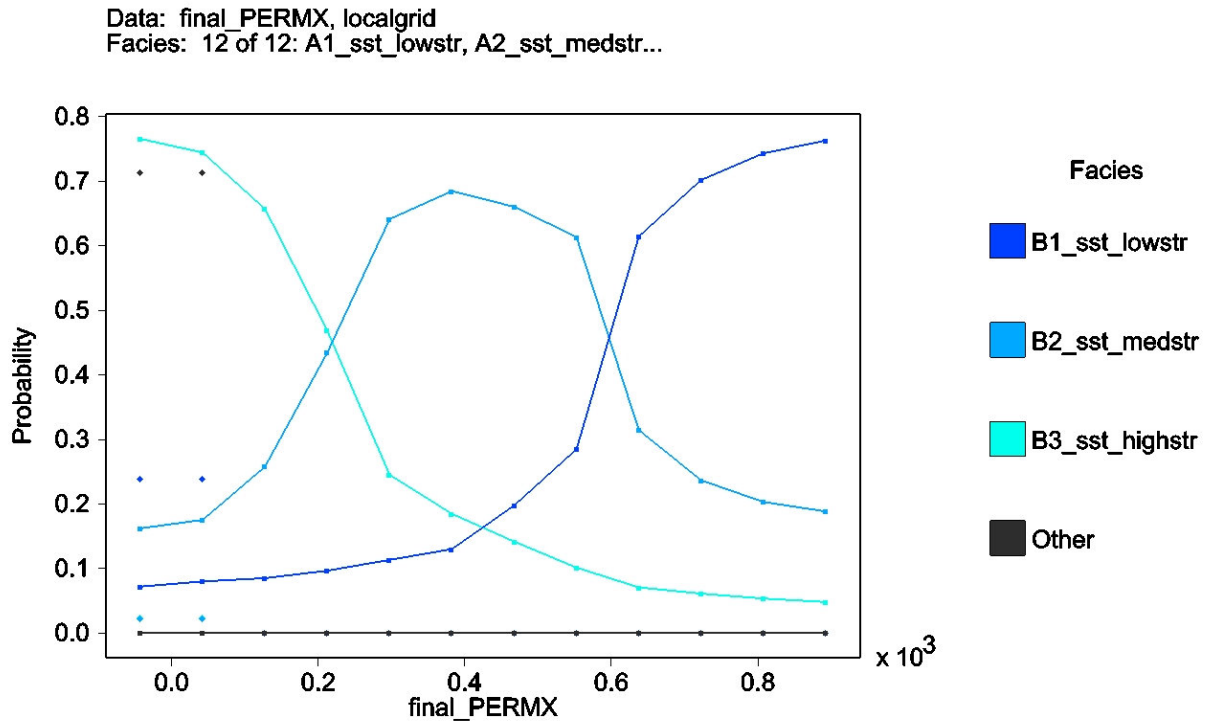
Figure 6.2.1   Example of the "Facies probability function…" in RMS. The user should be able to define the distribution probability of parameters quantitatively in a graphic display, guided by empirical data.

Up-scaling discrete element connectivity

When up-scaling a model with discrete fault facie objects such as sand lenses, the most determining factors for the flow simulation are the fault rock matrix permeability and the connectivity of fault rock lenses to the host rock rather than the sand lens permeability and sand lens fraction (Fredman et al. 2007). This means that if the grid contains lenses, the up-scaling should not be so coarse that the connectivity of fault rock lenses is lost. The fault rock lenses could perhaps even be modelled after the up-scaling, as they don't need to be as fine as the fault core modelling? Lenses were not modelled in my cases, and this could be something to be looked at and tested in the second part of the Fault Facies Project.

Distributing fault facies according to amount of strain is a good start, but a database should ideally be expanded to include : more sedimentary facies, burial depth, strain rate, the likelihood of drag zones or other sub-seismic geometries occurring and of course amounts of strain. An algorithm, , could be constructed to incorporate all of this, which makes it more user friendly to incorporate into a modelling workflow. This would allow a more accurate distribution of fault facies following trends based on extensive field work which could be updated easily with more data. The algorithm or

database needs be suited to predict reservoir flow better than what the SGR has been able to up till now, if it is to compete with the SGR in usefulness. In short, we need to improve our geological understanding and the statistical grounds for it if the fault facies modelling technique is to be an improvement on the transmissibility multiplier method.

Simulation Time

The time it takes to simulate on a fault facies grid (Table 4.1-3) may turn out to be too long for the method to become practical to use in the next year or two, but it is no huge disadvantage in the long run as if Moore's law continues to hold we will be able to double the number of calculations every two years.

7   Conclusion

The work performed:

- When I started on this thesis we hoped I would get time to perform comprehensive testing on the models to be able to make some statistics from the simulations, but as time went by it became clear that I would only get the time to compare the flow to the previous models in a brief manner.

- In hindsight, the ideal simulation for geologic realism would have been a case with 25m fault zone width (50m in total), no cap on strain in the IPL script pertaining to step 6 of the workflow and the initial permeability values. However, I did not get the time to test this setup as I struggled with the standard setup until the end.

Simulation:

- RMS cannot be used to simulate flow in grids with LGR's as seen in this thesis.

- An already well known fact when it comes to simulation times is apparent in this thesis as well, as it seems simulation time is not only dependant on the number of cells in the model, but also is influenced by the complexity of the flow-path.

Evaluation of the fault parameters:

- Even though the statistical evaluation of the method is not very strong due to the limited amount of samples, some tentative conclusion can be drawn pending further tests. The fault setup relative to the wells is by far the most influential flow controlling parameter, greatly surpassing the influence of the parameters controlling the faults transmissibility such as the thickness of the fault and the way strain modelling is handled.

Comparison to previous work:

- This is also to a certain degree comparable with the previous results from studies by Lescoffit & Townsend (2006), Ottesen et al. (2006), Manzocchi et al. (2008) and Tveranger et al. (in press) done on models with 2D representation of faults, which all emphasized the pattern of fault-set, the geometries in general and the importance of fault density, as more important than the permeability of the fault rock itself.

- Comparing to the work of Sæther (2006) we see the strong effect tight faults have on flow in compartmentalised reservoirs, and how little effect the faults have if there is any communication between the wells, bypassing the faults.

The bugs and the software:

- There are some bugs and improvements which need to be looked at, but none which are insurmountable in the foreseeable future.

- The interaction between RMS, Havana and Eclipse when using the additional functions of Havana, can be somewhat heavy-trodden and further work is needed to streamline the cooperation of the programs. This pertains specifically to the bug-workarounds, but will, needless to say, be less of an issue as the bugs are eliminated from the software.

The method:

- Flow simulation on a full field model with a geologically realistic scale of geometries and a level of detail similar to what has been employed in this thesis is impractical with the computing power commercially available in 2008, but may become possible in some years as computers grow ever more powerful and parallel processing is utilised to it's full potential.

- The workflow which is used when modelling fault facies is currently not user friendly and only suited for expert users, with complicated or non-intuitive parameters being used, and takes a lot of time to work through. However it be more streamlined as the Fault Facies project progresses further, and will in my personal opinion most likely be in industrial use in the future.

Footnotes:

[1]   - Table 4.1-2 [2], Only 4 realisations were made for the standard 75m case due to data trouble

[2]   - Table 4.1-2 [2],One simulation of each of the varying scenarios was supposed to be run for each case, but due to problems in getting the simulations to run properly using Eclipse, I eventually ran out of time, having to leave the data table somewhat lacking.

References

<u>*Antonellini and Aydin, 1994.*</u> *M.A. Antonellini and A. Aydin, 1994, Effect of faulting on fluid flow in porous sandstones: petrophysical properties. AAPG Bulletin* **78** *p. 355–377*

Bouvier, J. D., C. H. Kaars-Sijpesteijn, D. F. Kluesner, C. C. Onyejekwe, and R. C. Van der Pal, 1989, Three-dimensional seismic interpretation and fault sealing investigations, Nun River field, Nigeria: AAPG Bulletin, v. 73, p. 1397–1414.

Caine, J.S., Evans, J.P. and Forster, C.B., 1996, Fault zone architecture and permeability structure, Geology 24, 1025-1028

Cardozo, N., Røe, P., Soleng, H. H., Fredman, N., Tveranger, J., Schueller, S., 2008 A methodology for efficiently populating faulted corner point grids with strain, In press, Petroleum Geoscience.

Doughty, T., 2005, Clay smear seals and fault sealing potential of an exhumed growth fault, Rio Grande rift, New Mexico, AAPG Bulletin v.87, no. 3, p. 427 - 444

Fossen, H., Hesthammer, J., 2000, Possible absence of small faults in the Gullfaks Field, Northern North Sea: Implications for downscaling of faults in some porous sandstones, Journal of Structural Geology, 22, p. 851-863.

Fossen, H,. and Gabrielsen, R.H., 2005, Strukturgeologi, Fagbokforlaget

Fossen, H. and Bale, A., 2007, Deformation bands and their influence on fluid flow, AAPG Bulletin vol.91, nr12, p1685-1700

Fredman, N., Tveranger, J., Cardozo, N., Braathen, A. et al., 2008, Assessment of Fault Facies modelling; technique and approach for 3D conditioning and modelling of faulted grids. American Association of Petroleum Geologists Bulletin, accepted

Fredman, N., Tveranger, J., Semshaug, S., Braathen, A., Sverdrup, E., 2007, Sensitivity of fluid flow to fault core architecture and petrophysical properties of fault rocks in siliciclastic reservoirs: a synthetic fault model study <u>*Petroleum Geoscience*</u>*, Volume 13, Number 4, 2007 , p. 305-320(16)*

Gougel, J., 1952, Masson, Paris. Referance found in pecock et al 2000 Glossary of normal faults, Journal of structural geology

Harris, S.D., McAllister, E., Knipe, R.J., Odling, N.E., 2002, Predicting the three-dimensional population characteristics of fault zones: A study using stochastic models, Journal of Structural Geology vol. 25, p. 1281 - 1299

Hesthammer, J., Fossen, H., 2000 Uncertainties associated with fault sealing analysis, Petroleum Geoscience 6, p 37-45

Hollund, K., Mostad, P., Nielsen, B.F., Holden, L., Gjerde, J., Contursi, M.G., McCann A.J., Townsend, C., Sverdrup, E., 2002, HAVANA - A Fault Modeling Tool, Norwegian Petroleum Society Special Publication 11, p. 157 – 171, (Published by <u>*Elsevier*</u>*)*

Huggins, P., Watterson, J., Walsh J. J., and Childs C., 1995, Relay zone geometry and displacement transfer between normal faults recorded in coal-mine plans, Journal of Strucrural Geology, Vol. 17 p. 1741-1755

Knipe, R. J., 1997, Juxtaposition and seal diagrams to help analyze fault seals in hydrocarbon reservoirs. AAPG Bulletin v. 81, p. 187-195.

Larsen, P. H., 1988, Relay structures in a Lower Permian basement-involved extension system, East Greenland. J. Strucr. **Geol.** *10,3-8.*

Lescoffit, G., Townsend, C., 2005, Quantifying the impact of fault modelling parameters on production forecasting for clastic reservoirs, AAPG Hedberg Series no. 2, p. 137 – 149.

Lindsay, N. G., F. C. Murphy, J. J. Walsh, and J. Watterson, 1993, *Outcrop studies of shale smear on fault surfaces: International Association of Sedimentologists Special Publication 15, p. 113–123. (ref from Yielding et al. quantitative fault seal prediction.)*

Ma J., Couples G.D., 2007, *Construction of guiding grids for flow modelling in fault damage zones with through-going regions of connected matrix, Computers & Geosciences 33, p. 411–422 (was this used? Ref from chap. 1.2 damagezone)*

Mandl, G., 1987, *Tectonic deformation by rotating parallel faults: The bookshelf mechanism, Tectonophysics vol 141, p. 277-316*

Manzocchi, T., Walsh, J. J., Nell, P., Yielding, G., 1999, *Fault transmissibility multipliers for flow simulation models, Petroleum Geoscience, Vol. 5, p53-63*

Manzocchi, T., Carter,A., Skorstad,A. et al. 2008, *Sensitivity of the impact of geological uncertainty on production from faulted and unfaulted shallow-marine oil reservoirs: objectives and methods. Petroleum Geoscience, 14, p. 3-15.*

Manzocchi, T., Heath, A. E., Palananthakumar, B., Childs, C. and Walsh, J. J., 2008, *Faults in conventional flow simulation models: a consideration of representational assumptions and geological uncertainties. Petroleum Geoscience, vol. p. 14, 91-110.*

Manzocchi, T., Matthews, J.D., Strand, J.A., Carter, J.N., Skorstad, A., Howell, J.A., Stephen K.D. and Walsh, J.J., 2008, *A study of the structural controls on oil recovery from shallow-marine reservoirs, Petroleum Geoscience, Vol. 14, p. 55-70*

Odling, N.E., Harris, S.D, Knipe, R.J., 2004, *Permeability scaling properties of fault damage zones in siliclastic rocks, Journal of Structural Geology vol. 26, p. 1727 – 1747*

Ottesen, S., Townsend, C., Øverland, K.M., 2005, *Investigating the effect of varying fault geometry and transmissibility on recovery: Using a new workflow for structural uncertainty modelling in a clastic reservoir, AAPG Hedberg Series, no. 2, p. 125 – 136.*

Parnell, J., Watt, G. R., Middelton, D., Kelly, J., Baron, M., 2004, *Deformation band control on hydrocarbon migration, Journal of sedimentary research, Vol. 74, no. 4, p. 552-560*

Peacock, D. C. P., 2002, *Propagation, interaction and linkage in normal fault systems. Earth-Science reviews, Volume 58, 121-142*

Rotevatn, A., Hesthammer, J., Fossen, H., Aas T.E. & Howell, J.A. 2007, *Are relay ramps conduits for fluid flow? Structural analysis of a relay ramp in Arches National Park, Utah. In: Lonergan, L., Rawnsley, R.J.H. & Sanderson, D.J. (Eds) Fractured Reservoirs. Geological Society, London, Special Publications, 270, 55-71.*

Røe, P., Soleng, H.H., 2006, *Strain calculations in HAVANA: Algorithm and implementation, Norwegian Computing Center*

Shipton Z.K., Cowie P.A., 2001, *Damage zone and slip-surface evolution over um to km scales in high-porosity Navajo sandstone, Utah, Journal of structural Geology 23 p.1825-1844*

Shipton, Z.K., Evans, J.P., Robeson, J.P., Forster, C.B., and Snelgrove S. 2002, *Structural heterogeneity and permeability in faulted eolian sandstone: Implications for subsurface modelling of faults, AAPG Bulletin, v. 86, no. 5 p. 863–883*

Shipton, Z.K. and Evans, J.P. and Thompson, L.B., 2005, *The geometry and thickness of deformation-band fault core and its influence on sealing characteristics of deformation-band fault zones. American Association of Petroleum Geologists, pp. 181-195.*

Sperrevik, S., Færseth, R.B., Gabrielsen, R.H., 2000, *Experiments on clay smear formation along faults, Petroleum geoscience, v. 6, no. 2, p. 113 – 123*

Syversveen, A.R., Skorstad, A., Soleng, H.H., Røe, P. and Tveranger , J. 2005, *A prototype workflow for Fault Facies geo-modeling, Production Geoscience*

Sæther, E., 2006, Mastergradsoppgave; "Forkastningsparametre og produksjonsrespons i deformerte reservoarer", (Master thesis; "Fault parameters and production response in deformed reservoirs"), University of Bergen, Centre for Integrated Petroleum Researhc (CIPR), not published.

Tveranger, J., Braathen, A, & Skar, T. 2004: Incorporation of fault zones as volumes in reservoir models. Bolletino di Geofisica Teoretica et Applicata 45, 316-318.

Tveranger, J., Braathen, A., Skar, T., Skauge, A., 2005, Centre for integrated petroleum research: Research activities with emphasis on fluid flow in fault zones, Norwegian Journal of Geology

Tveranger, J., Braathen, A., Bastesen, E., Cardozo, N., Eigestad, G.T., Espedal, M., et al. 2008, Fault Facies Report

Tveranger, J., Braathen, A. & Skar (in press): Incorporation of fault zones as volumes in reservoir models using "Fault Facies". Geological Society of London Special Publication.

Yielding, G., Freeman, B., and Needham, D. T., 1997, Quantitative fault seal prediction, AAPG Bulletin v. 81; no. 6; p. 897-917

In prep./unpublished:
Fachri et al. In prep.
Tveranger et al. in prep.
Schueller et al. in prep.

Appendixes:

All appendixes are found on the DVD.

Appendix A – Petroplots

Appendix B – Tinyperm database

Appendix C – Tinyperm database with frequency diagrams

Appendix D – Facies data

Appendix E – RMS cases
-           Case 3
  - Rms project file
  - Eclipse data file
  - Input – fpar.dat file
  - Output – fault data plus coarsegrid and localgrid placement

-           Case 4.1
  - Rms project file
  - Eclipse data file
  - Input – fpar.dat file
  - Output – fault data plus coarsegrid and localgrid placement

-           Case 5
  - Rms project file
  - Eclipse data file
  - Input – fpar.dat file
  - Output – fault data plus coarsegrid and localgrid placement

-           Base case not included as the data used can be found in all the other cases.

Appendix F – Sæther's simulation parameters and results

Appendix G – Example of eclipse run file

Appendix H – IPL scripts

Appendix I – Case workflows. Step-by-step description of the RMS workflows.

Appendix J – Flow simulation results; Images of flow from all the cases and eclipse résumés containing the results